Author/s:
Geng, H;Zhong, QZ;Li, J;Lin, Z;Cui, J;Caruso, F;Hao, J

Title:
Metal Ion-Directed Functional Metal-Phenolic Materials

Date:
2022-07-13

Citation:
Geng, H., Zhong, Q. Z., Li, J., Lin, Z., Cui, J., Caruso, F. & Hao, J. (2022). Metal Ion-Directed Functional Metal-Phenolic Materials. Chemical Reviews, 122 (13), pp.11432-11473. https://doi.org/10.1021/acs.chemrev.1c01042.

Persistent Link:
https://hdl.handle.net/11343/304259

# Metal Ion-Directed Functional Metal–Phenolic Materials

*Huimin Geng,[†] Qi-Zhi Zhong,[†,‡] Jianhua Li,[§] Zhixing Lin,[‡] Jiwei Cui,[†,*] Frank Caruso,[‡,*] Jingcheng Hao[†,*]*

[†]Key Laboratory of Colloid and Interface Chemistry of the Ministry of Education, School of Chemistry and Chemical Engineering, and the State Key Laboratory of Microbial Technology, Shandong University, Jinan, Shandong 250100, China

[‡]Department of Chemical Engineering, The University of Melbourne, Parkville, Victoria 3010, Australia

[§]Department of Biomaterials, School and Hospital of Stomatology, Cheeloo College of Medicine, Shandong University, Jinan 250012, China

*Corresponding authors. E-mail addresses: jwcui@sdu.edu.cn (J.C.); fcaruso@unimelb.edu.au (F.C.); jhao@sdu.edu.cn (J.H.)

**Abstract**

Metal ions are ubiquitous in nature and play significant roles in assembling functional materials in fields spanning chemistry, biology, and materials science. Metal–phenolic materials are assembled from phenolic components in the presence of metal ions through the formation of diverse metal–organic complexes. Alkali, alkali-earth, and noble metal ions, as well as metalloids interacting with phenolic building blocks have been widely exploited to generate diverse hybrid materials. Despite extensive studies on the synthesis of metal–phenolic materials, a comprehensive summary of how metal ions guide the assembly of phenolic compounds is lacking. A fundamental understanding of the roles of metal ions in metal–phenolic material engineering will facilitate the assembly of materials with specific and functional properties. In this review, we focus on the diversity and function of metal ions in metal–phenolic material engineering and emerging applications. Specifically, we discuss the range of underlying interactions, including (i) cation–π, (ii) coordination, (iii) redox, and (iv) dynamic covalent interactions, and highlight the wide range of materials properties resulting from these interactions. Applications (e.g., biological, catalytic, and environmental) and perspectives of metal–phenolic materials are also highlighted.

**CONTENTS**

## 1. Introduction

Metal and metal ions are indispensable in daily life and participate in diverse biological activities, including photosynthesis, protein folding, nerve transmission, anaerobic digestion, and underwater adhesion of marine organisms.[1-5] These metal-containing systems provide valuable paradigms for designing synthetic materials with desired properties.[1,6] In particular, hybrid metal–organic materials, which typically consist of metal ions or metal clusters that are interconnected by organic ligands,[7,8] began to flourish with the revival of inorganic chemistry and coordination chemistry in the 1950s.[9-11] For example, metal–organic frameworks (MOFs) are porous supramolecular materials engineered through diverse metal–organic interactions. More than 20,000 types of MOFs have been reported and applied in catalysis, adsorption, filtration, energy storage, and biological applications.[12-16] The type of organic coordination ligands not only determines the structure of the metal–organic materials but also significantly influences the properties of the assemblies.[2,17] Surface-confined metal–organic materials, consisting of metal ions and phenolic ligands, have attracted widespread interest owing to the high affinity of phenolic compounds to a wide range of substrates.[18,19] Phenolic compounds are a class of bioactive chemicals that consist of one or more phenol, catechol, or pyrogallol (PG) groups, that interact with diverse macromolecules through various interactions, including hydrogen bonds and hydrophobic interactions.[20] They also have diverse interactions with metal ions, which are observed in various biological processes. For example, strong cation–π interactions between $K^+$ and phenolic moieties of proteins in cell membranes result in the considerably higher selectivity of $K^+$ channels toward $K^+$ over $Na^+$ (up to 1000:1).[21,22] Sandcastle worms can secrete adhesive glue to construct tubular shells composed of L-3,4-dihydroxyphenylalanine (DOPA)-containing proteins and metal ions (e.g., $Mg^{2+}$ and $Ca^{2+}$).[6] Mussel byssus exhibits a remarkable combination of high stiffness and extensibility due to the clustered distribution of $Fe^{3+}$–catechol complexes in cuticles.[23] Inspired by those biological process, considerable progress has been achieved in understanding the fundamental mechanisms and the engineering of metal–phenolic materials, which are assembled from a range of metal ions and phenolic ligands through diverse metal–

organic interactions. For example, the use of iron gall ink composed of tannins (e.g., tannic acid (TA) and gallic acid (GA)) and $Fe^{2+}$ can be traced back to the Middle Ages in Europe.[24] Metal–phenolic networks (MPNs) have also been exploited as a versatile platform for the surface modification of nanomaterials and biointerfaces.[18] In addition, in situ reduction of noble metal nanoparticles (NPs) mediated by phenolic compounds has been reported as an effective synthetic tool to prepare nanocatalysts,[25] and the potential of metalloid–phenolic interactions (e.g., boronate ester bonds) in materials science and drug delivery has been reported.[26]

Comprehensive reviews are available in the area of metal–phenolic materials but largely focus on the roles of phenolic compounds during the assembly process, on the MPNs, or on a specific application of the materials, such as biomedical applications.[19,27,28] There is a current need for an overview of the influence of metal ions on the engineering of metal–phenolic materials. The main theme of this review is centered on the role of metal ions in metal–phenolic material engineering, highlighting the diversity as well as functions of metal ions in phenolic chemistry. The review covers the essential principles and physicochemical properties of (i) cation–π interactions between alkali metal ions or alkaline-earth metal ions and phenolic compounds, (ii) coordination interactions that occur between transition metal ions and phenolic ligands to form MPNs, (iii) redox interactions between noble metal ions and phenolic compounds, and (iv) dynamic covalent interactions between metalloids and phenolics. This review also covers metal ions from alkali metal ions to metalloids, as well as a suite of phenolic compounds with intrinsic properties (e.g., radical scavenging, pH and redox responsiveness). Metalloids are included although they have properties that are intermediate between those of metals and nonmetals. By surveying the literature spanning from 2010 to 2021, this review summarizes the formation mechanisms, parameters of the assembly process, characterization techniques, the diverse structures of metal–phenolic materials, and potential applications. An outlook and the current challenges in the field of metal–phenolic materials are also presented. This review is expected to help unravel fundamental understandings in metal–phenolic systems and guide the design of sophisticated metal–phenolic materials for tailored applications.

## 2. Metal–Phenolic Interactions

There are 87 metals, 6 metalloids, and 18 nonmetals from element 1 (H) to element 111 (Rg) in the periodic table of elements. Both metal ions and metalloids have vacant orbitals in their electron configurations (thus they can serve as electron acceptors), whereas phenolic compounds are electron donors. Various interactions have been confirmed between phenolic molecules and metal ions, as illustrated in Figure 1a, spanning metal ions from alkali metal ions to metalloids (Figure 1b). Phenolic compounds contain numerous dihydroxyphenyl (catechol) and/or trihydroxyphenyl (PG) groups with high π-electron content and aromaticity, which provide potent negative binding sites for the cations to form cation–π interactions (see (i) in Figure 1a).[21] These cations include alkali or alkaline-earth metal ions with $ns^1$ or $ns^2$ electron configurations and are thus present as monovalent cations or divalent ions. However, covalent interactions appear to dominate noncovalent cation–π interactions in the presence of other competitive motifs to form stable metal–phenolic structures.[29] For instance, coordination bonds become the dominant forces in the presence of transition metal ions or main group metal ions with abundant vacant orbitals. The catechol or PG moieties of phenolic compounds are available as electron donors. Each hydroxyl oxygen atom can donate an electron pair to an empty orbital in the metal ions, leading to reversible coordination bonds and the resultant supramolecular structures known as MPNs (see (ii) in Figure 1a).[30] When noble metal ions (e.g., $Au^{3+}$, $Ag^{+}$, and $Pd^{2+}$) accept electrons donated by phenolic compounds, they can be reduced irreversibly to their stable metallic forms (e.g., Au, Ag, and Pd, respectively) (see (iii) in Figure 1a). During that process, it has been reported that the phenolic compounds are oxidized into quinones to further stabilize the noble metal atoms and form nanocomposite materials.[31] Notably, some multivalent transition metal ions with high reduction potentials, such as $Fe^{3+}$, can be reduced in the presence of phenolic compounds. Finally, metalloids, which are prototypical electron-deficient elements, can also accept electrons from the phenolic molecules. However, dynamic covalent bonds (e.g., boronate ester) show more covalent-like than coordination-like properties due to the high electronegativity of metalloids (see (iv) in Figure 1a).

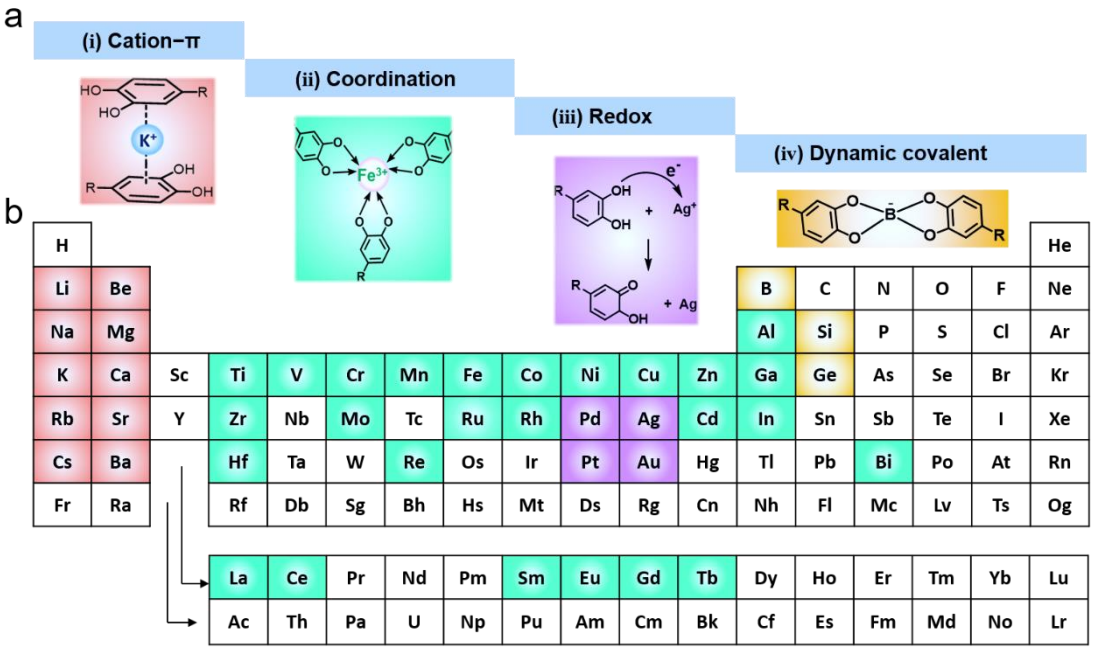


**Figure 1.** (a) Various metal/metalloid–phenolic interactions: (i) Cation–π interactions formed between e.g., $K^+$ and phenolic molecules; (ii) coordination interactions, operating within MPNs formed from e.g., $Fe^{3+}$ and phenolic molecules; (ii) redox interactions, involving the mechanism of redox reaction between e.g., $Ag^+$ and phenolic molecules; and (iv) dynamic covalent interactions involved in e.g., bis-complex formation between borate and phenolic molecules. (b) Periodic table: metal ions highlighted in red form cation–π interactions; metal ions highlighted in green form MPNs via coordination interactions; metal ions highlighted in purple are involved in redox interactions; and metalloid ions highlighted in yellow react with phenolic compounds via dynamic covalent interactions.

### 2.1. Cation–π

In 1996, inspired by cation-binding sites in protein structures, Dougherty and co-workers demonstrated that phenylalanine (Phe), tyrosine (Tyr), and tryptophan with electron-rich π systems could provide potent binding sites for cations (mainly alkali metal ions and alkaline-earth metal ions) to maintain the hierarchical structures of proteins.[21,32] Strong cation–π binding occurs when cations are perpendicular to the plane of the aromatic rings of phenolic compounds. In 2012, cation–π interactions were detected experimentally in the foot proteins from Asian green mussels

for strong underwater adhesion, which led to subsequent studies on cation–π interactions in mussel-inspired phenolic chemistry and the underwater adhesion of marine organisms.[33-35] The prevalent types of cation–π interactions are binary cation–π units and ternary π–cation–π units (Figure 2a). The former type of interaction plays an important role in generating interactions with a surface (e.g., mussel adhesion on rocks). The latter ternary π–cation–π interaction is important for maintaining the cross-linked structures (e.g., cohesion in mussel byssus and protein structures) in biological systems.[36,37] These types of interaction have been extensively studied experimentally via, for example, circular dichroism spectroscopy,[38] ultraviolet–visible (UV–vis) spectroscopy,[38] nuclear magnetic resonance spectroscopy,[39-41] resonance Raman spectroscopy,[42,43] X-ray crystallography.[44] In 2013, for the first time the nanomechanics of cation–π interactions in aqueous media were probed directly using a surface force apparatus (SFA).[45] To date, mechanical techniques, such as SFA and atomic force microscopy (AFM), have become effective approaches to study the influence of various parameters (e.g., hydrated cations, aromatic molecular structures and anion complexation) on the strength of cation–π interactions.[34,42,45-47]

Cation–π interactions are a type of electrostatic force in nature. Thus, the type of aromatic side groups (e.g., hydroxyl group, catechol, PG) with different electron densities can influence the strength of the cation–π interactions (Figure 2b). SFA measurements showed that the adhesion strength between positively charged poly-L-lysine (PLL) and three aromatic polymers followed the order of polytryptophan (PTrp) > polystyrene (PS) > polytyrosine (PTyr).[45] Gebbie et al. reported that the cohesion strength decreased in the order of Phe-rich peptide > Tyr-rich peptide ≈ DOPA-rich peptide.[39] This trend indicates that the presence of a single electronegative hydroxyl group can lead to a pronounced decrease in cation–π-mediated cohesion strength; however, the presence of an additional hydroxyl group only has a marginal additional effect on the strength.

Cation–π interactions are also influenced by the type of metal ions based on studies conducted on alkali metal ions (e.g., $Li^+$, $Na^+$, and $K^+$),[47,48] alkaline-earth metal ions (e.g., $Mg^{2+}$ and $Ca^{2+}$),[49,50] and transition metal ions (e.g., $Ag^+$ and $Cu^{2+}$).[38] In general, cation–π interactions involving alkali and alkaline-earth metal ions are stronger than those that involve transition metal ions.[29] The

experimental "binding" strength of mono-valent cations to PTrp measured by SFA in aqueous solution follows the order $NH_3R^+$, $NH_4^+ > K^+ > Na^+ > Li^+$ (Figure 2c).[45] This implies that although smaller ions (i.e., $Li^+$, $Na^+$) have stronger charge–quadrupole interactions, they have to overcome a higher desolvation energy barrier, which enables larger ions (i.e., $K^+$) to have stronger binding affinities. Understanding the differences of metal ions on cation–π interaction strength can help to provide insights in rationalizing biological assembly and engineering metal–phenolic materials.

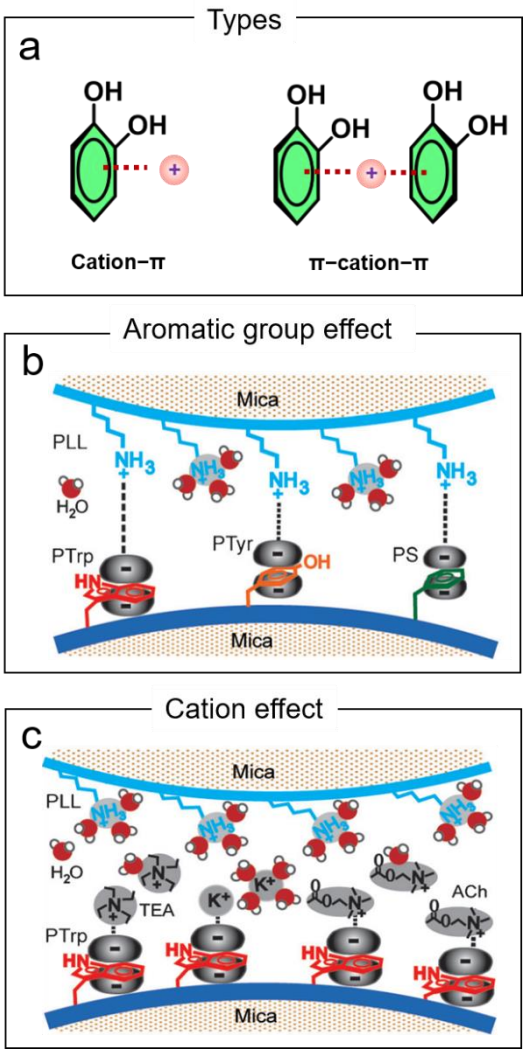


**Figure 2.** (a) Main types of cation–π interactions. Effects of (b) aromatic groups and (c) cations on cation–π interactions. Tetraethylammonium (TEA), nicotinic acetylcholine (Ach). (b, c) Adapted with permission from ref 45. Copyright 2013 Wiley-VCH.

## 2.2. Coordination

Metal–phenolic coordination occurs when two or more phenolic ligands donate a nonbonding electron pair to the empty orbitals of a metal ion. The rich choice of phenolic compounds (synthetic and naturally abundant phenolics, >8000 species)[27,51,52] and metal ions enables the assembly of modular and programmable MPNs, which allows for control over their structures and functionality. One of the features of MPNs is their strong pH dependency.[18] At low pH, mono-complexes form because most of the catechol groups are protonated, whereas bis- and tris-complexes are obtained at high pH (Figure 3).[53] For example, mono-, bis-, and tris-complexes of $Fe^{3+}$ and TA form at pH < 2, 3 < pH < 6, and pH > 7, respectively. These complexes in solution display characteristic ligand-to-metal charge transfer bands at >600, ~565 and ~510 nm, respectively, in their respective UV–vis spectra.[18,54] The stability of MPNs decreases at low pH due to the transition from bis- or tris-complexes to mono-complexes.[18] This pH-dependent coordination chemistry operates in mussels for establishing strong adhesion in the pad and cohesion in the byssus cuticles[23,55] and has been widely used in the design of self-healing materials.[56]

MPNs with different metal ions present different disassembly kinetics.[30] The electronic structure of metal ions also determines the color of MPNs. Multivalent metal ions (e.g., $Fe^{3+}$, $Ti^{4+}$, and $Mn^{2+}$) with partially filled d orbitals form strongly colored MPNs owing to the major contributions from d–d transitions.[57] In contrast, main group metal ions (e.g., $Al^{3+}$, $Ga^{3+}$, and $In^{3+}$) with empty or filled d/f-shells form light-colored MPNs.[57] These specific properties of MPNs provide the potential for engineering materials with different colors.

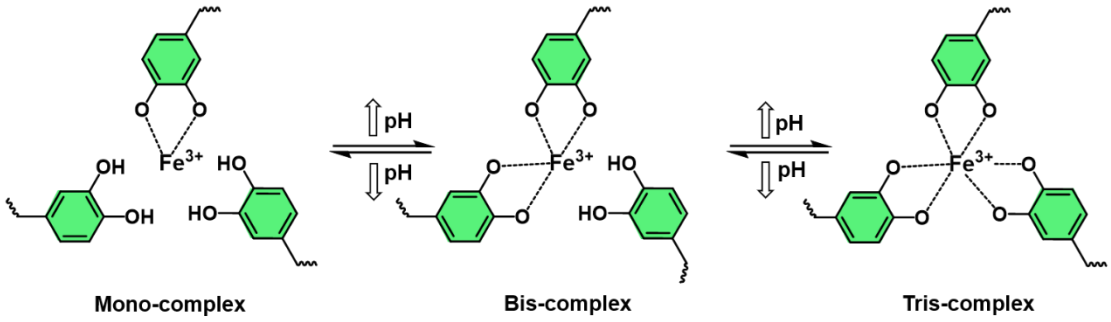

**Figure 3.** pH-dependent coordination of $Fe^{3+}$–catechol complexes. Adapted with permission from ref 53. Copyright 2011 National Academy of Sciences.

### 2.3. Redox

The reduction potentials of the noble metal ions including $Ag^0/Ag^+$, $Au^0/AuCl_4^-$, $Pt^0/PtCl_4^{2-}$, and $Pd^0/Pd^{2+}$ vs normal hydrogen electrode are 0.80, 1.0, 0.76, and 0.92 V, respectively.[58] In contrast, the catechol groups in polydopamine (PDA) and TA have standard electrode potentials of 0.53 and 0.89 V.[58,59] Therefore, the catechol moieties of phenolic molecules can be easily oxidized to the corresponding semiquinone/quinones by these noble metal ions,[58,60] and the noble metal ions are reduced to their metallic form (producing, for example, metal NPs) upon accepting the electrons donated by the phenolic compounds. The oxidized polyphenols can then function as capping agents to stabilize the noble metal NPs (Figure 4).[61-63] As alternatives to surfactants and strong oxidizing agents, phenolics and their derivatives have been used as green and effective chemicals for the in situ synthesis of noble metal NPs. The obtained noble metal NPs can be imaged by electron microscopy and detected experimentally by X-ray photoelectron spectroscopy, X-ray diffraction, energy-dispersive X-ray spectroscopy, and UV–vis spectroscopy in aqueous solution.[64,65] For example, the formation of Ag and Au NPs can be determined from the absorption peak around 420 and 525–560 nm, respectively, by UV–vis spectroscopy.[25,31] The oxidation of the catechol to quinone groups can be detected by UV–vis spectroscopy and Fourier transform infrared spectroscopy. Redox reactions can be monitored by cyclic voltammetry and electron paramagnetic resonance (EPR) analysis.[64,66]

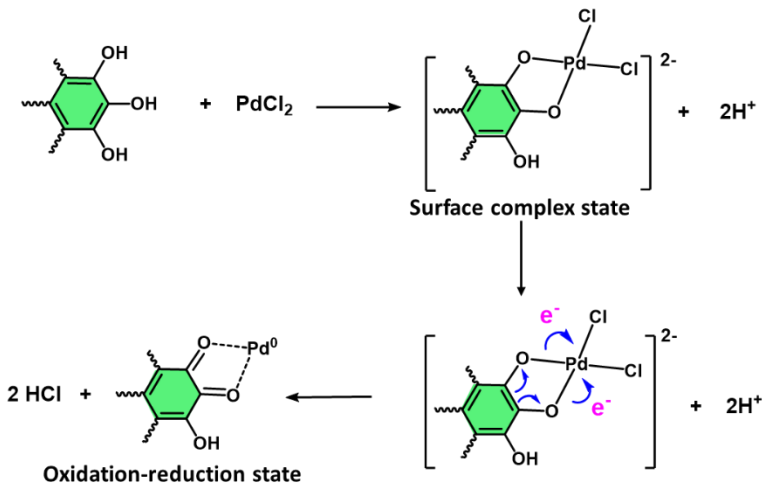


**Figure 4.** Schematic of the mechanism of the oxidation of phenolic molecules by $Pd^{2+}$. Adapted with permission from ref 61. Copyright 2015 Elsevier.

### 2.4. Dynamic Covalent Bonding

Metalloids are a class of chemical elements that present both metallic and nonmetallic physicochemical properties. B, Si, and Ge tend to form covalent bonds with ligands.[67-69] They have a high binding affinity to phenolic compounds, forming covalently cross-linked networks. Boronate–phenolic networks (BPNs) are formed from boronic acid and vicinal diol groups in phenolic molecules, which display a pH-dependent and *cis*-diol responsiveness.[70-72] It is worth noting that only when the surrounding pH is greater than the $pK_a$ values (4.5–10) of the boronic acid motifs, boron can transition from $sp^2$ hybridization to tetrahedral $sp^3$ hybridization and react with *cis*-diol to form cyclic boronate esters (Figure 5a). Thus, boronate covalent bonds are not stable in acidic conditions (when pH < $pK_a$), which impedes their further use under physiological conditions.[73-75] For application in a physiologically relevant pH range, a plethora of boronic acid ligands with adjustable $pK_a$ values, such as inorganic borates,[76] phenylboronic acid-based compounds,[70,75,77,78] boronic acid-conjugated (co)polymers,[79-84] and boron-containing drugs (e.g., bortezomib (BTZ))[82,85-87] have been developed. Incorporating an acidic moiety is another route to tune the pH of boronate–catechol complexation. Addition of acrylic acid (AA) into polymers consisting of dopamine (DA)-methacrylamide and 3-(acrylamido)phenylboronic acid could preserve catechol in its reduced state even at a pH of 8.5, potentially due to the localized buffering

capacity of AA.[88,89] Thus, hydrogels formed from polymers with catechol moieties, boronic acid groups, and carboxylic acid side chains demonstrated strong adhesion to a quartz substrate at a neutral-to-mild basic pH (7.5−8.5).[88]

Recently, there has been growing interest in probing the interactions between phenolics and other metalloids (e.g., Si and Ge).[69,90] Silicate–phenolic networks (SiPNs) were recently examined experimentally by Tiainen and co-workers.[91] Si binds to the vicinal phenolic O of the TA molecule to form a bis-complex (penta-coordinated Si(V) binding two phenolic ligands) and a tris-complex (hexa-coordinated Si(VI) binding three phenolic ligands) (Figure 5b and 5c).[91] Studies have shown that introducing Si NPs into phenolic adhesives can considerably improve the adhesive and mechanical properties of the resulting materials.[92,93] The interactions between germanium and phenolic molecules have been exploited to form germanium–phenolic networks (GePNs). The formation of bidentate Ge–O–C type covalent bonds is key for the formation of GePNs with pentagonal or hexagonal rings.[68,94,95] It is reported that GePN assemblies are also influenced by pH values, Ge/phenol ratio, and the presence of other metal ions.[90]

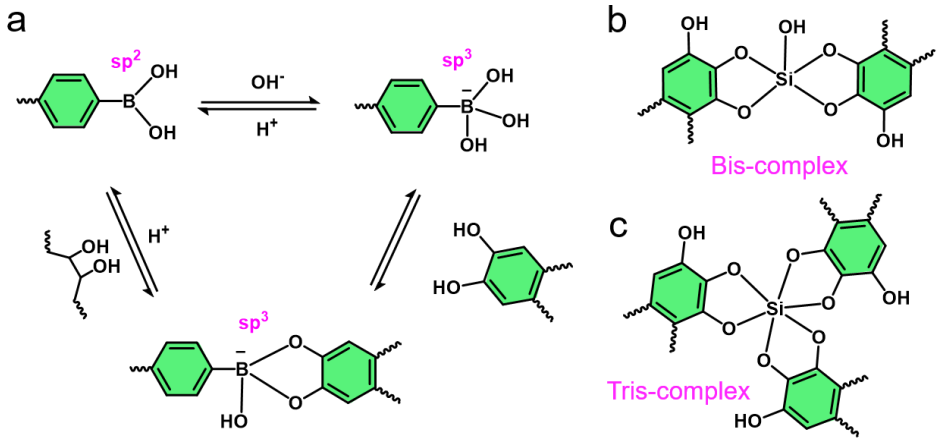


**Figure 5.** (a) Reaction scheme of the formation of boronate–catechol complexes. Schematic illustration of SiPNs forming (b) bis-complex and (c) tris-complex. (b, c) Adapted with permission from ref 91. Copyright 2019 Wiley-VCH.

## 3. Materials Formed via Cation–π Interactions

In the past decade, significant progress has been made in the engineering of various advanced materials driven by cation–π interactions.[96,97] Table 1 summarizes cation–π interaction studies involving different phenolic compounds and metal ions performed during the period 2010–2021. The cation–π interaction-driven functional materials, especially films and complex coacervates, hold potential in underwater adhesion applications.[96]

**Table 1.** Cation–π interactions formed between metal ions and phenolics obtained from experimental studies during 2010–2021.[a]

| Phenolic ligand | Metal ion | Assembled structures | Characterization | Binding energy | Ref. |
|---|---|---|---|---|---|
| Phenol | $Ag^+$, $Cu^+$, $Au^+$ | $Ag^+$–phenol cationic complex | IRMPD, quantum chemical calculations | $Au^+ > Cu^+ > Ag^+$ in gas phase | 98 |
| Phe–Phe dipeptide | $Ba^{2+}$, $Ca^{2+}$, $Li^+$, $Na^+$, $K^+$, $Cs^+$, $Ag^+$ | Cation–π ion cage | IRMPD, density functional theory | $Ca^{2+} > Ba^{2+} > Li^+ > Ag^+ > Na^+ > K^+ > Cs^+$ | 99 |
| mcfp-1 | $K^+$ | Films | SFA | $W_{ad}$ ~2.30 mJ $m^{-2}$, $W_{co}$ ~3.12 mJ $m^{-2}$ (0.2 M salt, pH 3) | 34 |
| PTyr | $Li^+$, $Na^+$, $K^+$ | Films | SFA | $K^+ > Na^+ > Li^+$ | 45 |
| rmfp-1 | $Na^+$ | Coacervates | SFA, UV resonance Raman spectroscopy | $W_{co}$ ~5.0 mJ $m^{-2}$ (0.6 M salt) | 42 |
| PDA | $Na^+$, $K^+$ | Films | UV–vis, XPS | $K^+ > Na^+$ | 48 |
| fp-3F | $Na^+$ | Coacervates | SFA | $SO_4^{2-} > Cl^- > NO_3^-$ (salt type) | 43 |
| PDA | $K^+$ | Films | SFA, UV–vis | | 100 |

| | | | | | |
|---|---|---|---|---|---|
| Poly(catechol) | $Li^+$, $Na^+$, $K^+$ | Films | SFA, XPS, AFM | $K^+ > Na^+ > Li^+$ | 36 |
| Tyr-rich peptide, DOPA-rich peptide | $K^+$ | Films | SFA | Tyr-rich peptide > DOPA-rich peptide (cohesion) | 101 |
| Poly($PO_4$-DHB) | $Li^+$, $Na^+$, $K^+$ | Films | SFA | Cation–π facilitated anion–π interactions | 102 |
| Lignin | $Na^+$, $K^+$ | Films | SPA | $K^+ > Na^+$ | 103 |

[a]Abbreviations: *Mytilus californianus* foot protein-1 (mcfp-1); polytyrosine (PTyr); recombinant mussel foot protein-1 (rmfp-1); foot protein type-3 fast variant (fp-3F); polydopamine (PDA); 2-*O*-phosphorylethanol 2,3-hydroxybenzamide ($PO_4$-DHB); infrared multiple photon dissociation (IRMPD); X-ray photoelectron spectroscopy (XPS); work of adhesion energy per unit area for the asymmetric configuration ($W_{ad}$); work of adhesion energy per unit area for the symmetric configuration ($W_{co}$).

### 3.1. Films

Cation–π interactions exhibit attractive short-range forces and therefore ternary π–cation–π units play an important role in film engineering. For example, the adhesion force measured in SFA experiments of poly(catechol) films is ~0.68 mN $m^{-1}$, which increases to ~1.32, ~4.42, ~11.44, ~23.75 mN $m^{-1}$, respectively, when the concentration of $K^+$ in buffer aqueous solutions is 10, 50, 100, 250 mM.[36] The $K^+$ can simultaneously interact with two π-conjugated groups on different poly(catechol) moieties through ternary π–cation–π interactions, hence enhancing the adhesion through physical bridging (Figure 6a). With gradual increase in the $K^+$ concentration to 250 mM, the aggregate size increased, which resulted in rough coatings with a surface roughness of ~3.32 nm (Figure 6b). Interestingly, when the $K^+$ concentration increases from 250 to 600 mM, the adhesion decreases to ~5.23 mN $m^{-1}$.[36] This decrease is attributed to the presence of excess of $K^+$ that could disrupt π–$K^+$–π complexes into binary $K^+$–π binding pairs, leading to the formation of smaller aggregates and smooth coatings with a surface roughness of ~1.2 nm at 600 mM $K^+$ (Figure 6c and 6d). Moreover, the adhesion strength and surface roughness of poly(catechol) coatings is enhanced in the presence of $Li^+$ or $Na^+$ at 250 mM.[36] In another example, PDA films delaminate from polyurethane substrates upon sodium hydroxide treatment due to the deprotonation of amine

groups. Owing to the larger binding force of the $K^+$–π interaction compared to the $Na^+$–π interaction, the disassembled PDA films in alkaline conditions re-assemble by adding $K^+$.[48] The thickness of the PDA films increased with an increase in the concentration of $K^+$ (green bars) and is similar to that before disassembly (blue bar) by adding 100 mM $K^+$. Moreover, the roughness and water contact angles of the $K^+$-mediated PDA films are controlled by the concentration of $K^+$, where the ionic intervention between PDA molecules results in hydrophilic surfaces. [48]

An increasing number of studies have shown that phenolic coatings or MPNs are formed under high ionic strength conditions.[104-107] Although the role of cation–π interactions was not examined in the studies, monovalent cations play an important role in controlling the final thickness and morphology of the phenolic films. Thus, the co-existence of alkali metal ions and phenolic molecules to form cation–π interactions is a potential factor for realizing material-independent surface coatings.

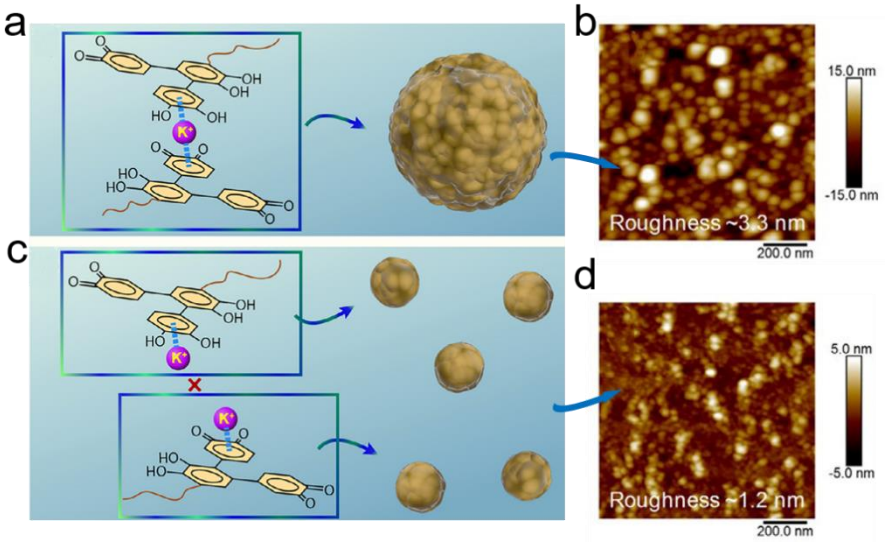


**Figure 6.** Schematic illustrations of (a) ternary π–cation–π complex promoting the assembly of larger poly(catechol) aggregates and (c) binary cation–π binding pairs induced by excess $K^+$ leading to smaller poly(catechol) aggregates. AFM images of poly(catechol) films after deposition in poly(catechol) solutions containing (b) 250 and (d) 600 mM $K^+$. Adapted with permission from ref 36. Copyright 2020 Elsevier.

### 3.2. Coacervates

Coacervates, an emerging class of soft materials, have attracted considerable interest owing to their implications for engineering lubricants and underwater adhesives.[40,41,108,109] Coacervates formed from charged polyanionic and polycationic protein species have been thoroughly studied.[110-112] Recently, coacervation driven by short-range cation–π interactions has been a focus of attention.[42,43,113] Recombinant mussel foot protein-1 (rmfp-1; 12 repetitions of the foot protein-1 decapeptide) has numerous cationic and phenolic groups, with no negatively charged residues (Figure 7a). rmfp-1 forms only finite complexes in the absence of $Na^+$, which may be triggered by the longer-ranged electrostatic repulsion between positively charged residues (e.g., $–NH_3^+$ of Lys) in rmfp-1 (Figure 7b). By increasing the concentration of $Na^+$ to a level equivalent to that in seawater (~0.7 M), infinite complexes of rmfp-1 formed into the coacervate phase (Figure 7c).[42] This is attributed to the screening of the electrostatic forces in rmfp-1 and the increasing prominence of cation–π interactions with increasing concentration of $Na^+$. The formation of mussel foot protein type-3 fast variant (fp-3F)-based coacervates was observed in salt-containing buffers but not in an acetic acid/acetate buffer, indicating the importance of salts to coacervation.[43] Besides, mussel foot protein-3S (mfp-3S) was triggered to form adhesive coacervates by liquid–liquid phase separation from equilibrium solution at a suitable pH and ionic strength.[46] Those phenomena are attributed to the high concentration of salts that can screen the longer-ranged electrostatic repulsion in the charged polymers. In contrast, the short-ranged cation–π interactions remain unaffected, resulting in macroscopic phase separation. Salt-triggered coacervation is a facile approach to develop high-performance coacervates, which have promising applications in lubricants and underwater adhesives.

The importance of cation–π interactions in attaining control over coacervation has been widely demonstrated. However, the development of synthetic metal–phenolic materials driven by cation–π interactions in bulk hydrogels or freestanding films is of considerable interest but remains a challenge. Moreover, the assembly mechanisms, for example, the effect of cations or substituents on cation–π assembly, are yet to be studied theoretically and experimentally.

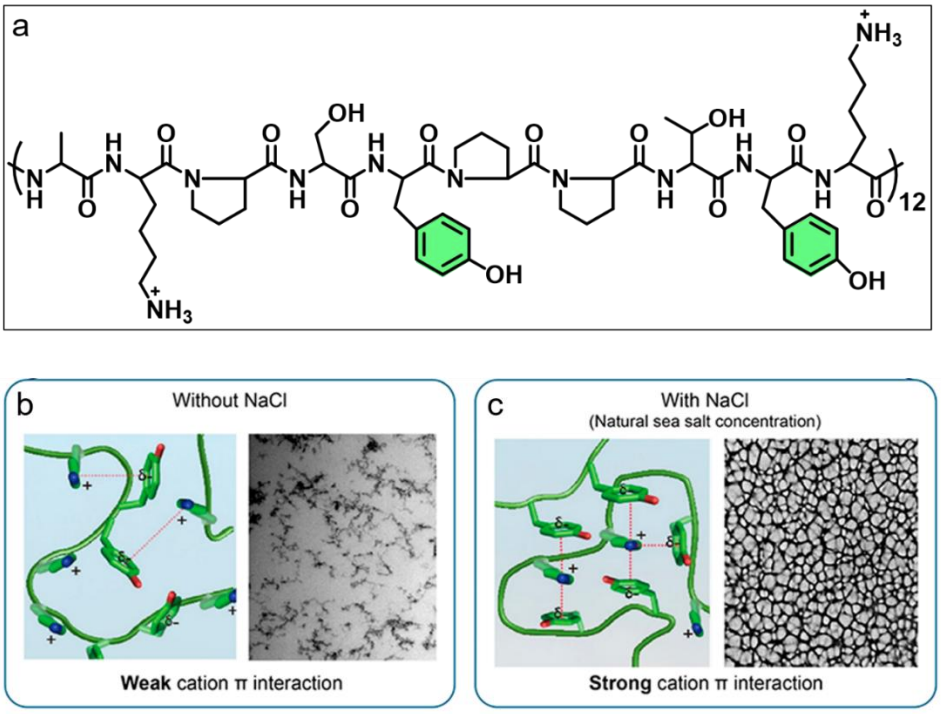


**Figure 7.** (a) Decapeptide sequence of rmfp-1. Schematics and cryogenic transmission electron microscope (cryo-TEM) images of (b) finite complexes of rmfp-1 in the absence of $Na^+$ and (c) dense coacervates formed by rmfp-1 and $Na^+$. (b, c) Adapted with permission from ref 42. Copyright 2017 American Chemical Society.

## 4. Materials Formed via Coordination Interactions

MPNs have emerged as a versatile platform to engineer various functional materials, and present many advantages, as illustrated in Figure 8. First, various phenolic ligands and metal ions used in MPN assembly allow for the facile generation of diverse materials with specific physiochemical properties.[27] Second, the phenolic moieties can generate diverse interactions with different molecules and substrates,[27] including hydrogen bonding (with poly(ethylene glycol) (PEG), as an example),[114] metal coordination (with $Fe^{3+}$ ions),[115] π–π interaction (with graphene oxide),[116] and hydrophobic interactions (with aliphatic side chains).[117] Thus, MPNs have been assembled into a range of materials, including NPs,[118] capsules,[119] conformal coatings,[120] and freestanding films.[24] Third, the dynamic coordination bonds between the metal ions and phenolic moieties can be broken and restored through various stimuli (e.g., pH and ionic strength), endowing MPN-based

materials with tunable permeability,[121] high toughness,[122] and self-healing properties.[123] Furthermore, owing to the hybrid and synergistic physicochemical properties imparted by the metal ions and phenolics, MPNs have potential in engineering materials with photothermal,[124] antioxidative,[125] and highly biocompatible properties,[18] with potential application in diverse fields ranging from confined catalysts,[126] underwater adhesives,[127,128] flexible electronics,[129,130] artificial cells,[131] separation membranes,[132,133] drug delivery[134] to soft actuators.[135]

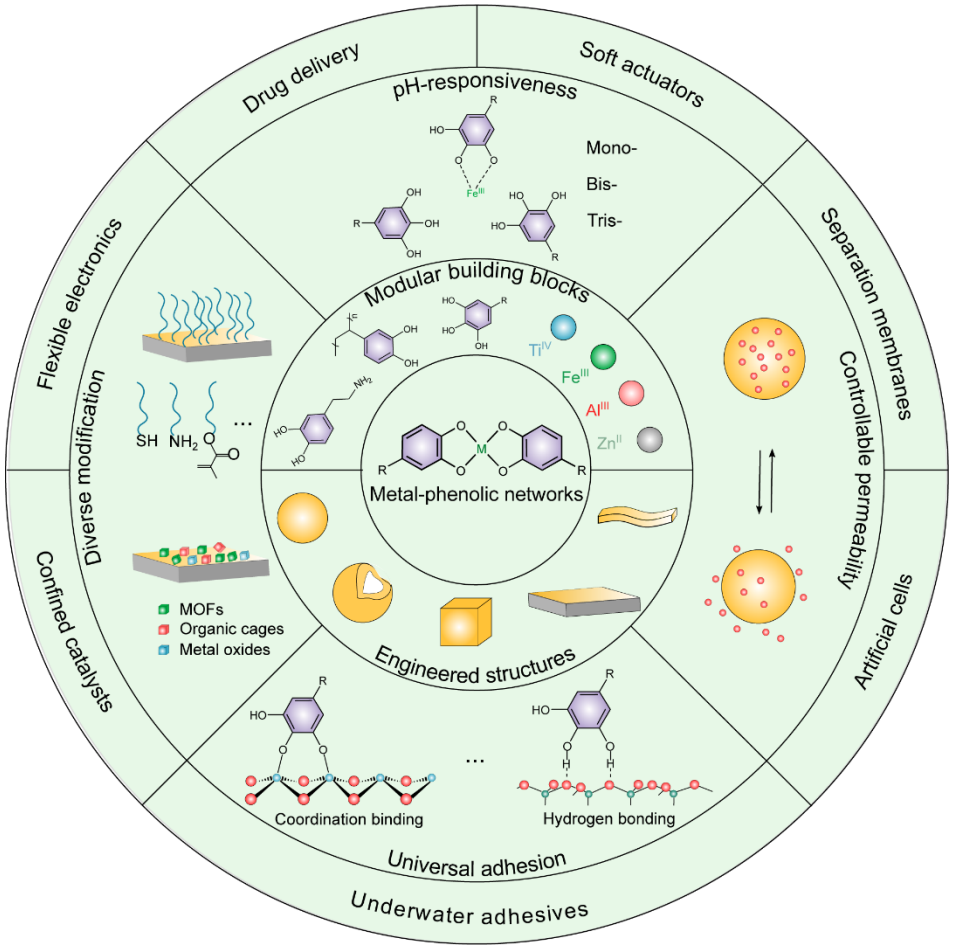


**Figure 8.** Overview of building blocks employed in the synthesis of MPN-based materials and a selection of the structures, properties, and potential applications of MPN-based materials.

Over the last decade, especially since the pioneering work of Caruso and co-workers in 2013,[18] significant progress has been achieved in MPN-based materials relating to the building blocks employed in their synthesis, and their preparation methods and potential applications. Figure 9 illustrates representative studies that highlight progress and breakthroughs in those areas: (i) the

choice of available building blocks has been expanded from natural to synthetic phenolic compounds, including monophenol-containing molecules; (ii) various methods are exploited to endow MPN-based materials with well-defined, hierarchal structures (e.g., mesoporous particles and hollow superstructured particles); and (iii) diverse applications have been explored from mussel-inspired byssus to environmental remediation, energy storage, and cancer therapy.

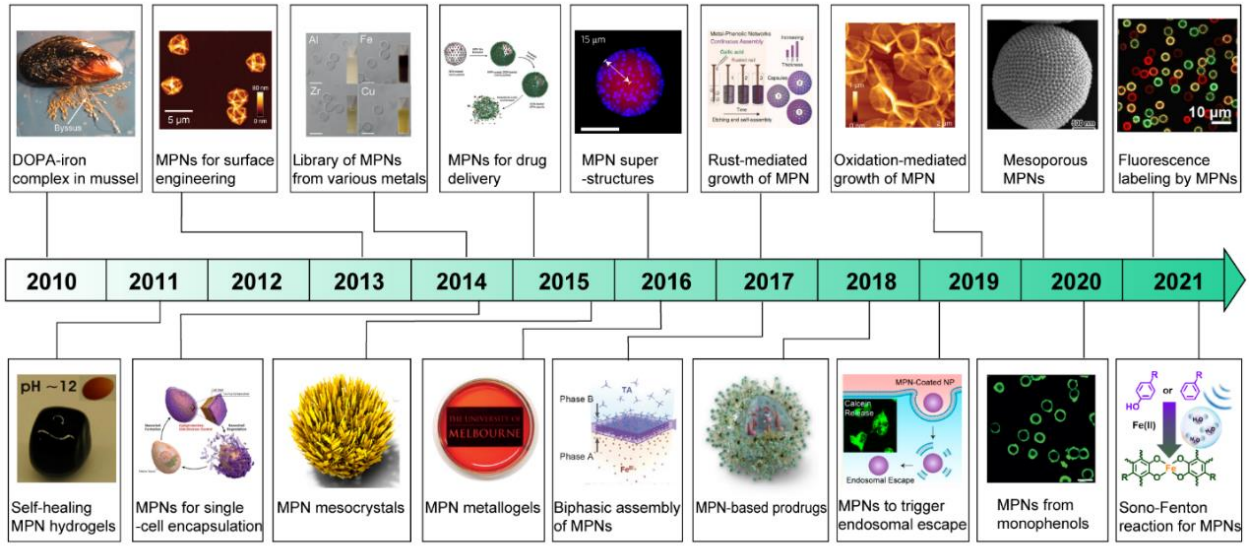


**Figure 9.** Timeline illustrating the progress achieved to date, including the building blocks employed during synthesis, assembly methods, material structures, and potential applications toward the development of MPN-based materials. Adapted with permission from the following references: Ref 23. Copyright 2010 The American Association for the Advancement of Science; Ref 53. Copyright 2011 National Academy of Sciences; Ref 18. Copyright 2013 The American Association for the Advancement of Science; Ref 30. Copyright 2014 Wiley-VCH; Ref 136. Copyright 2014 Wiley-VCH; Ref 137. Copyright 2015 Wiley-VCH; Ref 138. Copyright 2015 American Chemical Society; Ref 139. Copyright 2016 Wiley-VCH; Ref 140. Copyright 2016 Springer Nature; Ref 141. Copyright 2017 Wiley-VCH; Ref 142. Copyright 2017 Wiley-VCH; Ref 143. Copyright 2018 Wiley-VCH; Ref 144. Copyright 2019 Wiley-VCH; Ref 145. Copyright 2019 American Chemical Society; Ref 146. Copyright 2020 Wiley-VCH; Ref 147. Copyright 2020

American Chemical Society; Ref 148. Copyright 2021 Wiley-VCH; Ref 149. Copyright 2021 Wiley-VCH.

### 4.1. Films

Phenolic compounds tend to exhibit high adhesion to different substrates[150,151] and coordinate with metal ions for cross-linking. Therefore, MPNs have been widely used to fabricate substrate-independent thin films and coatings.[18,149] Due to the heterogeneous structures of polyphenols and the random complexation, most MPN films are amorphous. To this date, various naturally occurring polyphenols (Figure 10a) have been used to engineer MPNs with desired properties, including TA,[18] epigallocatechin-3-*O*-gallate (EGCG, as an anticancer drug),[152,153] and flavonoids (e.g., myricetin as a scavenger of reactive oxygen species (ROS)).[125] Besides natural polyphenols, catechol moieties can be conjugated to other molecules (Figure 10b), such as PEG[154] and hyaluronic acid,[155] to synthesize functional compounds. For instance, PEG-polyphenol was synthesized by conjugating catechol groups to the termini of a branched PEG and subsequently chelated to $Fe^{3+}$. Compared with $Fe^{3+}$–TA capsules, the $Fe^{3+}$–PEG-polyphenol capsules exhibited reduced nonspecific protein adsorption and more rapid disassembly at pH 5.[154] Additionally, an enzyme-mediated strategy was developed to convert monophenol moieties into catechol moieties, resulting in a range of monophenol-containing molecules (Figure 10c), including small molecules (e.g., Tyr), peptides (e.g., poly(4-vinylphenol)), and proteins (e.g., trypsin), that were used as building blocks for MPN film synthesis.[146] Recently it was demonstrated that the application of high-frequency ultrasound and the Fenton reaction synergistically convert phenol and phenyl derivatives into polyphenols for engineering MPNs.[148] The assembly process is initiated by acoustic cavitation-induced hydroxyl radicals (•OH) from water using high frequency ultrasound (412 kHz). The metal ions (e.g., $Fe^{2+}$, $Fe^{3+}$, $Cu^{2+}$, and $Co^{2+}$) can accelerate the generation of •OH via Fenton reactions to induce the hydroxylation/phenolation of phenol- and phenyl-based molecules and coordinate with the resultant polyphenols for film formation. These methods unlock numerous opportunities for exploring metal–phenolic materials with functional phenol- and phenyl-containing molecules.

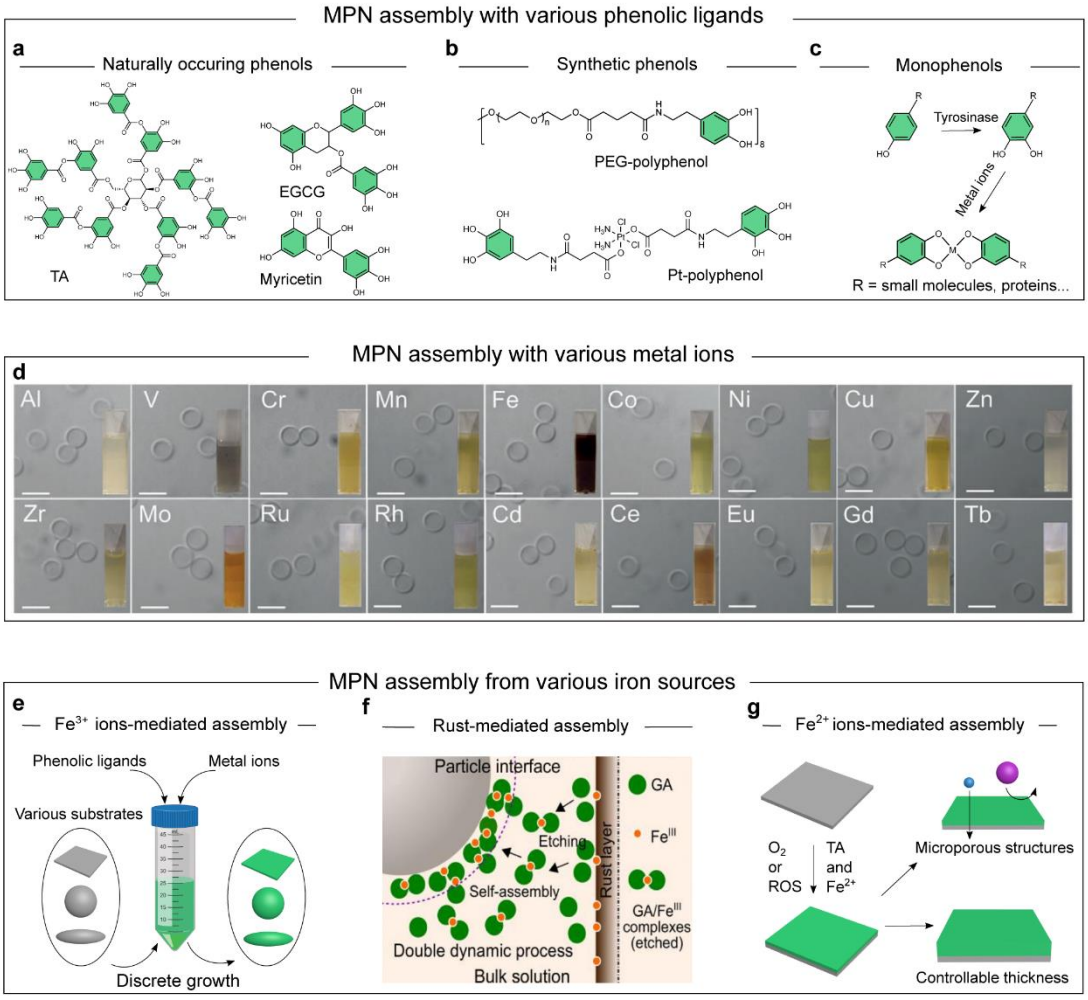


**Figure 10.** Examples of (a) naturally occurring, (b) synthetic, and (c) monophenol-containing phenols that are used for engineering MPN films and coatings. (d) Library of metal ions used for constructing MPN films. Scale bars are 5 μm. (e) Discrete growth of MPN films using phenolic ligands and $Fe^{3+}$ ions. Continuous growth of MPN films using (f) rust and (g) $Fe^{2+}$ ions as iron sources. (d) Adapted with permission from ref 30. Copyright 2014 Wiley-VCH. (e) Adapted with permission from ref 18. Copyright 2013 The American Association for the Advancement of Science. (f) Adapted with permission from ref 141. Copyright 2017 Wiley-VCH. (g) Adapted with permission from ref 144. Copyright 2019 Wiley-VCH.

The incorporation of different metal ions further expands the toolbox of building blocks for MPN film fabrication. Eighteen metal ions, including $Al^{3+}$, $V^{3+}$, $Cr^{3+}$, $Mn^{2+}$, $Fe^{3+}$, $Co^{2+}$, $Ni^{2+}$, $Cu^{2+}$, $Zn^{2+}$,

$Zr^{4+}$, $Mo^{2+}$, $Ru^{3+}$, $Rh^{3+}$, $Cd^{2+}$, $Ce^{3+}$, $Eu^{2+}$, $Gd^{3+}$, and $Tb^{3+}$, were demonstrated to coordinate with TA and assemble into thin films (i.e., capsules) with metal-specific properties (Figure 10d).[30] In particular, the use of $Fe^{3+}$, $Mn^{2+}$, and $Gd^{3+}$ endows MPNs with magnetic resonance imaging (MRI) properties, the use of $Tb^{3+}$ and $Eu^{2+}$ affords fluorescence imaging properties, and the use of $Cu^{2+}$ affords positron emission tomography (PET) imaging properties. In addition to obtaining MPN films with multiple functionalities, chelation with different metal ions fundamentally changes the pH response and Young's modulus ($E_Y$) of the resultant films. For example, films prepared from TA and $Zr^{4+}$, $Cu^{2+}$, or $Al^{3+}$ displayed different disassembly rates in the pH range of 5.0–7.4.[30] At pH 7.4, the $Zr^{4+}$–TA film showed negligible degradation even after incubation for 7 days, whereas ~40% of $Al^{3+}$–TA and ~80% of $Cu^{2+}$–TA films disassembled. In contrast, ~25% of $Cu^{2+}$–TA, $Al^{3+}$–TA, and $Zr^{4+}$–TA MPN capsules disassembled within 1, 6, and 168 h at pH 5.0.[30] The $Zr^{4+}$–TA film displayed the slowest disassembly rate, whereas the $Al^{3+}$–TA film showed intermediate disassembly properties, making them suitable vehicles for intracellular drug delivery.[137] The $Cu^{2+}$–TA and $Sr^{2+}$–TA films were more sensitive to the pH changes compared to the $Zr^{4+}$–TA and $Al^{3+}$–TA films.[30,156] The $Mn^{2+}$–TA films coated on rapamycin-formed NPs disassembled in a sustainable manner at pH 7.4, leading to rapamycin release of 55% over 48 h and 70% within 4 h at pH 5.5.[157] For the $Fe^{3+}$–TA films, it took about 4 h and 6 days to disassemble at pH 3.0 and 4.0, respectively. About ~70 and 90% of the $Fe^{3+}$–TA films still remained intact until 10 days at pH 5.0 and pH 7.4, respectively.[18] $Fe^{3+}$–TA films showed high stability under physiological conditions, which is due to the ionic radius of $Fe^{3+}$, which can form an octahedral complex with three catechol moieties.[158] MPN films prepared from TA and $Tb^{3+}$, $In^{3+}$, $Ga^{3+}$, or $Fe^{3+}$ displayed different $E_Y$ values: 21.9 ± 7.3 GPa for $Tb^{3+}$–TA, 5.9 ± 1.5 GPa for $In^{3+}$–TA, 5.9 ± 1.9 GPa for $Ga^{3+}$–TA, and 2.9 ± 1.0 GPa for $Fe^{3+}$–TA films.[158] Recently, MPN films self-assembled from $Fe^{3+}$, $Co^{2+}$, $Ni^{2+}$, and $Zn^{2+}$ ions were shown to exhibit varying binding affinities to antibodies. The $Co^{2+}$ system exhibited more than a 2-fold greater association than the other metal ion systems studied. The greater association of the $Co^{2+}$ MPN system is attributed to the coordination of $Co^{2+}$ to the histidine-rich portion of the antibody fragment, as revealed by molecular dynamics simulations.[159]

The state (solid or free ions), valence, and aggregation of metal ions can significantly influence the structures of the MPN films formed in terms of thickness and pore size.[141,144,160] Previous studies, where $Fe^{3+}$ ions were used as an iron source (Figure 10e), demonstrated the rapid termination of MPN film assembly within several minutes, resulting in a final film thickness of ~10 nm, independent of the ligand or assembly conditions used.[18] Such discrete assembly is possibly caused by kinetic trapping of the metal–phenolic complexes and symmetry breaking at the interface.[160] Recently, several methods, including rust-mediated (Figure 10f),[141] oxygen-mediated (Figure 10g),[24,144] and electro-triggered assembly approaches,[161] have been employed to circumvent this issue by enhancing the reversibility and self-correction of the iron–catechol bonding. When $Fe^{2+}$ ions were used as an iron source (Figure 10g), the low stability constant of $Fe^{2+}$–catechol (log $K_1$ = 8) allowed for increased reversibility,[24] and the relatively low concentration of free $Fe^{3+}$–TA complexes provided additional opportunities for conformational rearrangement and the self-correction of defects. As a result, MPN films can grow continuously with a thickness of up to ~2.5 μm at the water and air interface.[24] Moreover, as opposed to films obtained by the discrete assembly method, which showed pores larger than 6 nm, the oxygen-mediated strategy allowed for the formation of microporous MPN films with pores smaller than 1.7 nm.[144] Rust iron objects (solid-state iron source) can also afford the continuous growth of TA and GA films. Although the iron source is shown to strongly influence the structures of the MPN films formed, several questions related to the mechanisms remain unanswered. Specifically, (i) are there any common mechanisms (e.g., assembly kinetics)[106,162,163] between the rust-mediated (dissolution of solid rust to soluble $Fe^{3+}$ ions) and oxygen-mediated (oxidation of $Fe^{2+}$ to $Fe^{3+}$) methods that lead to the continuous growth of MPNs? and (ii) do the water molecules or μ-oxo species play a role in the coordination process and the resultant properties of the films?[164] Addressing the latter question will help gain a more detailed understanding of the coordination structures of $Fe^{3+}$–TA at the molecular level (bis- or tris- as the dominant coordination state).

Additionally, various other fabrication techniques, including layer-by-layer assembly,[165] spray coating,[54,166] mechanochemistry,[167] and biphasic assembly,[142] have been developed to endow MPN films with specific structures and properties.

Two-dimensional (2D) MPNs with crystalline structures have shown specific properties in electronics, sensing, and energy.[168,169] Generally, the metal ions that have been examined for the engineering of 2D MPNs include $Cu^{2+}$, $Co^{2+}$, and $Zn^{2+}$. Unlike the soft and asymmetric catechol-containing ligands (e.g., TA) that are used for preparing amorphous MPN films, rigid and symmetric phenolic ligands with a planar configuration, such as 2,3-dihydroxy-1,4-benzenedicarboxylic acid, hexahydroxybenzene (HHB), and 2,3,6,7,10,11-hexahydroxytriphenylene (HHTP), are necessary for the assembly and preparation of these 2D crystalline structures. A facile method that is used for constructing such films is surfactant-assisted assembly,[170] wherein the surfactants (e.g., sodium dodecyl sulfate) form a monolayer on the water surface, and the organic ligands adsorb and subsequently self-assemble under the surfactant monolayer. Metal ions (e.g., $Cu^{2+}$) subsequently cross-link the ligands and stabilize the 2D films.[171] Using this strategy, various nanofilms with well-defined structures were prepared, including $Cu^{2+}$–HHB (~8–10 layers of a single molecular layer), $Ni^{2+}$–HHB, and $Cu^{2+}$–HHTP (~10 layers) films.[172] Compared with the bulk MPN-based materials, such crystalline MPN films showed excellent performance in electronics owing to their high electrical conductivity, their well-defined porous structures, and the presence of more active sites on the films.[172,173]

### 4.2. Particles

Owing to the high chelation ability of multivalent metal ions to phenolic compounds, diverse MPN-based particulate nanostructures have been engineered, including particles (i.e., amorphous and crystalline MPN particles) and capsules. The phenolic building blocks that have been used are similar to those used for the preparation of thin films discussed in Section 4.1. The incorporation of metal ions can not only endow MPN nanostructures with distinct properties, including mechanical, electronic, magnetic, and optical properties, but also produces novel structures, including core–satellite and hollow superstructures.[134,140,174-176]

Amorphous MPN particles can be prepared by mixing, for example, TA and $Fe^{3+}$ in weak alkaline solutions in the absence of templates (Table 2). The $Fe^{3+}$–TA NPs were ~5 nm in diameter and could cause autophagic cell death by forming autophagosomes.[118] Through the chelation of $Fe^{3+}$ ions to polyphenol-modified anticancer drugs, various MPN-based prodrugs can be prepared. For example, Dai et al. reported the synthesis of Pt-PEG prodrug NPs (~100 nm in diameter) through metal–polyphenol complexation using an emulsification method. Water-in-oil nanoemulsions were formed by mixing a complexed solution of $Fe^{3+}$, Pt prodrug-polyphenols, and PEG-polyphenols with an oil phase, which were stabilized by another nanoemulsion containing Tris buffer to raise the pH.[177] The MPN-based particles could incorporate other functional molecules such as a photosensitizer (e.g., chlorin e6)[178] or an enzyme (e.g., myeloperoxidase)[179] for anticancer therapy. In another study, MPN particles were obtained by mixing poly(L-glutamic acid)-*graft*-methoxypoly(ethylene glycol), $Fe^{3+}$, and anthocyanins in solution in the absence of a template. The prepared NPs were ~70 nm in diameter and stable in various solutions and environments (e.g., 60 °C).[180] The hydrophobic drugs (i.e., anthocyanins), as the particle nuclei, enabled the growth of the MPN particles to the desired size.

Another class of MPN particles are formed by doping specific metal ions into preformed phenolic networks (Table 2). Such particles typically exploit covalent interactions to form the primary networks, and the added metal ions form the secondary networks via coordination interactions with the primary networks. Wei et al. demonstrated the synthesis of such MPN particles, where the phenolic oligomers chelated with a range of metals to form mono-metal ($Co^{2+}$, $Ni^{2+}$, $Cu^{2+}$, $Zn^{2+}$, $Fe^{3+}$, $Al^{3+}$, or $Ce^{3+}$), bi-metal ($Fe^{3+}/Co^{2+}$ and $Co^{2+}/Zn^{2+}$), and multimetal ($Fe^{3+}/Co^{2+}/Ni^{2+}/Cu^{2+}/Zn^{2+}$) particles. The resultant MPN particles showed potential as biosensors for the analysis of nucleic acid variants.[181]

Crystalline MPN particles have also been synthesized and reported. The phenolic ligands that have been explored include GA, ellagic acid (EA), tetrahydroxybenzoquinone, and HHTP (Table 2), and the investigated metal ions include $K^{+}$, $Na^{+}$, $Fe^{3+}$, $Fe^{2+}$, $Zn^{2+}$, $Mg^{2+}$, $Mn^{2+}$, $Co^{2+}$, $Bi^{3+}$, $Ni^{2+}$, $Cu^{2+}$, $Zr^{4+}$, $Ti^{4+}$, and $V^{4+}$.[138,182-188] For instance, $Bi^{3+}$ can chelate with EA to form hierarchical

mesocrystals with ordered quaternary structure in a spatiotemporally controlled manner.[189] $Bi^{3+}$–EA complexes driven by coordination interactions organized into secondary supramolecular threads via π–π interactions that further assembled into tertiary nanoscale filaments through dipole–dipole forces, and finally packing into quaternary mesocrystals.[189] Owing to the high $pK_a$ of the $Bi^{3+}$–catechol bonds, the resulting microporous $Bi^{3+}$–EA particles exhibited high chemical stability over a wide pH range (i.e., 2–14), harsh hydrothermal conditions, and organic solvents.[183] Although the field of crystalline MPN particles is in its infancy, crystalline metal–phenolic complexes are expected to broaden the properties of existing MOFs as they (i) are often highly biocompatible and bioactive; (ii) can be extracted from plant-based materials that are often considered as waste, such as tree barks and fruit peels; (iii) can act as rigid spacers between cations, contributing to the porosity of the resulting framework; (iv) and can have a high proton conductivity owing to the mixed oxidation states of metal ions.

**Table 2.** Summary of MPN particles.[a]

| Particle type | Metal ion | Phenolic ligand | Application | Comment | Ref. |
|---|---|---|---|---|---|
| Amorphous | $Fe^{2+}$ | GA | Glioblastoma therapy | Co-assembly with PVP | 190 |
| | $Fe^{3+}$ | CP | | Formation of protein-responsive assemblies | 191 |
| | $Fe^{3+}$ | Pt-polyphenol, PEG-polyphenol | Cancer therapy | | 177 |
| | $Fe^{3+}$ | TA | MRI contrast (in liver cell lines) | | 118 |
| | $Mn^{2+}$, $Fe^{3+}$, $Zn^{2+}$, $Co^{2+}$, $Ni^{2+}$, $Cu^{2+}$, $Ce^{3+}$ | TA | Sensors and electrode precursors | | 181 |

| | | | | | |
|---|---|---|---|---|---|
| | $Fe^{3+}$ | TA, catechin, EGCG, procyanidin | Cancer therapy | Co-assembly with bortezomib | 192 |
| | $Fe^{3+}$ | Anthocyanins | Cancer therapy | | 180 |
| | $Fe^{3+}$ | TA | Cancer therapy | Co-assembly with PLG-*g*-mPEG | 193 |
| | $VO_3^-$ | TA | Synergistic chemodynamic/photothermal therapy | Formation of nanoenzymes | 186 |
| | $Fe^{3+}$ | TA | Multimodal imaging-guided tumor-specific therapy | Co-assembly with protoporphyrin IX | 194 |
| | $Fe^{2+}$ | DA | Immunogenic cancer therapy | Co-assembly with PEG, Ce6, gossypol | 178 |
| | $Zn^{2+}$ | TA | Sepsis therapy | Co-assembly with gentamicin | 195 |
| | $Sm^{3+}$ | EGCG | Metastatic melanoma therapy | | 134 |
| Crystalline | $Mn^{2+}$, $Zn^{2+}$, $Fe^{3+}$ | EA | Photothermal therapy | Co-assembly with PVP | 196 |
| | $Zn^{2+}$ | EA | | Formation of mesocrystalline microparticles | 138 |
| | $Bi^{3+}$ | EA | | Green MOF particles | 183 |
| | $Bi^{3+}$ | EA | Energy storage devices (sodium ion batteries) | Formation of superstructured mesocrystals | 189 |
| | $Fe^{2+}$, $Co^{2+}$, $Mn^{2+}$ | THBQ | | Paramagnetic conducting MOFs | 197 |
| | $Cu^{2+}$ | HHB | | Formation of conductive MOFs | 173 |

| | | | | |
|---|---|---|---|---|
| | $Ti^{4+}$, $Fe^{3+}$, $V^{3+}$, $Fe^{2+}$ | HHTP | MOF particles with high proton conductivity | 184 |
| | $Fe^{3+}$ | GA | Formation of MOF particles | 198 |

[a]Abbreviations: Catechol-modified polymers (CP); tetrahydroxybenzoquinone (THBQ); poly(L-glutamic acid)-*graft*-methoxypoly(ethylene glycol) (PLG-*g*-mPEG); chlorin e6 (Ce6); polyvinylpyrrolidone (PVP); dopamine (DA).

When phenolics were used to coat MOF particles, an acidic solution of phenolic molecules (e.g., TA, GA) could etch the MOFs, resulting in the release free of metal ions,[199,200] which progressively coordinated with the surrounding phenolic molecules owing to the high affinity between catechol groups and metal ions.[201] The synergetic etching and coordination provides an opportunity to fabricate diverse nanostructures, including core–shell particles, hollow cages, and multishell particles. Although these MPN–MOF structures show desirable properties and functions for various applications, such as catalysis and drug delivery,[199,201] a more complete understanding of the mechanism of the etching process could provide insights into the chemistry of MPN coordination while unlocking the potential uses of MPNs in the field of fine chemicals, for instance as pharmaceutical crystals.[202,203]

To broaden the scope of MPN particles in various fields, hollow MPN particles (i.e., capsules) with tunable cavity and shell thickness have been engineered.[18] The preparation of capsules typically involves two stages: (i) film formation on particle templates and (ii) subsequent removal of the templates. The assembly details for MPN capsules have been reviewed.[19,204-206] Such structures have afforded the incorporation of higher amounts and diverse types of cargos, as relevant in the drug delivery field.[207] For instance, indocyanine green (ICG, a photosensitizer) was encapsulated into the pores of ZIF-8 NPs, after which a $Fe^{3+}$–TA shell was grown on the surface of the NPs. Removal of the ZIF-8 NPs resulted in ICG@$Fe^{3+}$–TA capsules that displayed photo/chemodynamic properties that are useful for cancer therapy.[200] MPN capsules were also applied as cell-mimic microreactors. Owing to the dynamic bonding of MPN capsules, the shell could function as a gate to cargos of different sizes.[131] In Table 3, we summarize the metal ions

and phenolic ligands used in the synthesis of core–shell particles and capsules and their associated application as a result of the properties conferred by the metal ions and phenolic ligands.

**Table 3.** Summary of MPN Core–Shell Particles and Capsules.[a]

| Type | Metal ion | Phenolic ligand | Template | Application | Comment | Ref. |
|---|---|---|---|---|---|---|
| Core–shell particles | $Fe^{3+}$ | TA | Paclitaxel nanocore | Cancer therapy | | 208 |
| | $Fe^{3+}$ | TA | HeLa, NIH 3T3 fibroblast, Jurkat cells | Cytoprotective coating | | 209 |
| | $Fe^{3+}$ | TA | Yeast cells, *E. coli*., PC-12 cells | Cellular surface engineering | | 210 |
| | $Fe^{3+}$ | TA | *Brome mosaic virus* | Virus stability | | 211 |
| | $Ti^{4+}$ | TA | Chitin microspheres | Enzyme immobilization | | 212 |
| | $Fe^{3+}$, $Al^{3+}$, $Eu^{3+}$ | TA | Zein/quaternized chitosan | Drug delivery | | 213 |
| | $Fe^{3+}$ | TA | Yeast, *S. cerevisiae* | Cytoprotective coating | | 136 |
| | $Fe^{3+}$ | TA | Polyethylenimine/ p53 plasmid complexes | Ferroptosis for cancer therapy | | 214 |
| | $Fe^{3+}$ | TA | Acrylic latex particles | Controlled release of urea | | 215 |
| | $Fe^{3+}$ | TA | $Fe_3O_4$, Au, CdS particles | Encapsulation of particles | | 216 |

| | | | | | |
|---|---|---|---|---|---|
| $^{89}Zr^{4+}$ | TA | Pluronic F-12 | Tumor NIRF/PET imaging | | 217 |
| $Fe^{3+}$ | TA | Oleic acid emulsions | | Low-fouling and pH-responsive particles | 218 |
| $Fe^{3+}$ | TA | $Fe_3O_4$@$SiO_2$ particles | Enzyme immobilization | | 219 |
| $Fe^{3+}$ | TA | Sorafenib nanocrystal | Imaging-guided photodynamic therapy | | 220 |
| $Fe^{3+}$ | TA | Den–DOX nanocomplexes | Cancer therapy | | 221 |
| $Fe^{3+}$ | TA | Starch NPs | | Antioxidant, antimicrobial, and pH-sensitive starch NPs | 222 |
| $Fe^{3+}$ | TA | PS, MF, mesoporous $SiO_2$ particles | Endosomal escape of particles | | 145 |
| $Fe^{2+}$ | Phenol, HQ, 4-CP, 4-BP, TyA, L-tyrosine, AP, RR, P4VP, PTyr, trypsin, GFP, CT, pepsin | PS, $SiO_2$, $CaCO_3$ particles | Surface modification | Tyrosinase-mediated assembly | 146 |
| $Cu^{2+}$ | TA | Mesoporous $SiO_2$-coated upconversion NPs | Controlled release | | 223 |

| | | | | | | |
|---|---|---|---|---|---|---|
| | $Ru^{3+}$ | TA | $BiVO_4$ particles | Photocatalysis | | 224 |
| | $Fe^{3+}$, $Cu^{2+}$, $Co^{2+}$, $Ni^{2+}$, $Zn^{2+}$ | TA | Au particles | Antibody assembly on particles | | 159 |
| | $Fe^{3+}$ | TA | PDA NPs | Cancer therapy | | 225 |
| | $Fe^{3+}$ | TA | PDA@$Fe_2O_3$ particles | MRI-guided cancer therapy | | 226 |
| | $Ni^{2+}$ | TA | $WO_3$/$BiVO_4$ heterojunction | Photolectrochemical water splitting | Fabrication of photoanodes with enhanced photolectrochemical activity and stability | 227 |
| | $Ga^{3+}$, $In^{3+}$ | TA | EGaIn ink particles | Surface patterning (pen writing) | Approach is applicable to a range of substrates | 228 |
| Capsules | $Fe^{3+}$, $V^{3+}$, $Gd^{3+}$, $Cr^{3+}$ | TA, EGCG | PS, $SiO_2$, $SiO_2$-$NH_2$, MF, *E. Coli*, *S. epidermidis*, $Fe_3O_4$, PDMS, PLGA, Au particles | | Engineering MPN capsules via discrete assembly | 18 |
| | $Fe^{3+}$, $Mn^{3+}$, $Gd^{3+}$, $Cu^{2+}$, $Eu^{3+}$, $Tb^{3+}$, $Rh^{3+}$, $V^{3+}$, $Cr^{3+}$, $Co^{2+}$, | TA | PS particles | | Multifunctional MPN capsules | 30 |

| | | | | | |
|---|---|---|---|---|---|
| $Ni^{2+}$, $Cu^{2+}$, $Zn^{2+}$, $Zr^{4+}$, $Mo^{2+}$, $Ru^{3+}$, $Rh^{3+}$, $Cd^{2+}$, $Ce^{3+}$ | | | | | |
| $Fe^{3+}$ | TA | ZIF-8 | Chemodynamic therapy | Enzyme encapsulation to trigger intracellular cascade reactions | 119 |
| $Ti^{4+}$ | TA | $CaCO_3$ particles | Enzyme encapsulation | | 229 |
| $Fe^{3+}$ | TA | $CaCO_3$ particles | | Magnetic and enzyme-loaded capsules | 230 |
| $Fe^{3+}$ | GA, PG, PC | PS particles | | Smallest phenolic molecules used for MPN capsules | 198 |
| $Al^{3+}$ | TA | $CaCO_3$ particles | Drug delivery | | 137 |
| $Fe^{3+}$ | Lignin | Emulsion | | Preparation of nanocapsules | 231 |
| $Fe^{3+}$ | PEG-polyphenol | $CaCO_3$ particles | | Low-fouling and pH-degradable capsules | 154 |
| $Fe^{3+}$ | HA-polyphenol | $CaCO_3$ particles | | Protein corona-coated MPN capsules | 232 |

| | | | | | |
|---|---|---|---|---|---|
| $Fe^{3+}$ | PEG-polyphenol, HA-polyphenol | $CaCO_3$ particles | Cancer cell targeting | | 155 |
| $Fe^{3+}$ | GA, TA | ZIF-8, MIL-68, Tb-CP, $Fe_3O_4$@ZIF-8 particles | Surface functionalization | | 199 |
| $Fe^{3+}$ | TA | Lignin particles | | MPN capsules | 233 |
| $Fe^{3+}$ | TA | PS particles | | MPN capsules | 165 |
| $Fe^{3+}$ | Que, Myr | PS particles | Radical scavenging | | 125 |
| Rust | GA, TA | PS particles | | Rust-mediated assembly | 141 |
| $Fe^{3+}$ | TA | Oil droplet, microbeads, yeasts | Cell encapsulation | Biphasic assembly | 229 |
| $Fe^{2+}$ | TA | Hexadecane droplet | | MPN capsules with controllable thickness | 24 |
| $Fe^{2+}$ | TA | PS particles | | Oxygen-mediated assembly methods ($O_2$ and ROS) | 144 |
| $Fe^{2+}$ | L-tyrosine | PS particles | | Engineering MPN capsules with monophenols | 146 |
| $Fe^{3+}$ | CG, CC | $CaCO_3$, PS particles | | MPN capsules with macrocyclic cyclodextrins | 234 |

| | | | | | |
|---|---|---|---|---|---|
| | | | | using host–guest chemistry | |
| $Fe^{3+}$ | TA | ZIF-L, GOx–ZIF-L, HRP–ZIF-L particles | Artificial cells | | 131 |
| $Fe^{3+}$ | Turkish galls gallotannins | $CaCO_3$ particles | Ulcerative colitis therapy | | 235 |
| $Fe^{3+}$ | Eucalyptus leaf extracts | PMMA particles | | Selective assembly of phenolic compounds with $Fe^{3+}$ ions | 120 |
| $Fe^{3+}$ | TA | PS particles | | Engineering MPN capsules using mechanochemistry | 167 |
| $Fe^{3+}$ | PDA | $CaCO_3$ particles | Surface modification | | 236 |
| $Al^{3+}$ | EGCG | Tumor cells | Vaccines | | 237 |
| $Fe^{3+}$, $Cu^{2+}$, $Zr^{4+}$ | GA, EGCG | PS-*b*-PEO particles | Enzyme encapsulation | Mesoporous MPN particles | 147 |
| $Fe^{3+}$ | TA | $CaCO_3$ particles | Controlled pulmonary deposition | | 238 |
| $Fe^{3+}$ | TA | ZIF-8 particles | Cancer therapy | Encapsulation of ICG | 200 |
| $Fe^{3+}$ | TA | PS particles | | MPN capsules with | 121 |

| | | | | | |
|---|---|---|---|---|---|
| | | | | programmable gating | |
| | $Co^{2+}$ | TA | ZIF-8 particles | Lithium ion recovery | 239 |
| | $Fe^{3+}$ | TA | $CaCO_3$ particles | Virus (Epstein–Barr) detection | 240 |
| | $Cu^{2+}$ | EGCG | $CaCO_3$ particles | Peripheral artery disease therapy | 152 |

[a]Abbreviations: Hydroquinone (HQ); 4-chlorophenol (4-CP); 4-bromophenol (4-BP); tyramine (TyA); acetaminophen (AP); resveratrol (RR); poly(4-vinylphenol) (P4VP); green fluorescent protein (GFP); catalase (CT); pyrocatechol (PC); hyaluronic acid (HA); quercetin (Que); myricetin (Myr); cyclodextrin catechol (CC); cyclodextrin galloyl (CG); *Saccharomyces cerevisiae* (*S. cerevisiae*); *Escherichia coli* (*E. coli*); *Staphylococcus epidermidis* (*S. epidermidis*); dendrimer–doxorubicin (Den–DOX); melamine formaldehyde (MF); eutectic gallium–indium alloy (EGaIn); polydimethylsiloxane (PDMS); poly(lactic-*co*-glycolic acid) (PLGA); Tb-coordination polymer (Tb-CP); glucose oxidase (GOx); peroxidase from horseradish (HRP); poly(methyl methacrylate) (PMMA); polystyrene-*block*-poly(ethylene oxide) (PS-*b*-PEO); near-infrared fluorescence (NIRF); positron emission tomography (PET); layer-by-layer (LbL).

Metal ions can also be used to connect polyphenol-coated micro- and nanoobjects to form complex superstructures, where the metal ions serve as the binders and curing agents. For example, 15 types of materials with different sizes, shapes, and compositions were assembled using MPNs or PDA as a surface coating and subsequently "locked together" by metal ions (e.g., $Fe^{3+}$ and $Al^{3+}$). As a result, complex three-dimensional (3D) superstructures, including core–satellite, hierarchically organized particles, and macroscopic materials, were engineered.[140] Superstructures of various shapes and sizes of 10–500 nm were assembled in a water/ethanol system using $Mo^{2+}$–PDA complexes as binders and various nanomaterials (e.g., $SiO_2$, nano Si, $Fe_2O_3$ nanocubes, $SiO_2$@C, $NiNH_4PO_4 \cdot H_2O$ nanorods, and $SnO_2$ hollow spheres) as building blocks. The shape of the superstructures was regulated from the morphology of the particle building blocks (nanospheres, nanocubes, nanorods, and hollow spheres).[241] Using MPN assembly to form hierarchical structures can open new avenues in synthetic cells or artificial organs.[28]

### 4.3. Hydrogels

As a promising type of soft material, hydrogels have been explored in various fields, including underwater adhesives, tissue engineering, artificial skin, and water treatment.[242-245] Despite their potential and progress achieved to date, conventional hydrogels present some challenges in their functionality in regard to the limited choice in the building blocks available for their synthesis and in generating adequate interactions (e.g., adhesion) with substrates (i.e., skin). To this end, MPN-based hydrogels have been engineered from modular building blocks, affording enhanced material properties including high adhesion with substrates.

MPN hydrogels have been extensively studied, as highlighted in recent reviews.[129,135,246] This section provides a general overview of MPN-based hydrogels with an emphasis on metal ion-directed gelation. Various metal ions have been reported to chelate with various catechol/PG-containing polymers, including PEG,[53,247,248] chitosan,[249] chondroitin sulfate,[250] gelatin,[251,252] polyallylamine,[57] generating reversible cross-linked hydrogel networks. For instance, a solution mixture of 4-arm-PEG-catechol and $Fe^{3+}$ with a low viscosity could transform into an elastomeric gel upon the formation of tris-$Fe^{3+}$–catechol complexes by raising the pH of the solution from ~5 to ~12.[53] The use of the metal ions $V^{5+}$, $Au^{3+}$, and $Ag^{+}$ also led to the gelation of 4-arm-PEG-catechol but with different gelation kinetics, mechanical properties, cross-link density, and self-healing capacity.[253] In contrast, the addition of $Cu^{2+}$, $Al^{3+}$, or $V^{4+}$ did not lead to the gelation of 4-arm-PEG-catechol, suggesting that the valency and redox potential of metal ions are important factors for the design of catechol-bearing hydrogel networks.[253] Metal oxide nanomaterials (e.g., nanosheets and NPs) were also used as building blocks for the preparation of hydrogels. For example, $Fe_3O_4$ NPs induced the gelation of 4-arm-PEG-catechol networks to produce a composite hydrogel. The hydrogel displayed a viscoelastic solid-like behavior, similar to covalently cross-linked hydrogels, but reversible mechanics.[254] Such material rheology properties were attributed to the dominant cross-links of particle–polymer interfacial $Fe^{3+}$–catechol coordination bonds and finely controlled by the number of polymer chains bound to each NP. Furthermore, $Fe_3O_4$ NPs were synthesized in situ by adding $Fe^{2+}$ to the 4-arm-PEG-catechol/$Fe^{3+}$ hydrogels under alkaline

conditions (Figure 11a).[248] The rheology measurements demonstrated that in situ mineralization significantly improved the mechanical performance of the hydrogels compared with that achieved by ex situ mineralization, mineral-free hydrogels and ligand-free hydrogels (Figure 11b–d). The strategy can be extended to other inorganic nanomaterials through coordination interactions, thus providing a facile approach to construct biological organic–inorganic composite materials.

Furthermore, the addition of preformed metal–phenolic complexes to polymer solutions, such as polyvinylpyrrolidone (PVP),[255,256] poly(sodium 4-styrenesulfonate), poly(dimethyldiallylammonium chloride), and PEG,[257] can lead to gelation through both hydrogen bonding and coordination bonding. Both synthetic molecules and naturally occurring phenolic compounds have been reported for engineering hydrogels via direct gelation. Supramolecular hydrogels were obtained by directly mixing TA with $Ti^{4+}$ or $Zr^{4+}$ ions in solution.[139] Incorporating diverse functional materials endowed TA/$Ti^{4+}$ hydrogels with multiple properties, including self-healing, pH-responsiveness, photothermal performance, and electrical conductivity.[139] TA/$Ti^{4+}$ metallogels were subsequently developed as a generic platform for the crystallization of active pharmaceutical ingredients (e.g., caffeine, carbamazepine, and piroxicam).[202] The biocompatibility and immunogenicity of TA/$Ti^{4+}$ metallogels were studied in immunocompetent mice over 14 weeks, which highlighted the potential suitability of the supramolecular hydrogels for biomedical applications.[258] The application of MPN-based hydrogels is thus widespread and has been demonstrated in a variety of fields, especially in biomedical engineering[246] (e.g., drug delivery[202,258] and tissue repair[259,260]), electronics[129] (e.g., skin-like sensors,[261,262] soft actuators,[255] and bioelectronic implants[263]), wet adhesives,[264] and environmental remediation and catalysis.[265]

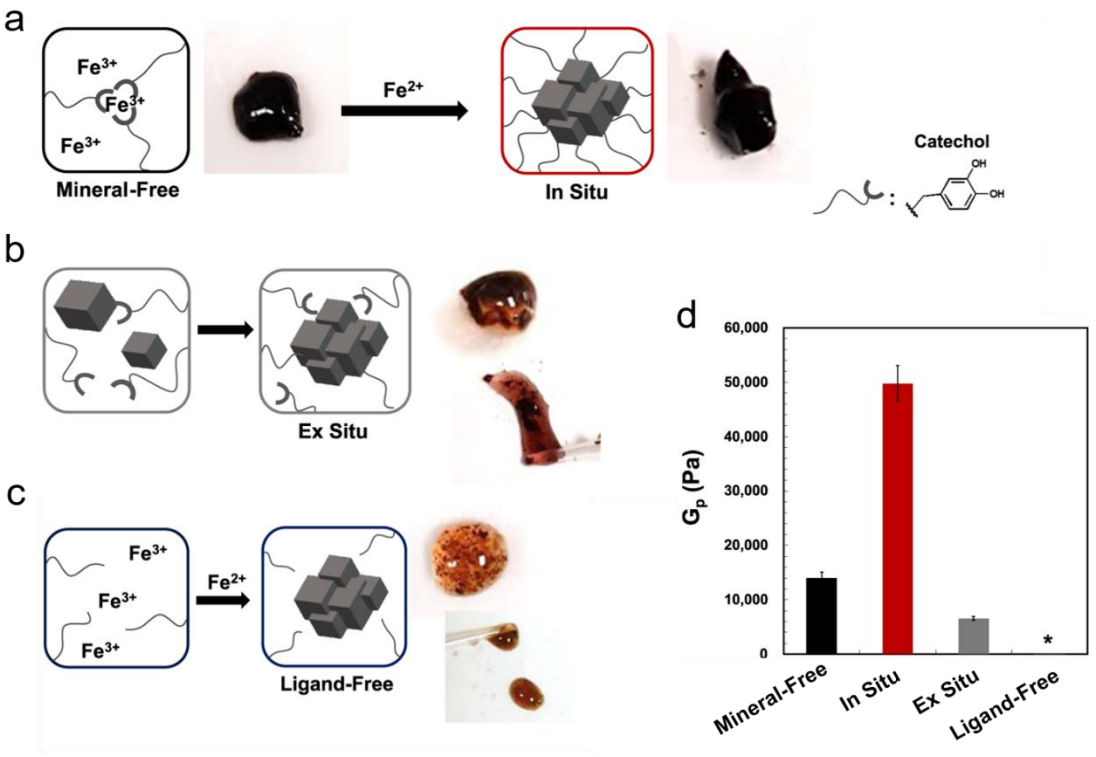


**Figure 11.** (a) In situ mineralization of a gel formed by introducing $Fe^{2+}$ to a mineral-free gel, cross-linked by 4-arm-PEG-catechol−$Fe^{3+}$ interactions. (b) Ex situ mineralization of a gel formed by mixing $Fe_3O_4$ minerals with 4-arm-PEG-catechol. (c) Preparation of a ligand-free hydrogel using the same protocol as that used for the in situ mineralized gel except that 4-arm PEG with no catechol modification was used. (d) Plateau modulus ($G_p$) values of the mineral-free gel, gels formed in situ and ex situ, and ligand-free gel at 1% strain. Adapted with permission from ref 248. Copyright 2021 Springer Nature.

## 5. Materials Formed via Redox Interactions

Recent advances in the field of in situ reduction of noble metal ions by phenolic compounds are demonstrated in Figure 12. Specifically, the choice of the phenolic building blocks employed has expanded from simple phenolic molecules to synthetic catechol-containing polymers, as well as biomass-derived lignin. Furthermore, well-defined nanostructures, such as multishell NPs, core–shell NPs, and multifunctional hydrogels have been effectively prepared through in situ reduction of noble metal ions by diverse phenolic building blocks.[31,266-270] Moreover, the dynamic redox

balance of phenol–quinone mediated by Ag NPs is a promising strategy for the development of long-lasting adhesive materials.[64,66,271] The particles and hydrogels formed via redox interactions not only retain the properties of the building blocks (e.g., antioxidant properties of phenolics), but also emerge new functions, such as enzyme-like activity of TA–Ag NPs.[66,272] The noble metal NPs obtained by the reduction of natural polyphenols represent potential applications in catalysis, sensing, and nanomedicine.

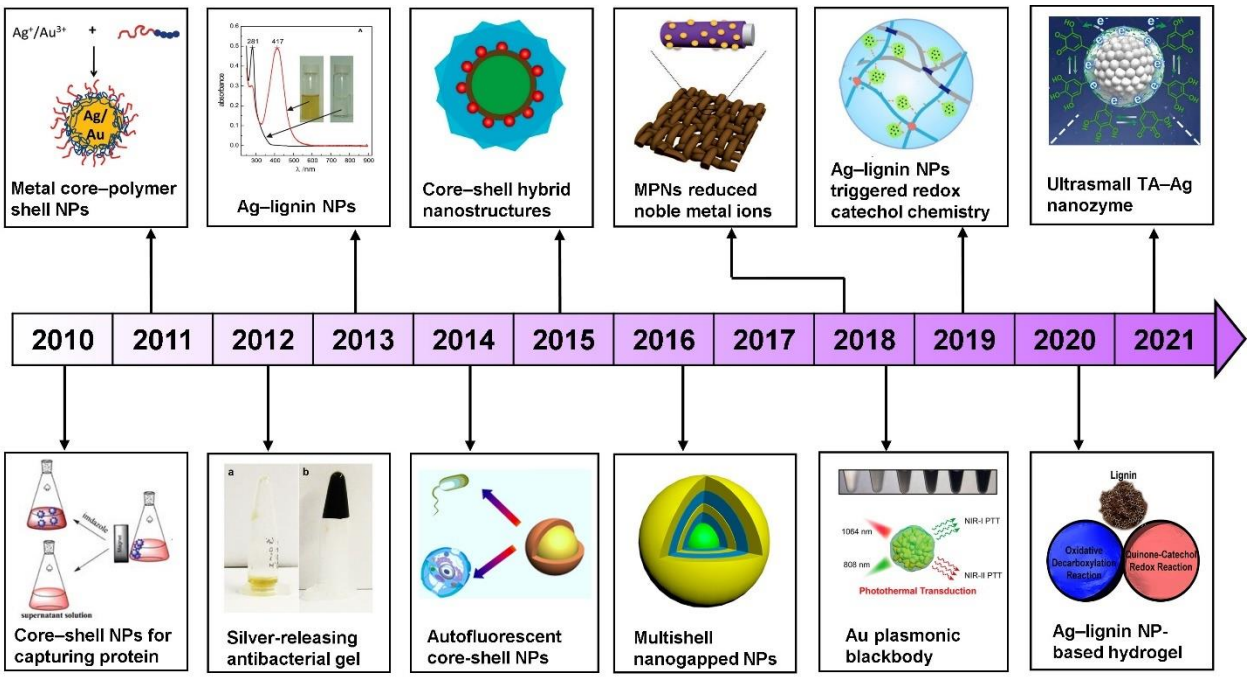


**Figure 12.** Recent progress in the redox interactions between noble metal ions and phenolic compounds. Adapted with permission from the following references: Ref 266. Copyright 2010 Royal Society of Chemistry; Ref 31. Copyright 2011 American Chemical Society; Ref 267. Copyright 2012 Elsevier; Ref 271. Copyright 2013 Elsevier; Ref 273. Copyright 2014 American Chemical Society; Ref 268. Copyright 2015 American Chemical Society; Ref 269. Copyright 2016 American Chemical Society; Ref 274. Copyright 2018 Wiley-VCH; Ref 275. Copyright 2018 American Chemical Society; Ref 66. Copyright 2019 Springer Nature; Ref 64. Copyright 2020 American Chemical Society; Ref 272. Copyright 2021 Elsevier.

### 5.1. Particles

Individual noble metal NPs, nanoplates, and nanofibers have been synthesized in various phenolic solutions such as TA,[59,276] DA,[58,275] GA[61,277,278] and various catechol-conjugated polymers.[65,279] Owing to the conformal coating properties displayed by phenolic compounds, noble metal NPs were fabricated on PDA or MPN-coated substrates such as polymer films,[280] metallic oxide NPs,[281] metal NPs,[282] gauze,[274,283] polymer microspheres,[59] 3D nickel hydroxide nanowalls,[284] and carbon nitride.[285]

Furthermore, complex nanostructures (e.g., multi-shell and core–shell NPs) were fabricated using a one-step redox reaction between phenolic compounds and noble metal ions. Well-defined core–shell nanocomposites were assembled by one-pot preparation under microwave irradiation in the presence of tea polyphenols (TPs) and $Ag^+$ or $Au^+$.[273] The core–shell Ag–TP nanocomposites showed strong inhibition activity toward the growth of *Escherichia coli* (*E. coli*) while showing negligible cytotoxicity against normal cells (i.e., COS-7, a monkey fibroblast-like cell line).[273] The use of microwave irradiation played an important role in the self-assembly and aggregation of the noble metal complexes. The addition of $AuCl_4^+$ or $Ag^+$ salts to DOPA-containing PEG solutions not only led to metal reduction but also simultaneously produced reactive quinones that covalently cross-linked the PEG shell onto the NP surfaces (Figure 13a).[31] A metal core and less electron dense coatings were shown in a transmission electron microscopy (TEM) image (Figure 13b). Owing to the protection provided by the PEG shell, the obtained metal NPs with polymeric shells provided high stability from aggregation in aqueous solutions even under high ionic strength conditions.[31] Potentially, this facile surface functionalization strategy can be broadened by using different catechol-containing molecules, such as PDA, DOPA-modified peptides, proteins, or polysaccharides for broader biological and catalytic applications. Duan and co-workers fabricated a series of multifunctional core–shell nanohybrids of NP@MOF and multishell nanogapped NPs.[268,269] The PDA-coated colloidal substrates enabled localized reduction of gold precursors and directed the subsequent heterogeneous nucleation of MOFs (e.g., ZIF-8, UiO-66) or the growth of Au shells. Specifically, simply repeating the cycles of PDA coating and metallization,

nanostructures with multiple concentric nanoshells around the core were obtained. As shown in Figure 13c, nanostructures with a single shell featured a 50 nm Au core and a 13 nm nanogap, where the size of single-shell nanostructures was smaller than that of the double-shell or triple-shell nanostructures based on the TEM images. The UV–vis absorption of the nanostructures increased significantly as the number of Au shells increased, and the surface-enhanced Raman scattering was strongly activated by nanogaps between the Au shells (Figure 13d and 13e).[269] The reduced Au sandwiched between the NP core and MOF or Au shell is expected to provide opportunities for flexible, rational functionality integration into the final materials. A class of compact monodisperse Au plasmonic blackbodies (AuPBs) were prepared via reduction of $AuCl_4^+$ by DA. The AuPBs exhibited intense and uniform broadband absorption in the first near-infrared and the second near-infrared (NIR-II) spectral windows.[275] In photothermal therapy (PTT) for tumors, the NIR-II laser could penetrate tissues 5 mm thick and induce prominent tumor cell death in 4T1 (a mouse breast cancer cell line) tumor-bearing mice after injection of the AuPBs.[275]

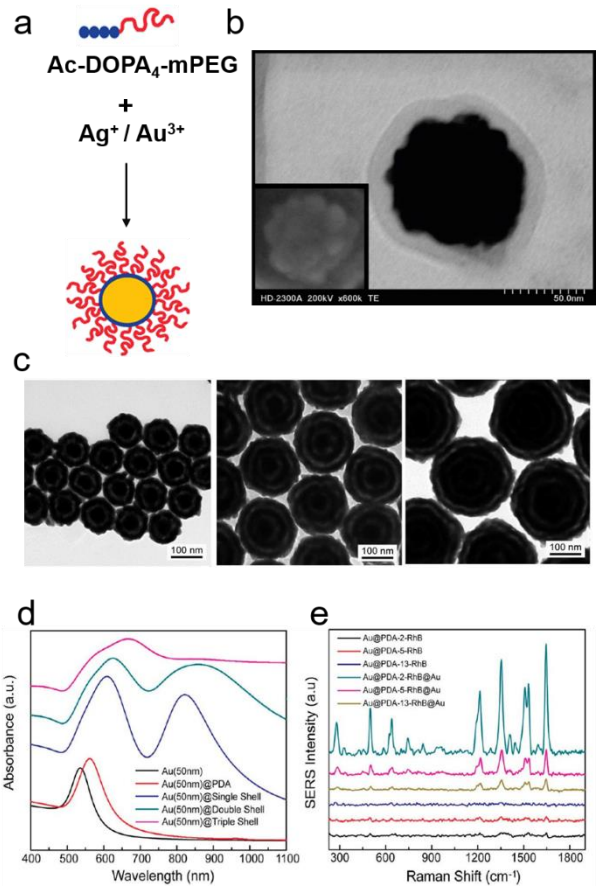

**Figure 13.** (a) Schematic and (b) TEM and SEM (inset) images of metal core–polymer shell NPs formed by DOPA-containing PEG polymers (Ac-$DOPA_4$-mPEG) and noble metal ions. (c) TEM images, (d) UV–vis spectra, and (e) surface-enhanced Raman scattering spectra of nanogapped Au NPs coated with PDA and single, double, or triple Au shells. (a, b) Adapted with permission from ref 31. Copyright 2011 American Chemical Society. (c–e) Adapted with permission from ref 269. Copyright 2016 American Chemical Society.

### 5.2. Hydrogels

Nanocomposite hydrogels are 3D hybrid networks that are formed by incorporation of nanomaterials (e.g., metallic, polymeric NPs) into bulk hydrogels.[242,286,287] The properties of the NPs and hydrogel constituents can be synergistically combined, enabling nanocomposite hydrogels with excellent mechanical properties and functionalities, such as conductivity, magnetic responsiveness, and photothermal effect.[286,288] The presence of metal NPs in phenolic hydrogel engineering presents several advantages. Firstly, the inclusion of metal NPs endows hydrogels with additional functions such as antibacterial properties (provided by Ag)[267] and catalytic activities (provided, for example, by Au).[289] Secondly, the composite hydrogels (with the incorporated metal NPs) present different physical properties including rheological properties, gelation kinetics, and cross-linking densities from those of hydrogels prepared without NPs.[253,289,290] Thirdly, the quinone–catechol redox reactions using noble metal ions as oxidizing agents leads to covalent cross-linking of the phenolic moieties that facilitate hydrogel formation,[267] thus promoting the adhesion and cohesion of the hydrogels.[66] As further exemplified in the literature, the oxidative covalent polymerization of catechols coupled with the reduction of $Ag^+$ to Ag NPs resulted in the formation of antibacterial hydrogels.[267] Biomass-derived lignin with numerous catechol and PG groups is an effective reducing agent. The lignin spontaneously loses electrons in the presence of metal ion precursors including $Ag^+$,[271] $Au^{3+}$, $Pd^{2+}$, $Ru^{3+}$, $Re^+$,[291] $Pd^{2+}$, $Cu^{2+}$, $Fe^{3+}$, $Ni^{2+}$, and $Zn^{2+}$,[64] resulting in the concurrent formation of metal–lignin NPs. Among lignin-based NPs, Ag–lignin NPs are stable redox pairs that can provide a long-lasting reductive–oxidative environment.[64,66] This redox system of generating catechol groups continuously is

attributed to the localized surface plasmon resonance effect of the Ag NPs, producing numerous photogenerated electrons that are accepted by quinones in lignin to form adherent phenolic hydroxyl groups.[64,66] The quinone–catechol reversible redox reaction has been widely used to trigger gelation based on free radical polymerization.[64,66,272,290] For example, Ag–lignin NPs combined with ammonium persulfate (APS) generated large amounts of free radicals, which initiated controlled free-radical polymerization of AA monomers into polyacrylic acid (PAA) to generate a hydrogel (Figure 14a).[66] Recently, it was reported that Ag–lignin NPs could catalyze oxidative decarboxylation reactions leading to intermolecular cross-linking of COOH-containing polymers in the presence of APS (Figure 14b).[64] Active radicals in the Ag–lignin NPs–PAA hydrogel were detected by EPR spectroscopy even after 24 h, suggesting that the radicals could maintain long lifetimes in the reductive environment provided by the Ag–lignin NPs (Figure 14c). In another study, Ag–TA NPs with an average diameter of 5 nm were prepared by in situ reduction of Ag NPs with TA. The Ag–TA NPs exhibited stable peroxidase-like catalytic activity (Figure 14d).[272] The resulting hydrogels formed from the Ag–TA NPs possessed conductive (Figure 14e), antibacterial, and adhesive properties. Thus, the Ag NPs and polyphenols can form suitable electron donor–acceptor complexes, which provides a facile and ecofriendly strategy for engineering durable adhesive and functional hydrogels. Nevertheless, a limitation that needs to be considered is the ability of lignin or TA and the corresponding quinones to act as radical scavengers, which could potentially inhibit intermolecular cross-linking, consequently preventing the formation of a self-standing hydrogel.

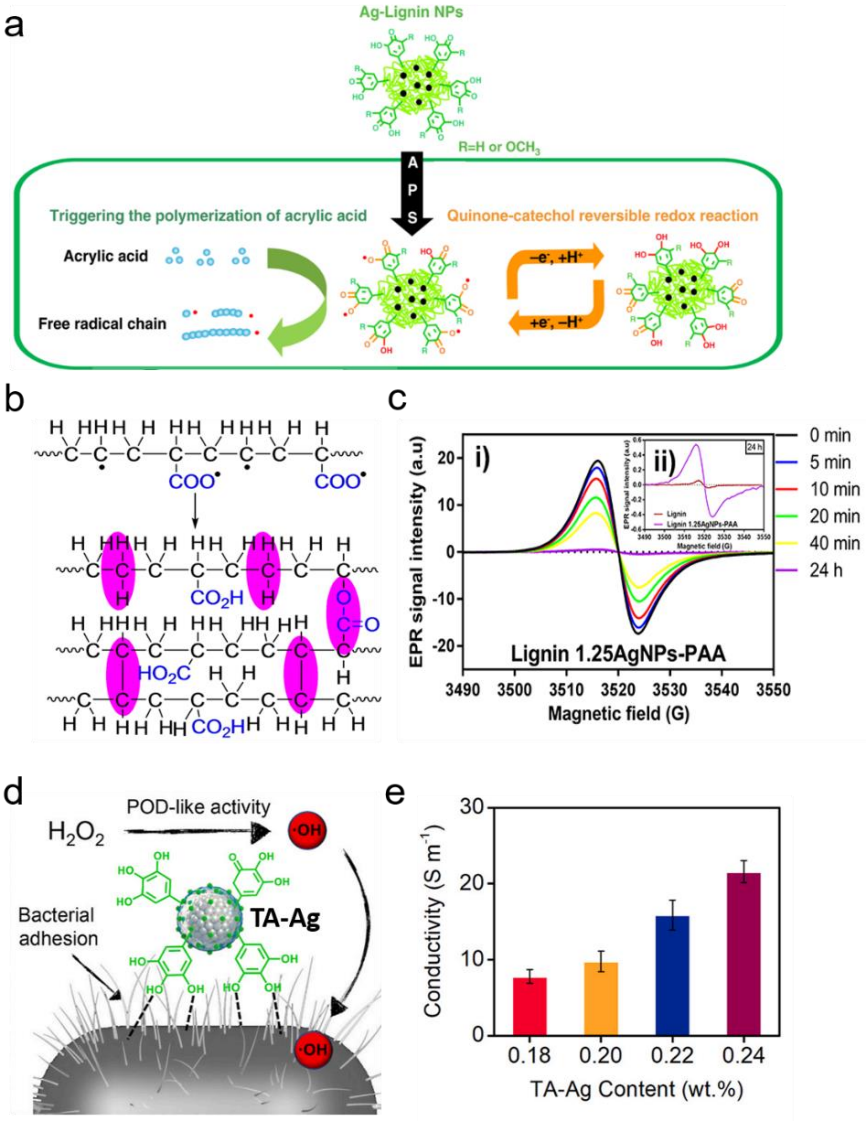


**Figure 14.** (a) Quinone–catechol reversible reactions of Ag–lignin NPs triggering gelation. Adapted with permission from ref 66. Copyright 2019 Springer Nature. (b) Intermolecular cross-linking of PAA via oxidative–decarboxylation reactions. (c) EPR spectra of the reaction for engineering Ag–lignin NPs–PAA hydrogel at various time points. (b, c) Adapted with permission from ref 64. Copyright 2020 American Chemical Society. (d) Schematic of the antibacterial activity displayed by Ag–TA NPs, as demonstrated via the generation of reactive oxygen species during a peroxidase (POD)-like catalytic process. (e) Conductivity of Ag–TA NP-containing hydrogels as a function of Ag–TA content. (d, e) Adapted with permission from ref 272. Copyright 2021 Elsevier.

## 6. Materials Formed via Dynamic Covalent Interactions

Recent findings in metalloid–phenolic networks including BPNs, SiPNs, and GePNs are shown in Figure 15. BPNs with pH- and sugar-responsiveness have gained considerable attention in material engineering from NPs,[80,292] micelles,[79,293] capsules,[70] bulk hydrogels[76,77,81,294,295] to coacervates,[88,296] and have shown potential applications in drug delivery,[79,82,85,86,297] tissue repair,[76-78] disease diagnostics,[75] 3D cell encapsulation,[73,294] molecular recognition,[75,266,298] and separation.[299] Other progress reported in the field of metalloid–phenolic networks relates to SiPNs.[69,91,300] The strong bonding interactions between Si and catechol or PG groups were demonstrated from the improved mechanical properties of polyphenol-containing hydrogels by addition of nanosilica (e.g., laponite, $Na_{0.7}^{+}(Mg_{5.5}Li_{0.3}Si_8)O_{20}(OH)_4)_{0.7}^{-}$),[301-304] as well as the formation of continuous TA nanocoatings mediated by silicic acid.[305] Studies have shown that introducing Si NPs into phenolic adhesives can considerably improve the adhesive and mechanical properties of the resulting materials.[92,93] In addition, GePNs have attracted increasing attention in engineering materials due to the strong interactions between Ge and phenolic materials. It is reported that the use of germanic acid together with TA enables a continuous coating.[305] Ge–mangiferin complexes have been shown to exhibit higher antioxidant and anti-cancer activities than free mangiferin or Ge.[306] Given the specific nature of metalloids, such as semiconducting properties and pharmacological effects, further studies on metalloid–phenolic networks will help to broaden the potential technological and biomedical applications of phenolic materials.

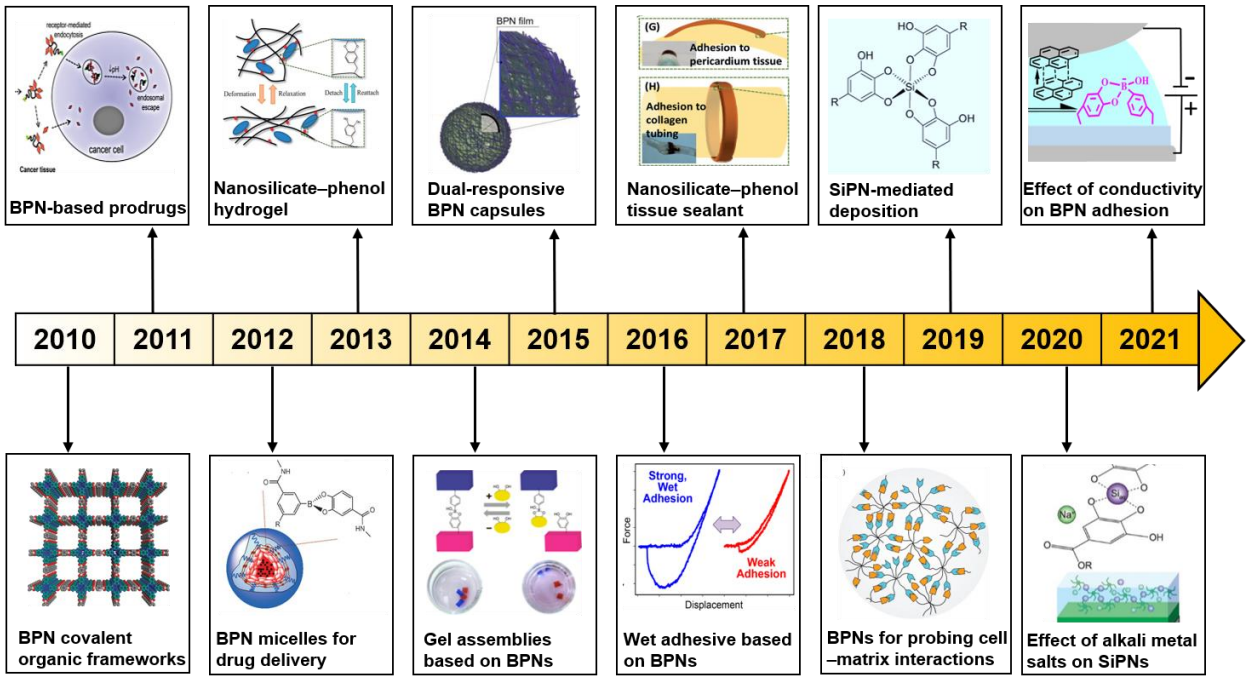


**Figure 15.** Timeline of recent development in metalloid–phenolic networks. Adapted with permission from the following references: Ref 292. Copyright 2010 Springer Nature; Ref 86. Copyright 2011 American Chemical Society; Ref 79. Copyright 2012 Wiley-VCH; Ref 302. Copyright 2013 Royal Society of Chemistry; Ref 83. Copyright 2014 American Chemical Society; Ref 70. Copyright 2015 Wiley-VCH; Ref 296. Copyright 2016 American Chemical Society; Ref 301. Copyright 2017 Wiley-VCH; Ref 294. Copyright 2018 Wiley-VCH; Ref 91. Copyright 2019 Wiley-VCH; Ref 105. Copyright 2020 American Chemical Society; Ref 307. Copyright 2021 American Chemical Society.

### 6.1. Particles

Boronate-based nanocarriers typically exhibit fast dual responsiveness to external pH and diols, which provides a facile way to release cargos in an acidic microenvironment (e.g., tumor sites) or in the presence of elevated glucose.[79,84,308,309] Lam and co-workers developed a class of stimuli-responsive micelles using reversible boronate ester bonds to cross-link dendritic PEG polymers (Figure 16a).[79] The cross-linked micelles remained stable under physiological conditions and dissociated at pH 5.0 or in 100 mM mannitol, which offers an opportunity for designing smart drug

delivery systems in a controllable manner (Figure 16b).[310] The micelles loaded with paclitaxel (PTX) displayed a long blood circulation time in vivo and the release of PTX via dissociation, triggered in acidic tumor microenvironments. Mannitol was administered intravenously, serving as an additional trigger to induce drug release on demand, thereby improving tumor therapeutic effects and extending survival of the mice.[293] Thus, multi-responsive boronate-based nanocarriers possess advantages in combination therapy for solid tumors, showing promise for improving therapeutic efficacy while minimizing side effects.

BTZ is not only a boronic acid analogue but also a commercial proteasome inhibitor for multiple myeloma and mantle cell lymphoma treatment (Figure 16c).[85,86] Substantial efforts have been focused on developing nanocarriers (e.g., NPs,[192] prodrugs,[86,87] micelles[82,85]) based on phenolic compounds and BTZ, which act as structural and functional components. PEG–catechol–BTZ conjugates showed a pH-dependent release behavior with high proteasome-inhibiting activity toward breast carcinoma cells.[86] To enhance drug delivery specificity to tumor sites, nanocarriers have often been incorporated with cell-targeting functions. For instance, tripeptide arginylglycylaspartic acid as a targeting ligand was grafted onto catechol/BTZ-modified polyamidoamine dendrimers to precisely deliver BTZ to MDA-MB-231 cells.[297] Another feasible strategy is to design nanocarriers that can undergo structural transformation in response to changes in temperature, magnetic field, or pH. For instance, BTZ-loaded micellar NPs were prepared from a diblock copolymer composed of PEG block and polycarbonate block linked through an acid-sensitive acetal junction. The NPs could shed the hydrophilic PEG shell in acidic tumor tissues or inside cancer cells, hence accelerating drug release at the target sites.[85] However, it was reported that boronate–catechol complexation could inhibit the therapeutic efficacy of BTZ to a certain degree.[192] Therefore, supramolecular self-assembly using small molecular natural polyphenols (e.g., TA, EGCG, catechin) and BTZ not only retains the bioactivity (e.g., anticancer activity) of the natural phenolic compounds but also reduces the inhibition effects on BTZ (Figure 16d).[192]

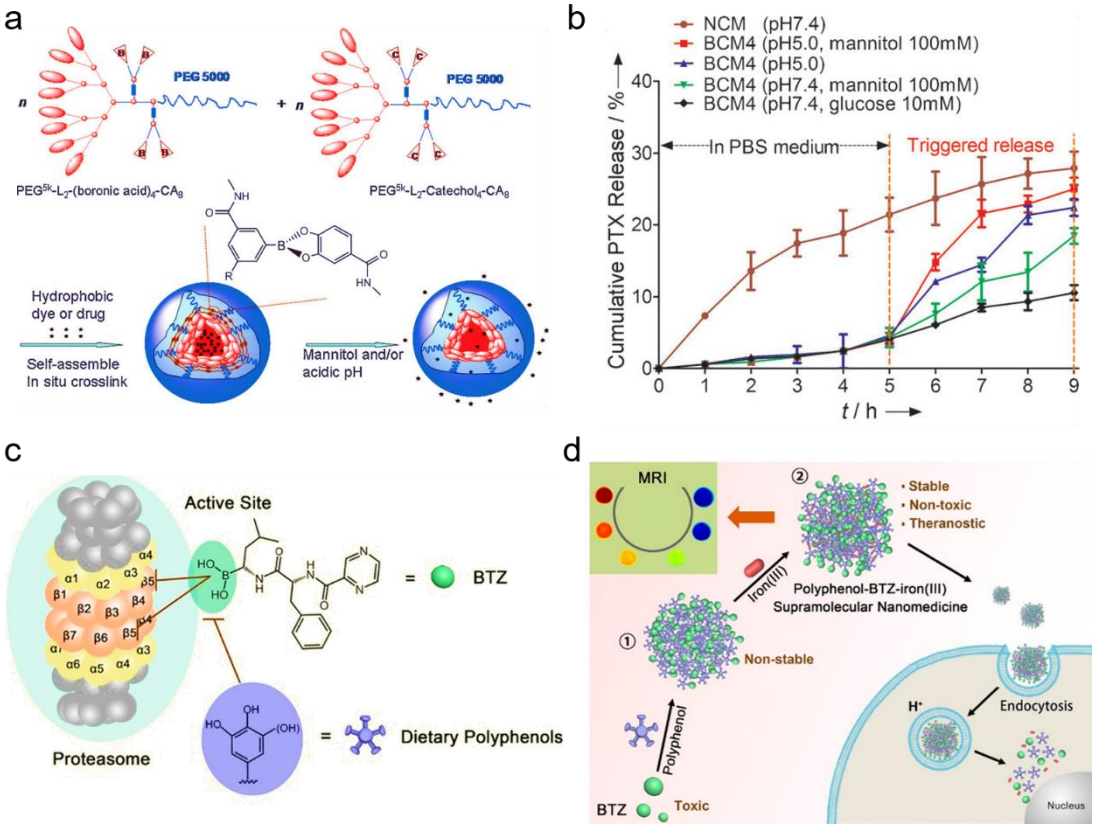


**Figure 16.** (a) Fabrication of micelles by using reversible boronate ester bonds to cross-link dendritic PEG polymers. (b) Controlled drug release profiles of the cross-linked micelles. (c) Proteasome inhibition by BTZ by chemically blocking the active sites. (d) Supramolecular nanomedicine involving natural polyphenols, BTZ, and $Fe^{3+}$ for cancer therapy. Cholic acid (CA); non-crosslinked micelle (NCM); boronate cross-linked micelles formed by $PEG^{5k}$-nitrophenylboronic $acid_4$-$CA_8$ and $PEG^{5k}$-$catechol_4$-$CA_8$ (BCM4). (a, b) Adapted with permission from ref 79. Copyright 2012 Wiley-VCH. (c, d) Adapted with permission from ref 192. Copyright 2018 American Chemical Society.

### 6.2. Hydrogels

The introduction of functional boronic acid moieties affords phenolic hydrogels with diverse properties such as pH-reversibility, self-healing, and glucose sensitivity.[78,83,295,311,312] Considering the bioactivities of phenolic compounds and negligible toxicity of boronic acid-derived compounds, BPN-based hydrogels are suitable for biomedical applications. A number of plant-

derived polyphenols as cross-linkers and therapeutics were used to form injectable hydrogels by mixing with boronic acid-modified PEG.[81] The reversible boronate ester bond afforded a long-term steady-state release of therapeutic polyphenols (i.e., EA) that led to a decrease in the survival rate of CAL-27 oral cancer cells.[81] Moreover, the dynamic nature of boronate ester bonds endows hydrogels with a stress-relaxing property (Figure 17a), which is important for 3D cell encapsulation to promote cell–matrix interactions. Human mesenchymal stem cells (hMSCs) were encapsulated in the fast stress-relaxing hydrogels promoted by both reversible boronate bonds and azide-alkyne cycloaddition.[294] hMSCs spread significantly within day 1, and cell volume was nearly four times as large as that in a control group comprising an elastic hydrogel prepared from permanent azide-alkyne cycloaddition chemistry alone at day 7 (Figure 17b).[294] The dynamic boronate ester bonds endow BPN hydrogels with high flexibility to afford tunable physicochemical properties and responsiveness for diverse applications.

Nanocomposite hydrogels that are formed from NPs and hydrogels hold promising prospects in many fields owing to their combined attributes from the respective NP and hydrogel components. The strong interfacial bonding between phenolic groups and nanosilicate (i.e., laponite) has been widely reported.[91,302] The addition of laponite enhanced the bulk mechanical and adhesive properties of catechol-conjugated polyacrylamide hydrogels[302,303] and catechol-modified PEG hydrogels.[301,304] For hydrogels formed by 8-armed PEG-catechol and laponite (PEG-Lapo), the storage modulus ($G'$) continued to increase over 4 days, and the damping ratio (loss modulus ($G''$)/G′) decreased with incubation time, indicated that the reversible laponite–catechol interactions in hydrogels were slowly replaced by covalent bonds of phenolic autoxidation.[301,302] As a result, PEG-Lapo hydrogels were remolded into different shapes according to surrounding environment features (e.g., adhesion to a convex pericardium or collagen tubing) and shape-fixed as the density of covalent cross-linking increased (Figure 17c), which provides a simple approach to construct moldable nanocomposite hydrogels.

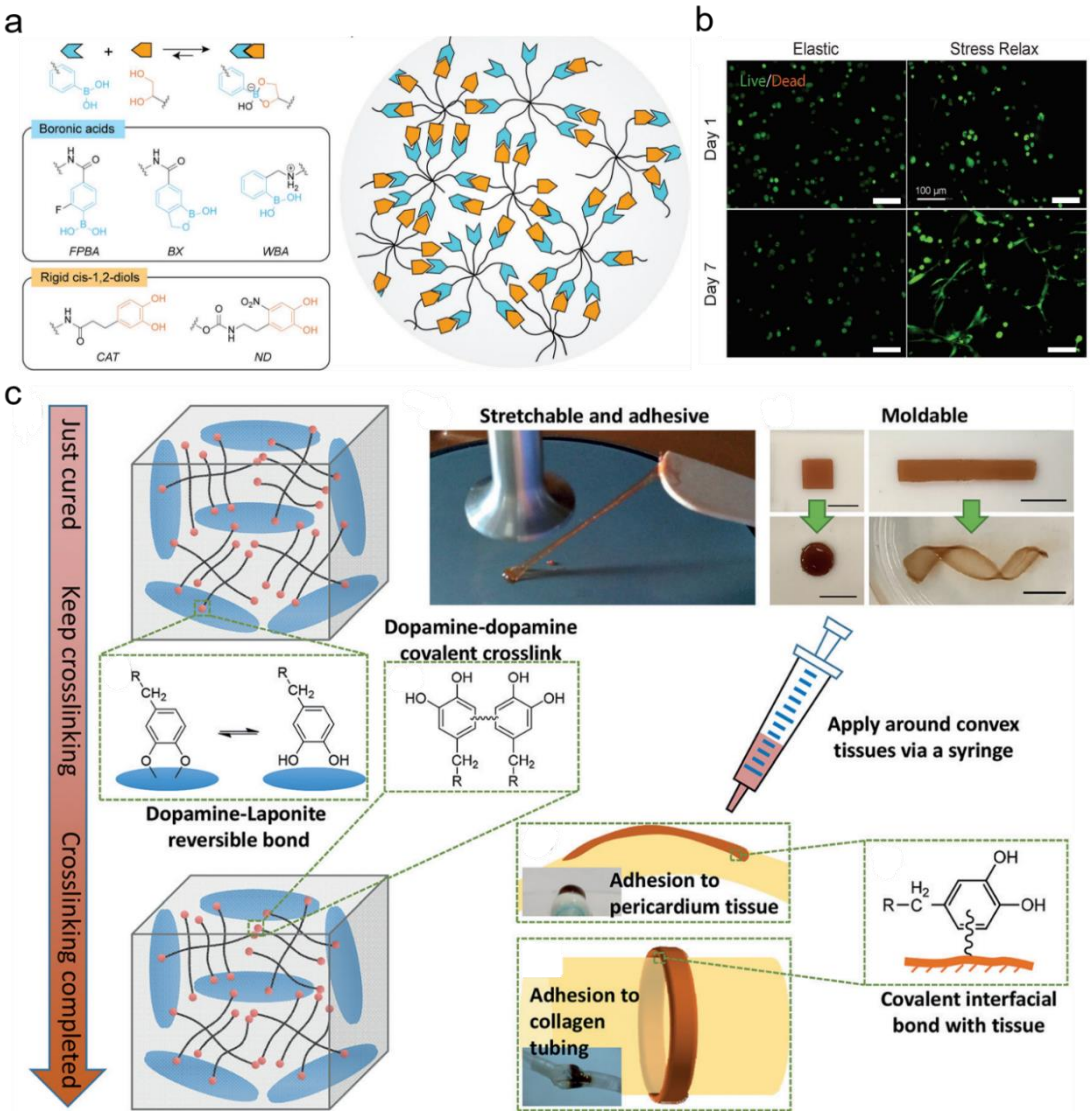


**Figure 17.** (a) Design of covalent adaptable networks based on dynamic boronate bonds. (b) Representative maximum intensity projection images of cells in elastic and stress-relaxing hydrogels on day 1 and day 7. Scale bars are 100 μm. (a, b) Adapted with permission from ref 294. Copyright 2018 Wiley-VCH. (c) Moldability and adhesiveness of a nanocomposite hydrogel formed from DA-modified PEG and laponite. Scale bars are 10 mm. 2-fluorophenylboronic acid (FPBA), boroxole (BX), Wulff-type-like boronic acid (WBA), catechol (CAT), and nitro-dopamine (ND). Adapted with permission from ref 301. Copyright 2017 Wiley-VCH.

## 7. Applications

Metal ions not only are important building blocks in the preparation of metal–phenolic materials but also endow metal–phenolic materials with diverse functionalities such as conductivity, imaging capability, and pH-responsiveness.[313] Such features allow the broad application of metal–phenolic materials in the biological, mechanical, catalytic, and environmental areas. Furthermore, liquid metals (LMs) have recently been developed as metal building blocks for metal–phenolic materials, which expands the use of metal–phenolic materials in soft electronics and sensors.[228,314] Scientific advances of metal–phenolic materials have been shown in emerging areas such as agriculture[315] and information visualization.[316,317] This section will give an overview of the applications of metal–phenolic materials.

### 7.1. Biological Applications

Numerous reviews on the biological applications of PDA or polyphenols have been published in the last few years, and many of them involve metal–phenolic materials, particularly MPNs.[19,27,60,313,318-320] Herein, we summarize some of the recent (2017–2021) reviews on the biological/biomedical applications of MPN-based materials (Table 4), followed by a focused discussion on predominant applications, such as theranostics, antibacterial, degradable biointerfaces, and the importance of metal ions.

**Table 4.** Overview of reviews published in 2017–2021 on the biological/biomedical applications of metal–phenolic materials

| Year | Material | Biological/biomedical application | Ref. |
|---|---|---|---|
| 2017 | MPNs | Engineering of various biointerfaces (bacteria, yeast, animal cells, viruses, teeth) | 19 |
| 2018 | Metal-containing PDA (nano)materials | Cancer therapy (imaging, therapy, nanotechnology) | 321 |
| | Metal-containing DA-based materials | Cancer diagnosis, therapy and theranostics | 322 |
| | Polyphenol-metal ion/boronate/noble | Cell encapsulation, antimicrobial and antioxidant | 323 |

| | | | |
|---|---|---|---|
| | metal NP complexes | applications | |
| 2019 | Metal-containing PDA platforms | Biosensing, bioimaging, cancer therapy, cancer theranostics, antimicrobials | 324 |
| | Metal-containing melanin/PDA-based nanomaterials | Bioimaging, disease treatment, theranostics, antibacterial applications, UV/radiation protection, biosensor, tissue engineering | 325 |
| | MPN-based particles | Cancer therapy, imaging and diagnosing, treatment of other diseases | 318 |
| | MPN films, particles and bulk materials | Drug delivery, sensing and imaging, artificial sporulation | 28 |
| 2020 | Metal–phenolic hydrogels | Antibacterial, wound dressing | 135 |
| | Metal–phenolic biomaterials | Drug delivery | 326 |
| | Metal-containing catechol-functionalized hydrogels | Tissue sealants and adhesives, antifouling and antimicrobial applications, drug delivery, cell encapsulation and delivery | 246 |
| | Metal-containing PDA nanomaterials | Theranostics, antifouling and antimicrobial applications | 313 |
| 2021 | Metal-containing polyphenol scaffolds | Tissue engineering | 327 |
| | Metal-phenolic particles and nanohybrid materials | Particle–cell interactions, pharmacokinetics, and toxicology, in vitro biosensing, in vivo bioimaging, disease therapy | 176 |
| | Metal–phenolic NPs | Biodetection, multimodal bioimaging, protein and gene delivery, bone repair, antibiosis, and cancer theranostics | 328 |
| | MPN-assembled complexes | Cancer theranostics | 329 |
| | MPNs | Cancer theranostics | 330 |
| | MPN coatings | Bioactive interfaces | 331 |

### 7.1.1. Theranostics

Metal ions play vital roles in the field of therapy and diagnosis.[332] Metal-containing phenolic NPs for various diagnostic and therapeutic applications have been discussed in other reviews.[313,318] Herein, we focus on the comparison of different metal–phenolic complexes (including those prepared from different metal ions and the same phenolics or from different phenolics and the same metal ions) applied in the theranostics field. MPNs are highly versatile in terms of their ability to incorporate various diagnostic metal ions. In addition, owing to the adhesion nature of MPNs, the functionalized (MPN-coated) templates could enable versatile cooperation with different theragnostic approaches. For example, a number of metal ion/TA assemblies were fabricated using poly(lactic-*co*-glycolic acid)-based nanovesicles (PNVs) as templates to explore the influence of metal ions on the photothermal effects of the assemblies.[124] Among the metal ions examined, $Gd^{3+}$-, $Cu^{2+}$-, $Mn^{2+}$-, and $Ni^{2+}$-based PNVs displayed negligible absorption, whereas the use of $Fe^{3+}$, $V^{3+}$, and $Ru^{3+}$ afforded excellent photothermal efficiency ($\eta$ ~40%). The photothermal performance increased in the order of $Ru^{3+}$–TA < $V^{3+}$–TA < $Fe^{3+}$–TA under 660 nm irradiation, which correlated to the color darkness of the assembly solution. Furthermore, PNV@$Fe^{3+}$–TA were applied in tumor-specific photoactivated PTT, photothermal imaging (PTI), photoacoustic imaging (PAI), and T1-weighted MRI (Figure 18a–e). PNV@$Fe^{3+}$–TA were endowed with T2-MRI imaging capability by additionally doping with $Mn^{2+}$ (Figure 18e) and with near-infrared fluorescence imaging capability by encapsulating hydrophilic NIR fluoroprobes (Figure 18f).[124] In addition to natural polyphenols, there are growing interests in synthesized phenolic compounds to form multifunctional MPNs due to their high physiological stability and bioavailability. Dai and co-workers designed a range of progressive therapeutic systems for cancer based on the coordination interactions of metal ions (e.g., $Fe^{3+}$) with catechol-modified PEG and PG-modified platinum prodrugs.[143,178,333] In addition, MPN-based NPs conjugated with $^{89}Zr$ or $^{64}Cu$ were applied for PET imaging.[143,179,334] As the $Gd^{3+}$ was encapsulated and chelated with polyphenols, MPN-based NPs were used as an excellent T1-weighted MRI contrast agent for monitoring acidic

tumor microenvironments.[334] Chelating hafnium with phenolic agents would be promising for MPN-based NPs as nano-radiosensitizers to improve radiotherapy performance.[335]

$Fe^{3+}$–phenolic complexes with different phenolic structures of non-*ortho*-substituted phenol (nophenol), catechol (odiphenol), and PG (otriphenol) moieties were synthesized, and their effects on particle size, absorption in the NIR region, and PTT and PAI properties were evaluated.[336] The $Fe^{3+}$–catechol and $Fe^{3+}$–PG complexes displayed higher PTT and PAI performance than $Fe^{3+}$–nophenol complexes, suggesting that at least one vicinal diol group is necessary to construct $Fe^{3+}$–phenolic complexes for PTT and PAI applications. To date, a variety of metal–phenolic nanomaterials have been widely designed for treatment of cancer and many other diseases, indicated their potential biomedical applications in various diagnostic and therapeutic applications.[221,329,337,338]

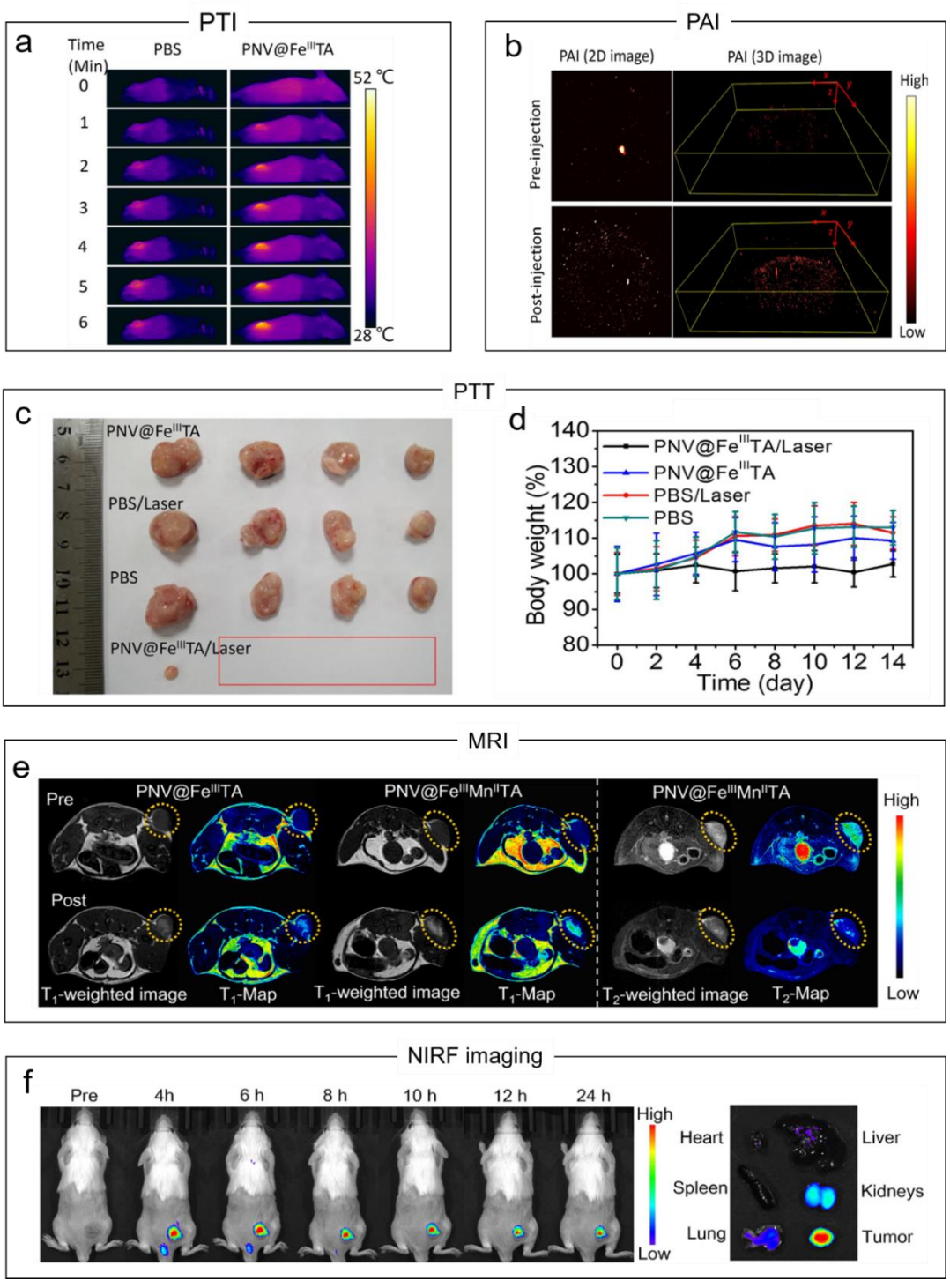


**Figure 18.** Application of PNV@$Fe^{3+}$–TA in (a) PTI, (b) PAI, (c, d) PTT in vivo, (e) MRI in the presence of $Mn^{2+}$, and (f) NIRF imaging of tumor and major organs with NIR fluoroprobes. Adapted with permission from ref 124. Copyright 2018 American Chemical Society.

### 7.1.2. Antibacterial

Metals (such as V, Ti, Cr, Co, Ni, Cu, Zn, Tb, W, Ag, Cd, Au, and Hg) have been used in various forms as antimicrobials for centuries.[339] The metal ions released from metal compounds can inhibit the growth of bacteria by breaking through cell walls, binding with intracellular DNA chains, producing ROS, eventually leading to bacterial death.[339] Owing to the importance of preparing antibacterial coatings and the facile incorporation of phenolic nanostructures with metal ions, metal–phenolic materials serve as a versatile platform to transport the desired metals for interaction with bacteria cells. For example, Ag NPs, one of the most commonly used metal antimicrobials, were synthesized on polyphenol or MPN-coated surfaces (e.g., textile) via in situ reduction of $Ag^{+}$ by polyphenols (Figure 19a). Textiles decorated with MPN@Ag NPs exhibited antibacterial activity against Gram-negative bacteria and outperformed a commercial bandage.[274] Transition metal ions coordinated with phenolics have demonstrated their potential as antibacterial coatings for medical devices or implants (Figure 19b); among the transition metal ions studied, $Cu^{2+}$ ions have been the most extensively studied.[340-342] In a representative study, Huang and co-workers harnessed the antibacterial and antithrombotic properties of $Cu^{2+}$ to fabricate metal–phenolic–amine network-based coatings.[341] The $Cu^{2+}$-chelating coatings endowed the polyvinyl chloride tubes with durable and excellent antibacterial performance, as well as the capability to produce the antithrombotic mediator nitric oxide gas in the presence of endogenous *S*-nitrosothiols from blood.[340] This $Cu^{2+}$–phenolic–amine surface functionalization strategy offers a simple and multifunctional solution to complications (e.g., infections, thrombosis) encountered in the use of indwelled blood-contacting biomedical devices.[340,343]

Rare-earth ions ($Re^{3+}$) have also been recently investigated for antibacterial applications (Figure 19c).[344,345] The inhibition effect of microbial growth by $Re^{3+}$ relies on the substitution of $Ca^{2+}$ (with $Re^{3+}$) from the binding sites of the cell membranes. Owing to the high adhesion of phenolic compounds, $Re^{3+}$-containing MPNs show good bioavailability and stability on the surface of cells. In a typical study, catechin (Cat), and $Re^{3+}$ ($La^{3+}$, $Gd^{3+}$, and $Tb^{3+}$) were used for the self-assembly of $Re^{3+}$–Cat NPs. The NPs were coated on the surface of a polyamide membrane to prevent the

adhesion of bacteria and subsequent formation of a biofilm. The $Re^{3+}$–Cat nanocoating showed excellent antibacterial (>90% inhibition activity) and anti-adhesion activities against *Pseudomonas aeruginosa*, as well as good reusability and long-term stability, therefore successfully inhibiting the formation of a biofilm on the polyamide membrane.[344]

In addition, antifouling polymers such as PEG or polycarboxybetaine conjugated with catechol moieties were assembled with metal ions to form antifouling and antimicrobial coatings (Figure 19d).[346,347] The metal ions (e.g., $Fe^{3+}$) not only cross-linked and stabilized the antifouling coatings but also were released to effectively suppress the growth of bacteria. Therefore, MPN-based materials offer an excellent platform to load antibacterial metal NPs and metal ions, as well as antifouling polymers, providing simple, yet effective antibacterial coatings for potential clinical applications.

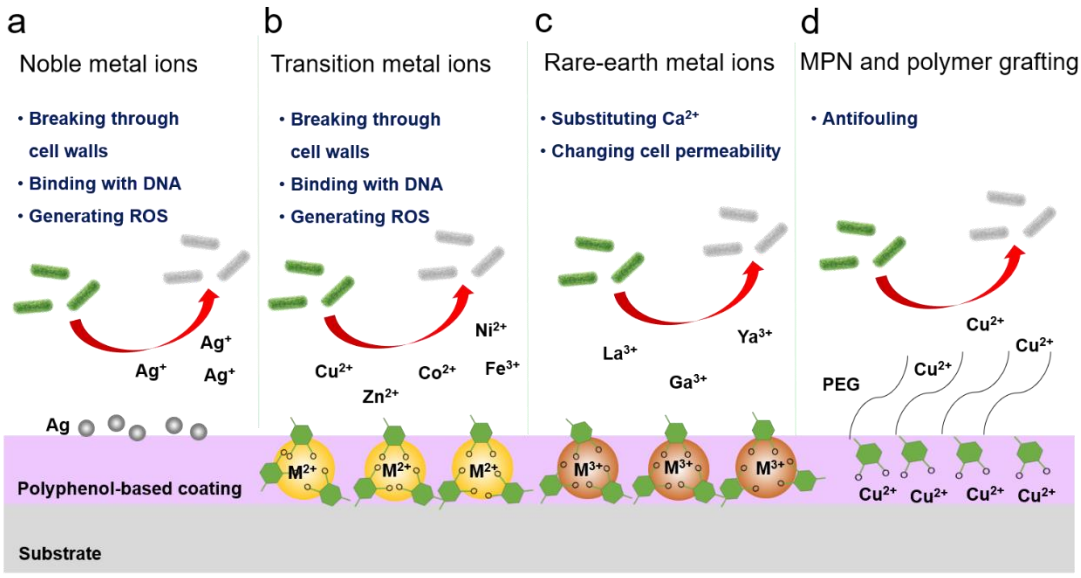


**Figure 19.** Preparation of polyphenol-based antibacterial coatings via (a) the formation of Ag NPs reduced by phenolic compounds, (b) the incorporation of transition metal ions, (c) association with rare-earth metal ions, and (d) conjugation with antifouling polymers.

### 7.1.3. Cell Encapsulation

Abiotic substrates including metal, organic, and inorganic materials can be functionalized by PDA or MPNs, as discussed in recent reviews.[28,324,348] Choi and co-workers have made significant

progress on the formation of biointerfaces using polyphenols or MPNs.[349] In 2011, PDA was first introduced onto living yeast cells, which provided a synthetic strategy for cell–surface modification beyond the traditional layer-by-layer method.[350] MPNs can disassemble under acidic conditions, which offers potential for forming cytoprotective shells that can degrade on demand.[136] Accordingly, the formation of a $Fe^{3+}$–TA shell on yeast cell surfaces that could degrade upon HCl treatment (Figure 20a) was successfully demonstrated. The $Fe^{3+}$–TA shell with average thickness of ~40 nm was observed in the TEM images (Figure 20b).[136] In addition to yeast, bacteria including *E. coli*[18,210] and *Staphylococcus epidermidis*,[18] individual mammalian cells, such as HeLa cells, NIH 3T3 fibroblast cells, Jurkat cells,[209] red blood cells,[351] and PC-12 cells,[210] were successfully coated with $Fe^{3+}$–TA complexes by one-step assembly.

A pericellular $Fe^{3+}$–TA shell was also formed by incubating $Fe^{3+}$-fed yeast cells in a TA solution via biphasic supramolecular self-assembly (Figure 20c).[142] The $Fe^{3+}$–TA shell could protect cells against external UV-C (200–275 nm) irradiation, Ag NPs, lyticase, and ROS. The shells degraded upon addition of acid or ethylenediaminetetraacetic acid.[136,142,210] Recently, it was found that L-ascorbic acid could also lead to the disassembly of MPN shells via the reduction of $Fe^{3+}$, resulting in the formation of loosely bound and readily degradable $Fe^{2+}$ complexes. Thus, the addition of L-ascorbic acid to yeast@$Fe^{3+}$–TA enabled the degradation of the shell under physiological conditions, without any negative effects on cell growth and proliferation.[352] To fabricate multifunctional coatings, magnetic NPs and DNA molecules were incorporated into the $Fe^{3+}$–TA shells for on-demand collection and release of cells (Figure 20d and 20e). In addition, $Fe^{3+}$–TA, $Mn^{2+}$–TA, or $Gd^{3+}$–TA shells on yeast cells could serve as MRI contrast agents, where MRI signals were enhanced with the increase in the concentrations of coated yeast cells (Figure 20f).[210] MPNs with degradable properties and a high affinity for biomolecules provide a versatile platform for cell surface engineering.

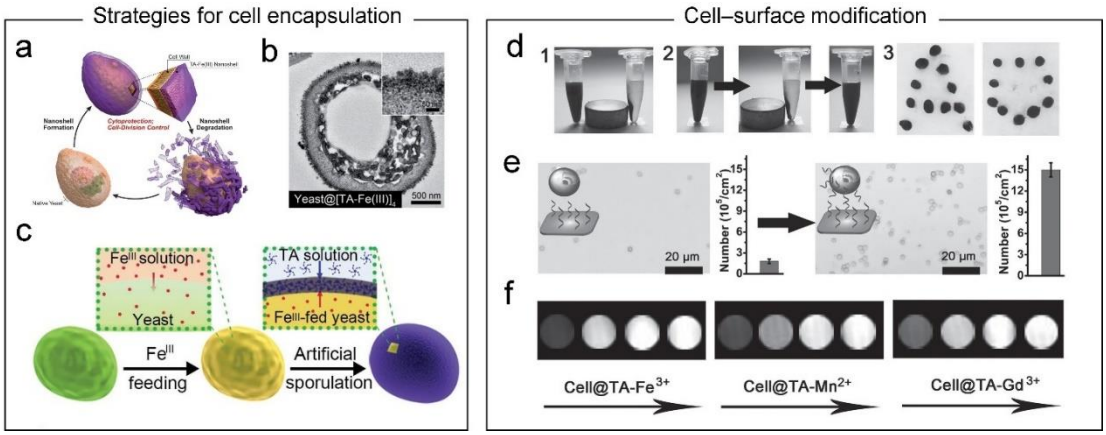


**Figure 20.** (a) Schematic of one-step assembly and degradation of the $Fe^{3+}$–TA shell on individual yeast cell. (b) TEM images of yeast cells with $Fe^{3+}$–TA shells. (c) Schematic of self-responsive $Fe^{3+}$–TA nanoshell formation on a yeast cell via biphasic supramolecular self-assembly. (d) On-demand collection, release and assembly of magnetic NP-modified yeast cells at $Fe^{3+}$–TA shells with magnetic field. (e) Comparison of the number of control yeast cells with $Fe^{3+}$–TA shells and DNA-linked yeast cells with $Fe^{3+}$–TA shells cultured on the complementary DNA-presenting substrate. (f) T1-weighted MRI images of the yeast cells with $Fe^{3+}$–TA shells, yeast cells with $Mn^{2+}$–TA shells, and yeast cells with $Gd^{3+}$–TA shells. (a, b) Adapted with permission from ref 136. Copyright 2014 Wiley-VCH. (c) Adapted with permission from ref 142. Copyright 2017 Wiley-VCH. (d–f) Adapted with permission from ref 210. Copyright 2015 Wiley-VCH.

## 7.2. Mechanical Applications

### 7.2.1. Flexible Electronic Devices

Incorporated metal ions not only direct the assembly of metal–phenolic materials but also can be employed as carriers for electronic conduction.[129,255,261,262,353] Phenol-containing electro-conductive hydrogels offer several advantages in designing bioelectronics, particularly wearable electronic devices, which could significantly facilitate interface affinity with human tissues and improve electronic performances.[129] Lu and co-workers developed self-catalytic and conductive hydrogels composed of metal ions (e.g., $Fe^{3+}$, $Co^{2+}$, $Ni^{3+}$, and $Zr^{3+}$), phenolic molecules (e.g., DA, TA, and TP), and vinyl-containing monomers (e.g., AA and acrylamide).[262] The conductivity of

DA-$Fe^{3+}$-AA hydrogels varied as a function of $Fe^{3+}$ content, reaching a maximum value of 38 S $m^{-1}$ at 1 wt% of $Fe^{3+}$. Moreover, a stronger conductivity was obtained by using higher valence state ions at a given metal ion concentration. Thus, $Al^{3+}$ and $Fe^{3+}$ have typically been chosen to endow hydrogels with conductivity properties.[354] The resulting hydrogels were applied for the detection of electrocardiogram and electromyography signals, as well as the facial movements of humans (Figure 21a and 21b).[262] The optical transparency of bioelectronics is another essential feature for wearable electronic devices. Improved transparency was achieved by fabricating ultrathin hydrogels,[255] as well as using metal ions with empty or filled d orbitals, such as $Al^{3+}$, $Ga^{3+}$, and $In^{3+}$, which formed lighter colored hydrogels.[57,354] Antifreezing and moisture retention properties are also essential and broaden the extreme environment adaptability and service life of hydrogel sensors. To achieve extreme environmental stability of hydrogel sensors, an organohydrogel-based electronic device was developed using TA-coated talc, $Al^{3+}$, and polyvinyl alcohol in ethylene glycol/$H_2O$.[354]

Hydrogels with high conductivity are used as implantable bioelectronics in tissue engineering to enhance signal transmission among cells.[263,353,355] A conducting polymer hydrogel fabricated from polypyrrole, TA, and $Fe^{3+}$ exhibited a high conductivity of 0.05–0.18 S $cm^{-1}$.[263] In general, $Fe^{3+}$ assisted the gelation process via promoting in situ polymerization of pyrrole and interacted with TA to form ionically cross-linked networks. The adhesive hydrogels with excellent electroactivity could activate endogenous neural stem cell neurogenesis in the lesion area (Figure 21c), thus promoting spinal cord injury recovery by restoring the interrupted spinal circuit. Metal–phenolic hydrogels with excellent self-adhesiveness and biocompatibility have been applied in the design of a wide variety of bioelectronics, ranging from wearable skin adhesive patches to implantable integrated scaffolds.[129]

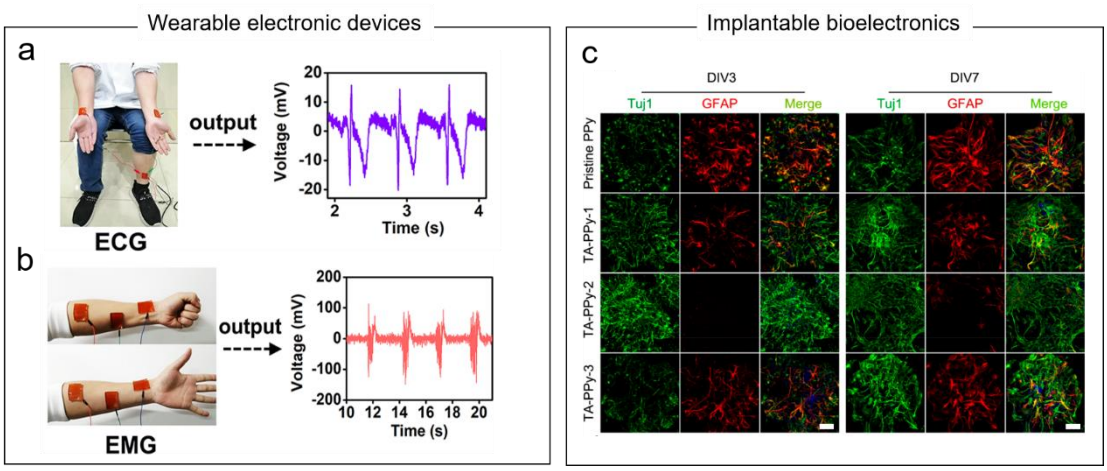


**Figure 21.** Conductive hydrogels acting as electrodes to detect (a) electrocardiogram (ECG) and (b) electromyography (EMG) signals. (c) Neural stem cell differentiation treated by pristine polypyrrole (PPy) and TA–PPy hydrogel ($Fe^{3+}$ acts as an oxidant and cross-linker) samples into neurons and for astrocytes. Scale bar are 50 μm. (a, b) Adapted with permission from ref 262. Copyright 2019 American Chemical Society. (c) Adapted with permission from ref 263. Copyright 2018 American Chemical Society.

### 7.2.2. Underwater Adhesives

Marine organisms (e.g., mussels and sandcastle worms) that are able to secrete complex coacervates underwater provide inspiration for the synthesis of waterproof adhesives.[150,356-358] Pairs generating cation–π interactions possess hydrophobic aromatic rings and hydrophilic cations, which can play a synergetic role in breaching the interfacial water barrier to engineer underwater adhesives.[39,40] Numerous mussel-inspired proteins or analogues, such as cationic rmfp-1,[42] fp-3F,[43] mfp-3S,[46] and mfp-3S analogue (containing 25 amino acids to mimic the native mfp-3S with 45 amino acids),[359] were triggered to form adhesive coacervates in the presence of cations and in the suitable pH environment. For example, the adhesion energy of rmfp-1 measured by SFA was ~5.0 mJ $m^{-2}$ with the addition of 600 mM NaCl in acetic acid solution.[42] Furthermore, those biomimetic adhesives showed diverse mechanical properties including low friction, high viscosity, and low interfacial tension, making them promising candidates for high-performance adhesives in underwater environments. Inspired by sandcastle worm glue proteins, Stewart and co-workers

created a water-borne polyacrylate adhesive containing phosphate, primary amine, catechol sidechains, and divalent cations. The adhesives showed adhesive ability on wet bones.[360,361] The modulus and bond strength increased with increasing concentration of the divalent cation (e.g., $Mg^{2+}$ and $Ca^{2+}$), which reached nearly 40% of the strength of commercial cyanoacrylate adhesives.[361] For potential application in the medical field, a biodegradable complex coacervate was prepared using aminated collagen, polymer with catechol and phosphate residues, and divalent cations (Figure 22a).[362] Increasing the ratio of the divalent cations and covalent cross-linking density of the catechol sidechains resulted in a higher bond strength. The maximum bond strength was 765 kPa in the presence of $Mg^{2+}$ at 1 wt%, which was more than twice the bond strength of *Phragmatopoma californica* glue.[362] When incubated with osteoblastic cells, the adhesives showed negligible cytotoxicity.[363] In cranial fracture rats, the adhesive fragments were associated with osteocytes and could hold wet bones together within the craniotomy region over 12 weeks (Figure 22b).[363] Furthermore, the adhesives were used as fetal membrane patches to seal iatrogenic defects of fetal membranes in an aqueous environment.[364]

MPN-based adhesive hydrogels for wet substrates and their applications have also been reported and reviewed in various fields such as tissue engineering, surgical glues, drug delivery, surface modification, supercapacitors, and catalysis.[19,246,365-369] Furthermore catechol-containing polymers are viable alternative underwater adhesives using metal ions as cross-linkers. Figure 22c shows a schematic of underwater adhesion displayed by adhesive polymers; the polymers are dissolved in organic solvents and applied onto a substrate underwater together with cross-linkers (e.g., $FeCl_3$). The adhesive polymer based on a catechol-modified PVP backbone exhibited bonding strength of ~0.74 MPa under wet conditions.[370] The bonding strength increased with the addition of $FeCl_3$, reaching a maximum bonding strength of 1.63 MPa (average 1.33 MPa) at an optimal $Fe^{3+}$-to-catechol molar ratio of 1:1.[370] The effect of cross-linker type (i.e., $FeCl_3$, iron(III) acetonylacetonate, $KMnO_4$, and $[(C_4H_9)_4N]IO_4$) on bonding strength was also investigated for poly(dopamine-*alt*-2,2-bis(4-glycidyloxyphenyl)propane) (poly(DA-*a*-BGOP)) copolymers. The highest bonding strength (average 0.57 MPa) was obtained by using $FeCl_3$ and iron

acetylacetonate), demonstrating that $Fe^{3+}$ was important toward realizing high underwater adhesive properties.[371] Under optimized formulation parameters (i.e., $Fe^{3+}$-to-catechol groups molar ratio of 1:3 and polymer concentration of 0.45 g $mL^{-1}$), poly(DA-*a*-BGOP) exhibited a dry-state bonding strength as high as 16.39 ± 2.13 MPa, and an underwater bonding strength of 0.91 ± 0.08 MPa on stainless steel substrates, which were higher than that of commercial glues, such as cyanoacrylates (≈ 0) and epoxy (0.23 ± 0.18 MPa) in an underwater condition.[371] Maximum adhesion strength was obtained at a different optimal $Fe^{3+}$-to-catechol molar ratio of 1:3[371] from that reported previously.[370] The different optimal ratio obtained may be attributed to differences in the polymer backbones displaying different polarity and hydrophobic/hydrophilic and cationic/anionic units and so on. For instance, Mu et al. investigated the underwater adhesive strength of four mussel-inspired polymers with similar catechol contents and molecular weights, but different amide/lactam contents, in the presence of same dosage of the cross-linker (i.e., $FeCl_3$). It was found that the underwater bonding strength increased with the increase in the amide/lactam content, which correlates to the polarity of polymers (Figure 22d).[372] The contribution of polarity of polymer backbones on bonding strength provides some guidance for designing novel underwater adhesives.

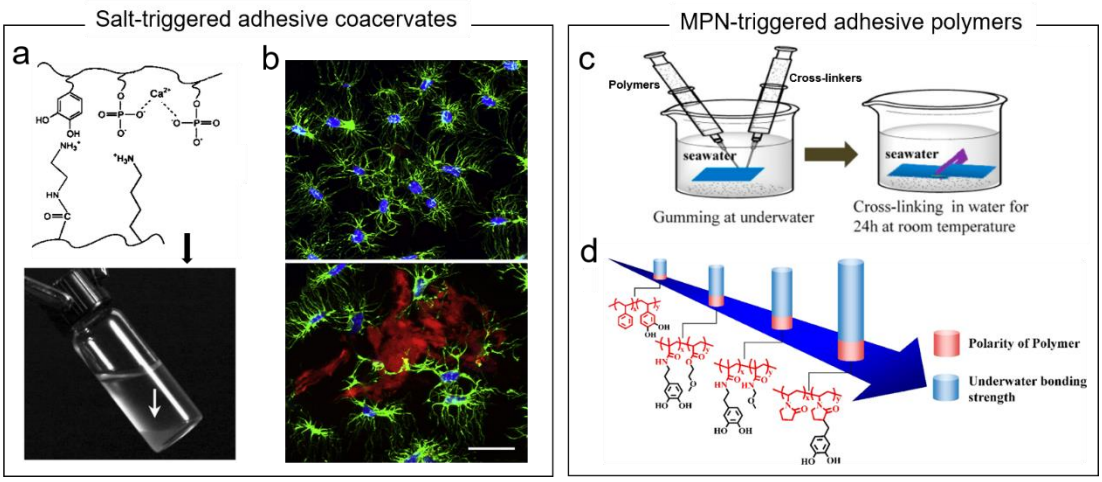


**Figure 22.** (a) Adhesives composed of polymers with catechol and phosphate residues, aminated collagen, and divalent cations. Adapted with permission from ref 362. Copyright 2010 Wiley-VCH. (b) Confocal laser scanning microscopy images of osteocytes in normal uninjured rat

calvaria (top) and with adhesive fragments (red) within the craniotomy region at 12 weeks (bottom). Scale bar is 50 μm. Adapted with permission from ref 363. Copyright 2010 Elsevier. (c) Schematic illustration of underwater adhesion of phenolic polymers. (d) Influence of polarity of polymer backbones on underwater bonding strength of mussel-inspired polymers. (c, d) Adapted with permission from ref 372. Copyright 2017 American Chemical Society.

### 7.3. Catalytic and Environmental Applications

#### 7.3.1. Catalysis

The ability to interact with a variety of metals makes phenolic materials attractive candidates as catalysts. Metal–organic catalysts are promising in environmentally benign organic synthesis.[373-375] Owing to the high-efficiency activity and tunable selectivity of nanostructured noble metal ions, the in situ reduction of metal ions by phenolic molecules or MPNs has widely been used to catalyze the reduction of nitroaromatics,[285,289,376-378] as well as the Suzuki–Miyaura coupling reactions[274,277,379] and styrene hydrogenation reactions.[58] For example, PDA-coated graphitic carbon nitride (g-$C_3N_4$) acted as both the reductant and stabilizer in the formation of Au NPs on surfaces.[285] Owing to the synergistic charge-transfer effects of plasmonic Au NPs, the PDA-g-$C_3N_4$@Au nanocatalysts achieved highly efficient reduction of various nitroaromatics (e.g., 2-nitrophenol, 4-dinitrophenol, methyl orange, congo red, and eriochrome black T), showing promising application in the removal of those organic pollutants from wastewater.[285] A redox reaction between DA and $Ag^+$ in solution induced the growth of an Ag shell on Au nanocrystals, which generated core–shell Au@Ag@PDA nanocrystals.[376] The Au@Ag@PDA nanocrystals showed excellent catalytic activity in the reduction of 4-nitrophenol to 4-aminopheol by $NaBH_4$ (Figure 23a). The decomposition of organic dyes (e.g., crystal violet, alizarin red S, malachite green, and rhodamine B) by singlet oxygen ($^1O_2$) was also reported. $^1O_2$ was generated by metal ion-mediated catechol oxidation (Figure 23b).[380] The Suzuki–Miyaura cross-coupling reaction is one of the most effective methods for synthesizing pharmaceuticals and biologically active compounds[277] and generally employs Pd NPs as the coupling catalyst. However, these reactions

are performed under organic conditions, which require laborious and time-consuming protocols to remove the residual organic solvents.[274,277] To circumvent these issues, Pd NPs were immobilized on PDA-decorated $Fe_3O_4$ or reduced in GA solution, thus allowing the Suzuki–Miyaura coupling reaction to proceed in water instead of organic solvents (Figure 23c).[277,379] The reaction showed >99% conversion in the presence of Pd NPs@$Fe^{3+}$–TA@textiles in water, which displayed high recyclability up to five cycles with negligible activity loss.[274]

### 7.3.2. Water Remediation

Surface modification strategies mediated by phenolics or MPNs provide opportunities for material design to address environmental issues, such as water pollution.[60,245] Considerable efforts have been devoted to purifying industrial wastewater using metal-directed phenolic materials (e.g., membranes and aerogels) for the removal of trace organic contaminants (Figure 23d),[381] heavy metals (Figure 23e),[382-384] degradation of soluble organic dyes,[385,386] inhibition of microorganism growth (Figure 23f),[382] and oil−water separation (Figure 23g).[54,387] For instance, a hydrophilic and underwater superoleophobic polyvinylidene fluoride (PVDF) membrane coated with EGCG and $Ag^+$ displayed a significantly higher permeate flux of 735 L $(m^2\,h)^{-1}$ for diesel-in-water emulsions compared to the uncoated PVDF membrane (0 L $(m^2\,h)^{-1}$).[388] The decomposition of soluble dyes was demonstrated using reduced Ag NPs with visible light photocatalytic activity.[385] TA and transitional metals, including $Ag^+$, $Co^{2+}$, $Ni^{2+}$, $Cu^{2+}$, and $Fe^{3+}$, have been successfully applied to prepare highly efficient membranes for wastewater remediation.[389] In particular, 3D porous structures were proven to be promising in oil–water separation. They could absorb and collect insoluble oil from water.[390] Ag–TA NP-functionalized sponges exhibited a high absorption capacity of 73–175× of their own weight for oils/organic solvents.[281] To improve the exposed area of adsorbents, MOFs were incorporated into $Fe^{3+}$–TA films. The resulting films featured superhydrophobic surfaces with a water contact angle greater than 150°.[216,391] A hydrophilic hierarchical hybrid layer derived from$Ti^{4+}$–TA networks and ZIF-8 endowed PVDF membranes with robust superhydrophilicity, underwater superoleophobicity, and high-efficiency oil/water

emulsion separation capability; the resulting membranes showed a high oil rejection rate (above 99.4%) and recyclable antifouling properties.[392]

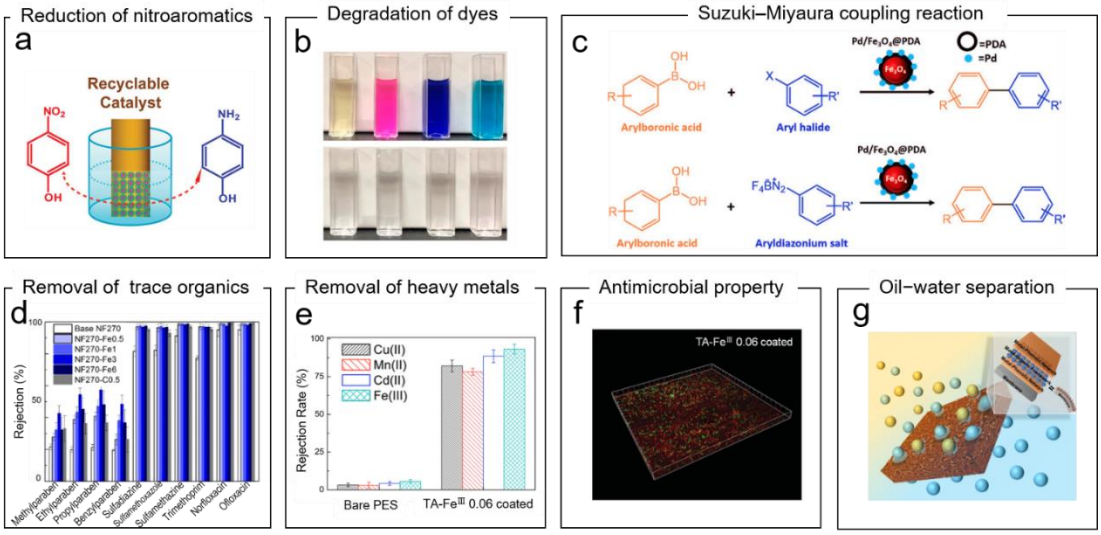


**Figure 23.** (a) Recyclable Au@Ag@PDA NPs for the catalytic reduction of nitroaromatics. Adapted with permission from ref 376. Copyright 2014 Wiley-VCH. (b) Photographs of dye solutions before and after incubation with catechol-containing $Fe_3O_4$ NPs. Adapted with permission from ref 380. Copyright 2020 American Chemical Society. (c) $Pd/Fe_3O_4$@PDA nanocatalysts for Suzuki–Miyaura cross-coupling reaction. Adapted with permission from ref 313. Copyright 2020 Wiley-VCH. (d) Rejection values of trace organic contaminants for $Fe^{3+}$–TA-coated membranes. Adapted with permission from ref 381. Copyright 2017 American Chemical Society. (e) Rejection rates of heavy metal ions of $Fe^{3+}$–TA-coated poly(ether sulfone) (PES) membranes. (f) Antimicrobial property of $Fe^{3+}$–TA-coated PES membrane. (e, f) Adapted with permission from ref 382. Copyright 2015 Wiley-VCH. (g) Oil–water separation capability of $Ti^{4+}$–TA/ZIF-8/$Ti^{4+}$–TA-modified PVDF membrane. Adapted with permission from ref 392. Copyright 2020 American Chemical Society.

### 7.4. Emerging Applications

Functional assemblies formed from interactions between metal ions and phenolic compounds have attracted increasing interest in many emerging fields. For instance, although iron gall inks

have been used historically, a reformative visual information storage strategy was recently developed that involved surface modification of substrates with polyphenols and subsequently with various metal ions (e.g., $Cu^{2+}$, $Fe^{3+}$, and $Ti^{4+}$) as inks (Figure 24a).[316] The use of LMs as inks for surface patterning is a facile approach to develop functional substrates. Furthermore, the adhesive ink obtained by mixing TA and EGaIn enabled patterning on diverse substrates and broadened the interactions of LMs with substrate surfaces.[228] These inks not only were applied for hand-written texts using a ballpoint pen but also achieved complex conductive patterns using an automated setup (Figure 24b). The application of MPNs as hair dyes was also examined owing to strong interactions between phenolic molecules and hair surface proteins driven by hydrophobic interactions and hydrogen bonds. In addition, the desired colors were achieved by adjusting the type of metal ions.[393,394] The experimental results showed that $Fe^{2+}$ was superior for dyeing black hair to other metal ions, including commonly used $Fe^{3+}$ (Figure 24c).[393-396] The superior performance was attributed to the slow oxidation process of $Fe^{2+}$ to $Fe^{3+}$, which provides additional opportunities for the adjustment of MPN conformations on the hair surfaces.[393] Recently, an oil-in-water emulsion by homogenizing a mixture of polyphenols, $Fe^{2+}$, and natural oil was used for black hair dyeing.[396] The $Fe^{2+}$–polyphenol complexes were used to stabilize the emulsion and for hair dyeing, whereas the natural oil was used to strengthen the hair. The advanced hair dyes in a form of surfactant-free emulsions presented distinct advantages in haircare applications.[396] The development of suitable hair dyes featuring biocompatibility, stable ingredients, and color resistance to detergents, and that are easy to use is desirable.

In the agriculture area, various smart delivery systems have been developed to transport micronutrients to plants through foliar uptake. To enhance the load capability of poly(allylamine) hydrochloride microgels for micronutrients (e.g., metal ions), the surface of the microgels was modified with 2,3-dihydroxybenzoic acid (DHBA) to enable binding to $Fe^{3+}$ (Figure 24d).[315] The $Fe^{3+}$–DHBA microgel provided a controllable and sustainable release of the nutrient $Fe^{3+}$ to the iron-deficient cucumber leaf surfaces (Figure 24e). As a result, the leaf showed significant “re-greening” and increased chlorophyll content. Excessive aluminum in soils inhibits growth and

function of the plant roots. Polyphenols have been identified as effective aluminum-detoxifying agents due to their high affinity for aluminum.[397] Exogenously added polyphenols in culture solution is an easy way to achieve aluminum resistance in plants. PEG/dextran phase-separated microdroplets containing $Fe^{3+}$–TA complexes were prepared and used for protein condensation owing to the high affinity between polyphenols and proteins.[398] Bovine serum albumin in the PEG phase was collected into small coacervate particles and TA moved into the PEG phase from the dextran phase in the microdroplets (Figure 24f). Another example of using the specific interactions between polyphenols and biomolecules is via patterning MPNs on proteins, lipids, nucleic acids, polysaccharides, and fingerprints.[317] The MPNs grew preferentially on biomolecule patterns. By subsequently reducing Ag NPs on the deposited MPNs in situ, patterns were visualized.[317] Inspired by this visualization method, the latent fingerprint patterns became visible after MPN growth. Furthermore, visualization of the fingerprint pattern was enhanced through Ag NP formation (Figure 24g). This platform has potential application in relevant areas of forensics and biomedicine.[317]

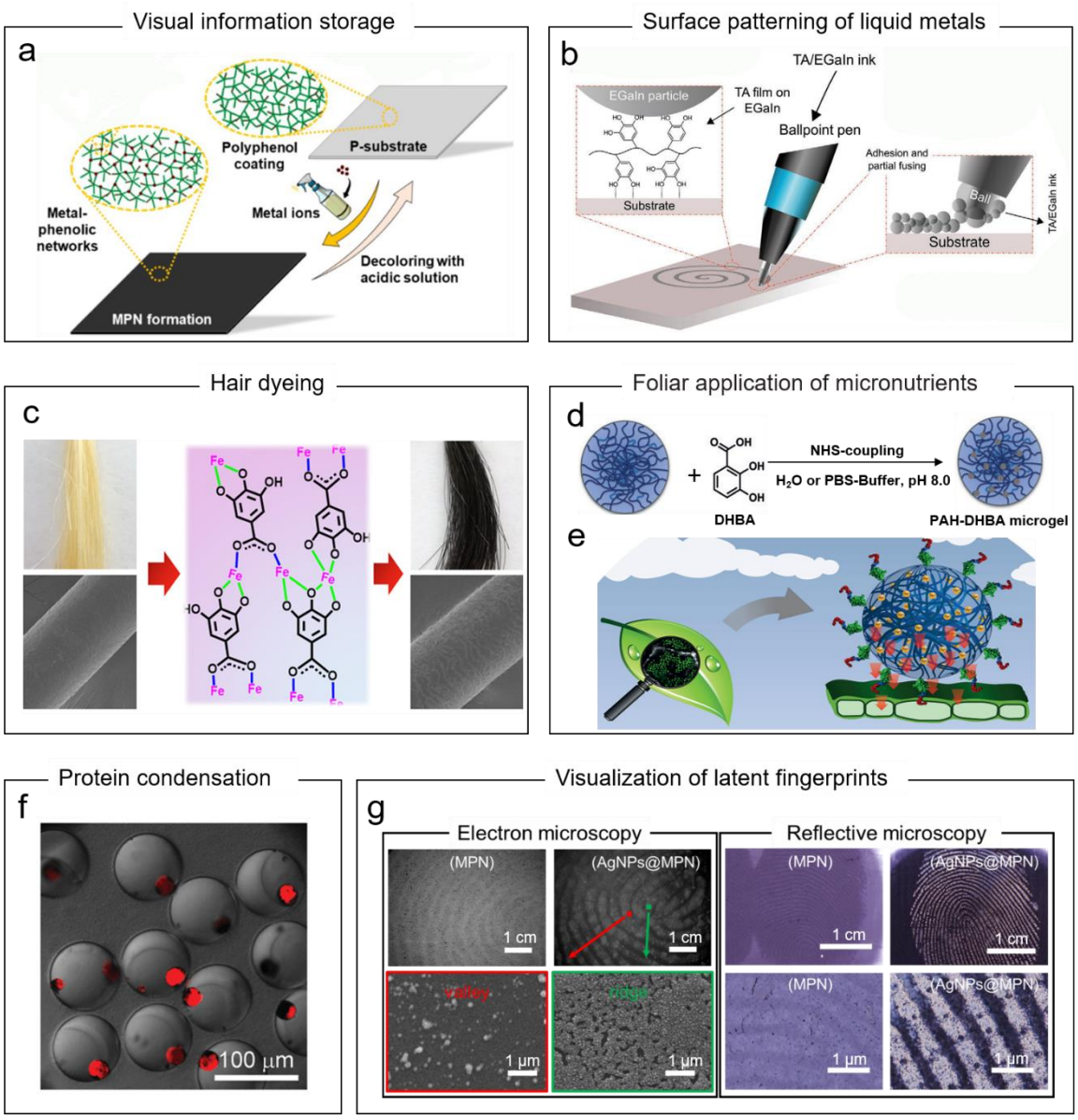


**Figure 24.** (a) Metal ions used as inks on polyphenol-coated substrates for visual information storage via the formation of MPNs. Adapted with permission from ref 316. Copyright 2019 American Chemical Society. (b) Writing process using a ballpoint pen filled with TA/EGaIn inks. Adapted with permission from ref 228. Copyright 2020 Wiley-VCH. (c) Optical images and SEM images of native hair (left) and metal–phenolic network (middle)-coated hair (right). Adapted with permission from ref 393. Copyright 2020 American Chemical Society. (d) Functionalization of microgels with DHBA. N-hydroxysuccinimide (NHS); poly(allylamine) hydrochloride (PAH). (e) Functional microgel-based fertilizers for controlled foliar delivery of nutrients to plants. (d, e)

Adapted with permission from ref 315. Copyright 2017 Wiley-VCH. (f) Fe3+–TA coacervate particles in PEG/dextran microdroplets for protein condensation. Adapted with permission from ref 398. Copyright 2019 Royal Society of Chemistry. (g) SEM and reflectance microscopy images of the films before and after the formation of Ag NPs on MPN-coated fingerprints. Adapted with permission from ref 317. Copyright 2020 Wiley-VCH.

## 8. Conclusions and Outlook

Exploiting the interactions between metal ions and phenolic compounds has proved to be a versatile strategy to engineer functional materials. Cation–π interactions play important roles in protein structures and molecular recognition, which present advantages in designing materials for underwater adhesion.[39,96] MPNs and metalloid–phenolic interactions both involve dynamic covalent bonds and are widely used in the fabrication of various functional materials such as NPs, hydrogels, and films. In addition, MPN coatings, as a versatile surface modification platform, are promising for engineering materials with desired properties that are conferred by the metals and phenolic building blocks.[19] In situ reduction reactions between noble metal ions and phenolic conjugates are not only relevant to chemical catalysis but also a useful strategy for constructing hierarchal structures.[268,269,272] Despite the significant achievements that have been attained in engineering metal–phenolic materials, there are still ample opportunities for further improvement in future research.

(i) Elucidation of how the physicochemical properties (e.g., size, valence state, electron configuration, reduction potential, and stability constant) of metal ions alter the stability and responsiveness of metal–phenolic interactions is an essential fundamental question to address. In addition, a thorough understanding of the fundamental mechanisms (e.g., kinetics and dynamics) of the different interactions between metal ions and phenolic compounds is desirable.

(ii) Expanding the choice of phenol derivatives and metallic building blocks offers a wide range of possibilities for developing novel metal–phenolic assemblies, and subsequently realizing synergistic or emergent properties.[148] For example, cation–π interactions reported to date are typically limited to catechols, phenols, and benzene rings. Alternatively, PG-containing molecules

could potentially provide potent binding sites for cations but are yet to be reported for materials engineering based on cation–π interactions. Most MPN-based supramolecular structures are mainly formed by first-row transition metal ions and phenolics. Exploring other transition metal ions (e.g., late transition metals and rare-earth metals) as building blocks is expected to broaden the scope of MPNs and endow MPNs with specific properties.

(iii) Incorporation of new characterization (e.g., X-ray absorption fine structure spectroscopy) and computer simulations to characterize supramolecular metal–phenolic structures at the molecular or atomic level, especially amorphous assemblies, will shed light on the assembly/disassembly mechanisms of metal–phenolic materials. Further exploiting force techniques (e.g., SFA and single-molecule force spectroscopy based on AFM) to probe the energetics and nanomechanics of various metal–phenolic interactions will be important for further manipulation of metal–phenolic materials in a controlled manner.

In summary, the developments of metal–phenolic materials in the past decade represent significant advances. Powerful analytical techniques, computational chemistry, and advanced processing technologies are expected to further elucidate the relationships of structure–property–function in the formation of metal ion-directed phenolic materials. We envision that a comprehensive understanding of the effects of metal ions on diverse interactions in metal–phenolic materials will provide further advances and opportunities in promising applications.

## AUTHOR INFORMATION


### Corresponding Authors

*jwcui@sdu.edu.cn (Jiwei Cui)

*fcaruso@unimelb.edu.au (Frank Caruso)

*jhao@sdu.edu.cn (Jingcheng Hao)


### Notes

The authors declare no competing interest.

Biographies

Huimin Geng received her Ph.D. in Materials Science and Engineering from Beijing Institute of Technology in 2018. She is currently a postdoctoral fellow in the School of Chemistry and Chemical Engineering at Shandong University. Her research interests are focused on the engineering of functional hydrogels for biomedical applications.

Qi-Zhi Zhong received his Ph.D. in Chemical Engineering from The University of Melbourne in 2021 under the supervision of Prof. Frank Caruso. He is currently conducting his postdoctoral research at the University of Bristol under the supervision of Prof. Stephen Mann. His research interests focus on protocell assembly and functional porous materials.

Jianhua Li is a Professor in the School of Stomatology at Shandong University. He received his Ph.D. from Shandong University in 2016. His research focuses on functional biomaterials for exploration of their applications in cell fate control, nanomedicine, and tissue engineering.

Zhixing Lin received his Ph.D. in 2021, researching metal–phenolic networks, under the supervision of Prof. Frank Caruso at The University of Melbourne and is currently a Research Fellow in Prof. Frank Caruso's group. His research is focused on exploring various applications of metal–organic materials.

Jiwei Cui is a Professor in the School of Chemistry and Chemical Engineering at Shandong University. He received his Ph.D. in Colloid and Interface Chemistry from Shandong University in 2010. His research interests include colloidal assembly, interface engineering, bio–nano interactions, and therapeutic delivery.

Frank Caruso is a Melbourne Laureate Professor and an NHMRC Senior Principal Research Fellow at The University of Melbourne. He received his Ph.D. in 1994 from The University of Melbourne and thereafter conducted postdoctoral research at CSIRO Division of Chemicals and

Polymers. In 1997–2002, he was a Humboldt Research Fellow and group leader at the Max Planck Institute of Colloids and Interfaces (Germany). Since 2003, he has been a Professor at The University of Melbourne and has held ARC Federation and ARC Australian Laureate Fellowships. His research is focused on developing advanced nano- and biomaterials for biotechnology and medicine.

Jingcheng Hao is a Professor in the School of Chemistry and Chemical Engineering at Shandong University. He received his Ph.D. from Lanzhou Institute of Chemical Physics, Chinese Academy of Sciences in 1995. His research is focused on colloid and interface science, including surfactants in solution and self-assembly at all scales in bulk solutions and at interfaces.

## ACKNOWLEDGMENTS

The work was funded by the National Natural Science Foundation of China (21872085, 22072075), Innovation Project of Jinan Science and Technology Bureau (2020GXRC022), Project for Scientific Research Innovation Team of Young Scholar in Colleges and Universities of Shandong Province (2020KJC001), and Natural Science Foundation of Shandong Province (ZR2019BB056). F.C. acknowledges support from the Australian Research Council under the Discovery Project scheme (DP200100713).

## ABBREVIATIONS

•OH: hydroxyl radicals; $^1O_2$: singlet oxygen; 2D: two-dimensional; 3D: three-dimensional; 4-BP: 4-bromophenol; 4-CP: 4-chlorophenol; AA: acrylic acid; Ach: nicotinic acetylcholine; AFM: atomic force microscopy; AP: acetaminophen; APS: ammonium persulfate; BPNs: boronate–phenolic networks; BTZ: bortezomib; BX: boroxole; CA: cholic acid; Cat: catechin; CC: cyclodextrin catechol; Ce6: chlorin e6; CG: cyclodextrin galloyl; CP: Random polymer conjugated with catechol moieties; cryo-TEM: cryogenic transmission electron microscopy; CT: catalase; DA: dopamine; Den–DOX: dendrimer–doxorubicin; DHBA: 2,3-dihydroxybenzoic acid; DOPA: L-3,4-dihydroxyphenylalanine; *E. coli*.: *Escherichia coli*; EA: ellagic acid; ECG: electrocardiogram;

EGaIn: eutectic gallium–indium alloy; EGCG: epigallocatechin-3-*O*-gallate; EMG: electromyography; EPR: electron paramagnetic resonance; $E_Y$: Young's modulus; fp-3F: foot protein type-3 fast variant; FPBA: 2-fluorophenylboronic acid; *G′*: storage modulus; *G″*: loss modulus; GA: gallic acid; g-$C_3N_4$: graphitic carbon nitride; GePNs: germanium–phenolic networks; GFP: green fluorescent protein; GOx: glucose oxidase; HA: hyaluronic acid; HHB: hexahydroxybenzene; HHTP: 2,3,6,7,10,11-hexahydroxytriphenylene; hMSCs: human mesenchymal stem cells; HQ: hydroquinone; HRP: peroxidase from horseradish; ICG: indocyanine green; IRMPD: infrared multiple photon dissociation; LbL: layer-by-layer; LM: liquid metal; mcfp-1: *Mytilus californianus* foot protein-1; MF: melamine formaldehyde; mfp-3S: mussel foot protein-3S; mfp-5: mussel foot protein 5; MOF: metal–organic framework; MPN: metal–phenolic network; MRI: magnetic resonance imaging; Myr: myricetin; NCM: non-crosslinked micelles; ND: nitro-dopamine; NHS: N-hydroxysuccinimide; NIR-II: second near-infrared; NIRF: near-infrared resonance fluorescence; NP: nanoparticle; P4VP: poly(4-vinylphenol); PAA: polyacrylic acid; PAH: poly(allylamine) hydrochloride; PAI: photoacoustic imaging; PBS: phosphate-buffered saline; PC: pyrocatechol; PDA: polydopamine; PDMS: polydimethylsiloxane; PEG: poly(ethylene glycol); PES: poly(ether sulfone); PET: positron emission tomography; PG: pyrogallol; Phe: Phenylalanine; PLGA: poly(lactic-*co*-glycolic acid); PLG-*g*-mPEG: poly(L-glutamic acid)-*graft*-methoxypoly(ethylene glycol); PLL: poly-L-lysine; PMMA: poly(methyl methacrylate); PNV: poly(lactic-*co*-glycolic acid)-based nanovesicle; $PO_4$-DHB: 2-*O*-phosphorylethanol 2,3-hydroxybenzamide; POD: peroxidase; poly(DA-*a*-BGOP): poly(dopamine-*alt*-2,2-bis(4-glycidyloxyphenyl)propane); PPy: polypyrrole; PS: polystyrene; PS-*b*-PEO: polystyrene-*block*-poly(ethylene oxide); PTI: photothermal imaging; PTrp: polytryptophan; PTT: photothermal therapy; PTX: paclitaxel; PTyr: polytyrosine; PVDF: polyvinylidene fluoride; PVP: polyvinylpyrrolidone; Que: quercetin; rmfp-1: recombinant mussel foot protein-1; ROS: reactive oxygen species; RR: resveratrol; *S. cerevisiae*: *Saccharomyces cerevisiae*; *S. epidermidis*: *Staphylococcus epidermidis*; SEM: scanning electron microscopy; SFA: surface force apparatus; SiPNs: silicate–phenolic networks; TA: tannic acid; Tb-CP: Tb-

coordination polymer; TEA: tetraethylammonium; TEM: transmission electron microscopy; THBQ: tetrahydroxybenzoquinone; TP: tea polyphenol; TyA: tyramine; Tyr: tyrosine; UV–vis: ultraviolet–visible; WBA: Wulff-type-like boronic acid; $W_{co}$: work of adhesion energy per unit area for the symmetric configuration; $W_{ad}$: work of adhesion energy per unit area for the asymmetric configuration; XPS: X-ray photoelectron spectroscopy.

REFERENCES

(1) Khare, E.; Holten-Andersen, N.; Buehler, M. J. Transition-Metal Coordinate Bonds for Bioinspired Macromolecules with Tunable Mechanical Properties. *Nat. Rev. Mater.* **2021**, *6*, 421–436.

(2) Haas, K. L.; Franz, K. J. Application of Metal Coordination Chemistry To Explore and Manipulate Cell Biology. *Chem. Rev.* **2009**, *109*, 4921–4960.

(3) Rozov, A.; Khusainov, I.; El Omari, K.; Duman, R.; Mykhaylyk, V.; Yusupov, M.; Westhof, E.; Wagner, A.; Yusupova, G. Importance of Potassium Ions for Ribosome Structure and Function Revealed by Long-Wavelength X-Ray Diffraction. *Nat. Commun.* **2019**, *10*, 2519.

(4) Österberg, R. Origins of Metal Ions in Biology. *Nature* **1974**, *249*, 382–383.

(5) Holm, R. H.; Kennepohl, P.; Solomon, E. I. Structural and Functional Aspects of Metal Sites in Biology. *Chem. Rev.* **1996**, *96*, 2239–2314.

(6) Ma, S.; Wu, Y.; Zhou, F. Bioinspired Synthetic Wet Adhesives: From Permanent Bonding to Reversible Regulation. *Curr. Opin. Colloid Interface Sci.* **2020**, *47*, 84–98.

(7) Zhang, Z.; Zaworotko, M. J. Template-Directed Synthesis of Metal–Organic Materials. *Chem. Soc. Rev.* **2014**, *43*, 5444–5455.

(8) Carné, A.; Carbonell, C.; Imaz, I.; Maspoch, D. Nanoscale Metal–Organic Materials. *Chem. Soc. Rev.* **2011**, *40*, 291–305.

(9) Lions, F.; Martin, K. V. Tridentate Chelate Compounds. I. *J. Am. Chem. Soc.* **1957**, *79*, 2733–2738.

(10) Sacconi, L.; Paoletti, P.; Maggio, F. Studies in Coördination Chemistry. II. Spectrophotometric Investigation of Some Hydrazidic Tetracovalent Nickel(II) Complexes. *J. Am. Chem. Soc.* **1957**, *79*, 4067–4069.

(11) Courtney, R. C.; Gustafson, R. L.; Westerback, S. J.; Hyytiainen, H.; Chaberek Jr., S. C.; Martell, A. E. Metal Chelate Compounds as Catalysts in the Hydrolysis of Isopropyl Methylphosphonofluoridate and Diisopropylphosphorofluoridate. *J. Am. Chem. Soc.* **1957**, *79*, 3030–3036.

(12) Zhang, H.; Liu, X.; Wu, Y.; Guan, C.; Cheetham, A. K.; Wang, J. MOF-Derived Nanohybrids for Electrocatalysis and Energy Storage: Current Status and Perspectives. *Chem. Commun.* **2018**, *54*, 5268–5288.

(13) Wang, Q.; Astruc, D. State of the Art and Prospects in Metal–Organic Framework (MOF)-Based and MOF-Derived Nanocatalysis. *Chem. Rev.* **2020**, *120*, 1438–1511.

(14) Falcaro, P.; Ricco, R.; Doherty, C. M.; Liang, K.; Hill, A. J.; Styles, M. J. MOF Positioning Technology and Device Fabrication. *Chem. Soc. Rev.* **2014**, *43*, 5513–5560.

(15) Gao, P.; Chen, Y.; Pan, W.; Li, N.; Liu, Z.; Tang, B. Antitumor Agents Based on Metal–Organic Frameworks. *Angew. Chem. Int. Ed.* **2021**, *60*, 16763–16776.

(16) Riccò, R.; Liang, W.; Li, S.; Gassensmith, J. J.; Caruso, F.; Doonan, C.; Falcaro, P. Metal–Organic Frameworks for Cell and Virus Biology: A Perspective. *ACS Nano* **2018**, *12*, 13–23.

(17) Zou, R.; Wang, Q.; Wu, J.; Wu, J.; Schmuck, C.; Tian, H. Peptide Self-Assembly Triggered by Metal Ions. *Chem. Soc. Rev.* **2015**, *44*, 5200–5219.

(18) Ejima, H.; Richardson, J. J.; Liang, K.; Best, J. P.; van Koeverden, M. P.; Such, G. K.; Cui, J.; Caruso, F. One-Step Assembly of Coordination Complexes for Versatile Film and Particle Engineering. *Science* **2013**, *341*, 154–157.

(19) Ejima, H.; Richardson, J. J.; Caruso, F. Metal–Phenolic Networks as a Versatile Platform to Engineer Nanomaterials and Biointerfaces. *Nano Today* **2017**, *12*, 136–148.

(20) Quideau, S.; Deffieux, D.; Douat-Casassus, C.; Pouységu, L. Plant Polyphenols: Chemical Properties, Biological Activities, and Synthesis. *Angew. Chem. Int. Ed.* **2011**, *50*, 586–621.

(21) Dougherty, D. A. Cation–π Interactions in Chemistry and Biology: A New View of Benzene, Phe, Tyr, and Trp. *Science* **1996**, *271*, 163–168.

(22) Ma, J. C.; Dougherty, D. A. The Cation–π Interaction. *Chem. Rev.* **1997**, *97*, 1303–1324.

(23) Harrington, M. J.; Masic, A.; Holten-Andersen, N.; Waite, J. H.; Fratzl, P. Iron-Clad Fibers: A Metal-Based Biological Strategy for Hard Flexible Coatings. *Science* **2010**, *328*, 216–220.

(24) Lee, H.; Kim, W. I.; Youn, W.; Park, T.; Lee, S.; Kim, T.-S.; Mano, J. F.; Choi, I. S. Iron Gall Ink Revisited: In Situ Oxidation of Fe(II)–Tannin Complex for Fluidic-Interface Engineering. *Adv. Mater.* **2018**, *30*, 1805091.

(25) Jacob, J. A.; Mahal, H. S.; Biswas, N.; Mukherjee, T.; Kapoor, S. Role of Phenol Derivatives in the Formation of Silver Nanoparticles. *Langumir* **2008**, *24*, 528–533.

(26) Lü, J.; Ma, R.; Shi, L. Advances of Phenylboronic Acid-Containing Materials in Drug Delivery. *Chin. Sci. Bull.* **2016**, *61*, 2113–2123.

(27) Zhou, J.; Lin, Z.; Ju, Y.; Rahim, M. A.; Richardson, J. J.; Caruso, F. Polyphenol-Mediated Assembly for Particle Engineering. *Acc. Chem. Res.* **2020**, *53*, 1269–1278.

(28) Rahim, M. A.; Kristufek, S. L.; Pan, S.; Richardson, J. J.; Caruso, F. Phenolic Building Blocks for the Assembly of Functional Materials. *Angew. Chem. Int. Ed.* **2019**, *58*, 1904–1927.

(29) Mahadevi, A. S.; Sastry, G. N. Cation–π Interaction: Its Role and Relevance in Chemistry, Biology, and Material Science. *Chem. Rev.* **2013**, *113*, 2100–2138.

(30) Guo, J.; Ping, Y.; Ejima, H.; Alt, K.; Meissner, M.; Richardson, J. J.; Yan, Y.; Peter, K.; von Elverfeldt, D.; Hagemeyer, C. E.; et al. Engineering Multifunctional Capsules through the Assembly of Metal–Phenolic Networks. *Angew. Chem. Int. Ed.* **2014**, *53*, 5546–5551.

(31) Black, K. C. L.; Liu, Z.; Messersmith, P. B. Catechol Redox Induced Formation of Metal Core–Polymer Shell Nanoparticles. *Chem. Mater.* **2011**, *23*, 1130–1135.

(32) Mecozzi, S.; West, A. P., Jr.; Dougherty, D. A. Cation–π Interactions in Aromatics of Biological and Medicinal Interest: Electrostatic Potential Surfaces as a Useful Qualitative Guide. *Proc. Natl. Acad. Sci. U. S. A.* **1996**, *93*, 10566–10571.

(33) Hwang, D. S.; Zeng, H.; Lu, Q.; Israelachvili, J.; Waite, J. H. Adhesion Mechanism in a DOPA-Deficient Foot Protein from Green Mussels. *Soft Matter* **2012**, *8*, 5640–5648.

(34) Lu, Q.; Hwang, D. S.; Liu, Y.; Zeng, H. Molecular Interactions of Mussel Protective Coating Protein, mcfp-1, from *Mytilus Californianus*. *Biomaterials* **2012**, *33*, 1903–1911.

(35) Dougherty, D. A. The Cation–π Interaction. *Acc. Chem. Res.* **2013**, *46*, 885–893.

(36) Xiang, L.; Zhang, J.; Wang, W.; Gong, L.; Zhang, L.; Yan, B.; Zeng, H. Nanomechanics of π–Cation–π Interaction with Implications for Bio-Inspired Wet Adhesion. *Acta Biomater.* **2020**, *117*, 294–301.

(37) Liu, T.; Zhu, W.; Gu, J.; Shen, J.; Luo, X.; Chen, G.; Puah, C. M.; Silman, I.; Chen, K.; Sussman, J. L.; et al. Additivity of Cation–π Interactions: An ab Initio Computational Study on π–Cation–π Sandwich Complexes. *J. Phys. Chem. A* **2004**, *109*, 9400–9405.

(38) Yorita, H.; Otomo, K.; Hiramatsu, H.; Toyama, A.; Miura, T.; Takeuchi, H. Evidence for the Cation–π Interaction between $Cu^{2+}$ and Tryptophan. *J. Am. Chem. Soc.* **2008**, *130*, 15266–15267.

(39) Gebbie, M. A.; Wei, W.; Schrader, A. M.; Cristiani, T. R.; Dobbs, H. A.; Idso, M.; Chmelka, B. F.; Waite, J. H.; Israelachvili, J. N. Tuning Underwater Adhesion with Cation–π Interactions. *Nat. Chem.* **2017**, *9*, 473–479.

(40) Fan, H.; Wang, J.; Tao, Z.; Huang, J.; Rao, P.; Kurokawa, T.; Gong, J. P. Adjacent Cationic-Aromatic Sequences Yield Strong Electrostatic Adhesion of Hydrogels in Seawater. *Nat. Commun.* **2019**, *10*, 5127.

(41) Xiao, X.; Chen, H.; Dong, X.; Ren, D.; Deng, Q.; Wang, D.; Tian, W. A Double Cation–π-Driven Strategy Enabling Two-Dimensional Supramolecular Polymers as Efficient Catalyst Carriers. *Angew. Chem. Int. Ed.* **2020**, *59*, 9534–9541.

(42) Kim, S.; Yoo, H. Y.; Huang, J.; Lee, Y.; Park, S.; Park, Y.; Jin, S.; Jung, Y. M.; Zeng, H.; Hwang, D. S.; et al. Salt Triggers the Simple Coacervation of an Underwater Adhesive When Cations Meet Aromatic π Electrons in Seawater. *ACS Nano* **2017**, *11*, 6764–6772.

(43) Yang, B.; Jin, S.; Park, Y.; Jung, Y. M.; Cha, H. J. Coacervation of Interfacial Adhesive Proteins for Initial Mussel Adhesion to a Wet Surface. *Small* **2018**, *14*, 1803377.

(44) Hu, J.; Barbour, L. J.; Gokel, G. W. Probing Alkali Metal–π Interactions with the Side Chain Residue of Tryptophan. *Proc. Natl. Acad. Sci. U. S. A.* **2002**, *99*, 5121–5126.

(45) Lu, Q.; Oh, D. X.; Lee, Y.; Jho, Y.; Hwang, D. S.; Zeng, H. Nanomechanics of Cation–π Interactions in Aqueous Solution. *Angew. Chem. Int. Ed.* **2013**, *52*, 3944–3948.

(46) Wei, W.; Tan, Y.; Rodriguez, N. R. M.; Yu, J.; Israelachvili, J. N.; Waite, J. H. A Mussel-Derived One Component Adhesive Coacervate. *Acta Biomater.* **2014**, *10*, 1663–1670.

(47) Fan, H.; Guo, H.; Wang, J.; Gong, J. P. Competitive Cation–π Interactions between Small Cations and Polycations with Phenyl Groups in Poly(Cation–π) Hydrogels. *Giant* **2020**, *1*, 100005.

(48) Hong, S.; Wang, Y.; Park, S. Y.; Lee, H. Progressive Fuzzy Cation–π Assembly of Biological Catecholamines. *Sci. Adv.* **2018**, *4*, eaat7457.

(49) Reddy, A. S.; Sastry, G. N. Cation [M = $H^+$, $Li^+$, $Na^+$, $K^+$, $Ca^{2+}$, $Mg^{2+}$, $NH_4^+$, and $NMe_4^+$] Interactions with the Aromatic Motifs of Naturally Occurring Amino Acids: A Theoretical Study. *J. Phys. Chem. A* **2005**, *109*, 8893–8903.

(50) Khanmohammadi, A.; Raissi, H.; Mollania, F.; Hokmabadi, L. Molecular Structure and Bonding Character of Mono and Divalent Metal Cations ($Li^+$, $Na^+$, $K^+$, $Be^{2+}$, $Mg^{2+}$, and $Ca^{2+}$) with Substituted Benzene Derivatives: AIM, NBO, and NMR Analyses. *Struct. Chem.* **2014**, *25*, 1327–1342.

(51) Bravo, L. Polyphenols: Chemistry, Dietary Sources, Metabolism, and Nutritional Significance. *Nutr. Rev.* **1998**, *56*, 317–333.

(52) Pandey, K. B.; Rizvi, S. I. Plant Polyphenols as Dietary Antioxidants in Human Health and Disease. *Oxid. Med. Cell. Longevity* **2009**, *2*, 270–278.

(53) Holten-Andersen, N.; Harrington, M. J.; Birkedal, H.; Lee, B. P.; Messersmith, P. B.; Lee, K. Y. C.; Waite, J. H. pH-Induced Metal-Ligand Cross-Links Inspired by Mussel Yield Self-Healing Polymer Networks with Near-Covalent Elastic Moduli. *Proc. Natl. Acad. Sci. U. S. A.* **2011**, *108*, 2651–2655.

(54) Zhong, Q.-Z.; Pan, S.; Rahim, M. A.; Yun, G.; Li, J.; Ju, Y.; Lin, Z.; Han, Y.; Ma, Y.; Richardson, J. J.; et al. Spray Assembly of Metal–Phenolic Networks: Formation, Growth, and Applications. *ACS Appl. Mater. Interfaces* **2018**, *10*, 33721–33729.

(55) Priemel, T.; Palia, G.; Förste, F.; Jehle, F.; Sviben, S.; Mantouvalou, I.; Zaslansky, P.; Bertinetti, L.; Harrington, M. J. Microfluidic-Like Fabrication of Metal Ion–Cured Bioadhesives by Mussels. *Science* **2021**, *374*, 206–211.

(56) Andersen, A.; Chen, Y.; Birkedal, H. Bioinspired Metal–Polyphenol Materials: Self-Healing and Beyond. *Biomimetics* **2019**, *4*, 30.

(57) Krogsgaard, M.; Hansen, M. R.; Birkedal, H. Metals & Polymers in the Mix: Fine-Tuning the Mechanical Properties & Color of Self-Healing Mussel-Inspired Hydrogels. *J. Mater. Chem. B* **2014**, *2*, 8292–8297.

(58) Wei, F.; Liu, J.; Zhu, Y.-N.; Wang, X.-S.; Cao, C.-Y.; Song, W.-G. In Situ Facile Loading of Noble Metal Nanoparticles on Polydopamine Nanospheres via Galvanic Replacement Reaction for Multifunctional Catalysis. *Sci. China Chem.* **2017**, *60*, 1236–1242.

(59) Kim, J.; Kim, K. R.; Hong, Y.; Choi, S.; Yavuz, C. T.; Kim, J. W.; Nam, Y. S. Photochemically Enhanced Selective Adsorption of Gold Ions on Tannin-Coated Porous Polymer Microspheres. *ACS Appl. Mater. Interfaces* **2019**, *11*, 21915–21925.

(60) Liu, Y.; Ai, K.; Lu, L. Polydopamine and Its Derivative Materials: Synthesis and Promising Applications in Energy, Environmental, and Biomedical Fields. *Chem. Rev.* **2014**, *114*, 5057–5115.

(61) Can, M.; Bulut, E.; Özacar, M. Reduction of Palladium onto Pyrogallol-Derived Nano-Resin and its Mechanism. *Chem. Eng. J.* **2015**, *275*, 322–330.

(62) Kumar, K. M.; Mandal, B. K.; Tammina, S. K. Green Synthesis of Nano Platinum Using Naturally Occurring Polyphenols. *RSC Adv.* **2013**, *3*, 4033–4039.

(63) Guo, L.; Liu, Q.; Li, G.; Shi, J.; Liu, J.; Wang, T.; Jiang, G. A Mussel-Inspired Polydopamine Coating as a Versatile Platform forthe In Situ Synthesis of Graphene-Based Nanocomposites. *Nanoscale* **2012**, *4*, 5864–5867.

(64) Afewerki, S.; Wang, X.; Ruiz-Esparza, G. U.; Tai, C.-W.; Kong, X.; Zhou, S.; Welch, K.; Huang, P.; Bengtsson, R.; Xu, C.; et al. Combined Catalysis for Engineering Bioinspired, Lignin-Based, Long-Lasting, Adhesive, Self-Mending, Antimicrobial Hydrogels. *ACS Nano* **2020**, *14*, 17004–17017.

(65) Son, H. Y.; Ryu, J. H.; Lee, H.; Nam, Y. S. Bioinspired Templating Synthesis of Metal–Polymer Hybrid Nanostructures within 3D Electrospun Nanofibers. *ACS Appl. Mater. Interfaces* **2013**, *5*, 6381–6390.

(66) Gan, D.; Xing, W.; Jiang, L.; Fang, J.; Zhao, C.; Ren, F.; Fang, L.; Wang, K.; Lu, X. Plant-Inspired Adhesive and Tough Hydrogel Based on Ag-Lignin Nanoparticles-Triggered Dynamic Redox Catechol Chemistry. *Nat. Commun.* **2019**, *10*, 1487.

(67) Rupar, P. A.; Staroverov, V. N.; Baines, K. M. A Cryptand-Encapsulated Germanium(II) Dication. *Science* **2008,** *322*, 1360–1363.

(68) Patel, M.; Karamalidis, A. K. Germanium: A Review of Its US Demand, Uses, Resources, Chemistry, and Separation Technologies. *Sep. Purif. Technol.* **2021**, *275*, 118981.

(69) Hartmann, D.; Thorwart, T.; Müller, R.; Thusek, J.; Schwabedissen, J.; Mix, A.; Lamm, J.-H.; Neumann, B.; Mitzel, N. W.; Greb, L. The Structure of Bis(catecholato)silanes: Phase Adaptation by Dynamic Covalent Chemistry of the Si–O Bond. *J. Am. Chem. Soc.* **2021**, *143*, 18784–18793.

(70) Guo, J.; Sun, H.; Alt, K.; Tardy, B. L.; Richardson, J. J.; Suma, T.; Ejima, H.; Cui, J.; Hagemeyer, C. E.; Caruso, F. Boronate–Phenolic Network Capsules with Dual Response to Acidic pH and *cis*-Diols. *Adv. Healthcare Mater.* **2015**, *4*, 1796–1801.

(71) Guan, Y.; Zhang, Y. Boronic Acid-Containing Hydrogels: Synthesis and Their Applications. *Chem. Soc. Rev.* **2013**, *42*, 8106–8121.

(72) Nakahata, M.; Sakai, S. Cross-Linking Building Blocks Using a “Boronate Bridge” to Build Functional Hybrid Materials. *ChemNanoMat* **2019**, *5*, 141–151.

(73) Chen, Y.; Diaz-Dussan, D.; Wu, D.; Wang, W.; Peng, Y.-Y.; Asha, A. B.; Hall, D. G.; Ishihara, K.; Narain, R. Bioinspired Self-Healing Hydrogel Based on Benzoxaborole-Catechol Dynamic Covalent Chemistry for 3D Cell Encapsulation. *ACS Macro Lett.* **2018**, *7*, 904–908.

(74) Cambre, J. N.; Sumerlin, B. S. Biomedical Applications of Boronic Acid Polymers. *Polymer* **2011**, *52*, 4631–4643.

(75) Li, D.; Chen, Y.; Liu, Z. Boronate Affinity Materials for Separation and Molecular Recognition: Structure, Properties and Applications. *Chem. Soc. Rev.* **2015**, *44*, 8097–8123.

(76) Cheng, X.; Li, M.; Wang, H.; Cheng, Y. All-Small-Molecule Dynamic Covalent Gels with Antibacterial Activity by Boronate-Tannic Acid Gelation. *Chin. Chem. Lett.* **2020**, *31*, 869–874.

(77) Geng, H.; Dai, Q.; Sun, H.; Zhuang, L.; Song, A.; Caruso, F.; Hao, J.; Cui, J. Injectable and Sprayable Polyphenol-Based Hydrogels for Controlling Hemostasis. *ACS Appl. Bio Mater*. **2020**, *3*, 1258–1266.

(78) Zhao, P.; Wei, K.; Feng, Q.; Chen, H.; Wong, D. S. H.; Chen, X.; Wu, C.-C.; Bian, L. Mussel-Mimetic Hydrogels with Defined Cross-Linkers Achieved via Controlled Catechol Dimerization Exhibiting Tough Adhesion for Wet Biological Tissues. *Chem. Commun.* **2017**, *53*, 12000–12003.

(79) Li, Y.; Xiao, W.; Xiao, K.; Berti, L.; Luo, J.; Tseng, H. P.; Fung, G.; Lam, K. S. Well-Defined, Reversible Boronate Crosslinked Nanocarriers for Targeted Drug Delivery in Response to Acidic pH Values and *cis*-Diols. *Angew. Chem. Int. Ed.* **2012**, *51*, 2864–2869.

(80) Montanari, E.; Gennari, A.; Pelliccia, M.; Gourmel, C.; Lallana, E.; Matricardi, P.; McBain, A. J.; Tirelli, N. Hyaluronan/Tannic Acid Nanoparticles Via Catechol/Boronate Complexation as a Smart Antibacterial System. *Macromol. Biosci.* **2016**, *16*, 1815–1823.

(81) Huang, Z.; Delparastan, P.; Burch, P.; Cheng, J.; Cao, Y.; Messersmith, P. B. Injectable Dynamic Covalent Hydrogels of Boronic Acid Polymers Cross-Linked by Bioactive Plant-Derived Polyphenols. *Biomater. Sci.* **2018**, *6*, 2487–2495.

(82) Zhu, J.; Huo, Q.; Xu, M.; Yang, F.; Li, Y.; Shi, H.; Niu, Y.; Liu, Y. Bortezomib-Catechol Conjugated Prodrug Micelles: Combining Bone Targeting and Aryl Boronate-Based pH-

Responsive Drug Release for Cancer Bone-Metastasis Therapy. *Nanoscale* **2018**, *10*, 18387–18397.

(83) Nakahata, M.; Mori, S.; Takashima, Y.; Hashidzume, A.; Yamaguchi, H.; Harada, A. pH- and Sugar-Responsive Gel Assemblies Based on Boronate–Catechol Interactions. *ACS Macro Lett.* **2014**, *3*, 337–340.

(84) Yang, B.; Lv, Y.; Zhu, J.; Han, Y.; Jia, H.; Chen, W.; Feng, J.; Zhang, X.; Zhuo, R. A pH-Responsive Drug Nanovehicle Constructed by Reversible Attachment of Cholesterol to PEGylated Poly(L-Lysine) via Catechol–Boronic Acid Ester Formation. *Acta Biomater.* **2014**, *10*, 3686–3695.

(85) Liu, S.; Ono, R. J.; Yang, C.; Gao, S.; Tan, J. Y. M.; Hedrick, J. L.; Yang, Y. Y. Dual pH-Responsive Shell-Cleavable Polycarbonate Micellar Nanoparticles for in Vivo Anticancer Drug Delivery. *ACS Appl. Mater. Interfaces* **2018**, *10*, 19355–19364.

(86) Su, J.; Chen, F.; Cryns, V. L.; Messersmith, P. B. Catechol Polymers for pH-Responsive, Targeted Drug Delivery to Cancer Cells. *J. Am. Chem. Soc.* **2011**, *133*, 11850–11853.

(87) Wang, M.; Wang, Y.; Hu, K.; Shao, N.; Cheng, Y. Tumor Extracellular Acidity Activated "off-on" Release of Bortezomib from a Biocompatible Dendrimer. *Biomater. Sci.* **2015**, *3*, 480–489.

(88) Narkar, A. R.; Lee, B. P. Incorporation of Anionic Monomer to Tune the Reversible Catechol–Boronate Complex for pH-Responsive, Reversible Adhesion. *Langmuir* **2018**, *34*, 9410–9417.

(89) Narkar, A. R.; Kelley, J. D.; Pinnaratip, R.; Lee, B. P. Effect of Ionic Functional Groups on the Oxidation State and Interfacial Binding Property of Catechol-Based Adhesive. *Biomacromolecules* **2018**, *19*, 1416–1424.

(90) Zhang, L.; Liu, Y.; Hu, X.; Wang, Y.; Xu, M. Binding and Precipitation of Germanium(IV) by Penta-*O*-galloyl-*β*-D-glucose. *J. Agric. Food Chem.* **2018**, *66*, 11000–11007.

(91) Weber, F.; Liao, W.-C.; Barrantes, A.; Edén, M.; Tiainen, H. Silicate-Phenolic Networks: Coordination-Mediated Deposition of Bioinspired Tannic Acid Coatings. *Chem. Eur. J.* **2019**, *25*, 9870–9874.

(92) Wang, Y.; Jeon, E. J.; Lee, J.; Hwang, H.; Cho, S.-W.; Lee, H. A Phenol-Amine Superglue Inspired by Insect Sclerotization Process. *Adv. Mater.* **2020**, *32*, 2002118.

(93) Pinnaratip, R.; Forooshani, P. K.; Li, M.; Hang Hu, Y.; Rajachar, R. M.; Lee, B. P. Controlling the Release of Hydrogen Peroxide from Catechol-Based Adhesive Using Silica Nanoparticle. *ACS Biomater. Sci. Eng.* **2020**, *6*, 4502–4511.

(94) Pokrovski, G. S.; Martin, F.; Hazemann, J.-L.; Schott, J. An X-Ray Absorption Fine Structure Spectroscopy Study of Germanium-Organic Ligand Complexes in Aqueous Solution. *Chem. Geol.* **2000**, *163*, 151–165.

(95) Nikolaevskaya, E. N.; Saverina, E. A.; Starikova, A. A.; Farhati, A.; Kiskin, M. A.; Syroeshkin, M. A.; Egorov, M. P.; Jouikov, V. V. Halogen-Free $GeO_2$ Conversion: Electrochemical Reduction vs. Complexation in $(DTBC)_2Ge[Py(CN)_n]$ ($n$ = 0...2) Complexes. *Dalton Trans.* **2018**, *47*, 17127–17133.

(96) Park, S.; Kim, S.; Jho, Y.; Hwang, D. S. Cation–π Interactions and Their Contribution to Mussel Underwater Adhesion Studied Using a Surface Forces Apparatus: A Mini-Review. *Langmuir* **2019**, *35*, 16002–16012.

(97) Zhu, X.; Wei, C.; Chen, H.; Zhang, C.; Peng, H.; Wang, D.; Yuan, J.; Waite, J. H.; Zhao, Q. A Cation-Methylene-Phenyl Sequence Encodes Programmable Poly(Ionic Liquid) Coacervation and Robust Underwater Adhesion. *Adv. Funct. Mater.* **2021**, *32*, 2105464.

(98) Lagutschenkov, A.; Sinha, R. K.; Maitre, P.; Dopfer, O. Structure and Infrared Spectrum of the $Ag^+$–Phenol Ionic Complex. *J. Phys. Chem. A* **2010**, *114*, 11053–11059.

(99) Dunbar, R. C.; Steill, J. D.; Oomens, J. Encapsulation of Metal Cations by the PhePhe Ligand: A Cation–π Ion Cage. *J. Am. Chem. Soc.* **2011**, *133*, 9376–9386.

(100) Zhang, C.; Xiang, L.; Zhang, J.; Gong, L.; Han, L.; Xu, Z.-K.; Zeng, H. Tough and Alkaline-Resistant Mussel-Inspired Wet Adhesion with Surface Salt Displacement via Polydopamine/Amine Synergy. *Langmuir* **2019**, *35*, 5257–5263.

(101) Wonderly, W. R.; Cristiani, T. R.; Cunha, K. C.; Degen, G. D.; Shea, J.-E.; Waite, J. H. Dueling Backbones: Comparing Peptoid and Peptide Analogues of a Mussel Adhesive Protein. *Macromolecules* **2020**, *53*, 6767–6779.

(102) Zhang, J.; Xiang, L.; Yan, B.; Zeng, H. Nanomechanics of Anion–π Interaction in Aqueous Solution. *J. Am. Chem. Soc.* **2020**, *142*, 1710–1714.

(103) Zheng, P.; Xiang, L.; Chang, J.; Lin, Q.; Xie, L.; Lan, T.; Liu, J.; Gong, Z.; Tang, T.; Shuai, L.; et al. Nanomechanics of Lignin–Cellulase Interactions in Aqueous Solutions. *Biomacromolecules* **2021**, *22*, 2033–2042.

(104) Hong, S.; Yeom, J.; Song, I. T.; Kang, S. M.; Lee, H.; Lee, H. Pyrogallol 2-Aminoethane: A Plant Flavonoid-Inspired Molecule for Material-Independent Surface Chemistry. *Adv. Mater. Interfaces* **2014**, *1*, 1400113.

(105) Weber, F.; Sagstuen, E.; Zhong, Q.-Z.; Zheng, T.; Tiainen, H. Tannic Acid Radicals in the Presence of Alkali Metal Salts and Their Impact on the Formation of Silicate-Phenolic Networks. *ACS Appl. Mater. Interfaces* **2020**, *12*, 52457–52466.

(106) Guo, J.; Richardson, J. J.; Besford, Q. A.; Christofferson, A. J.; Dai, Y.; Ong, C. W.; Tardy, B. L.; Liang, K.; Choi, G. H.; Cui, J.; et al. Influence of Ionic Strength on the Deposition of Metal–Phenolic Networks. *Langmuir* **2017**, *33*, 10616–10622.

(107) Park, T.; Kim, W. I.; Kim, B. J.; Lee, H.; Choi, I. S.; Park, J. H.; Cho, W. K. Salt-Induced, Continuous Deposition of Supramolecular Iron(III)-Tannic Acid Complex. *Langmuir* **2018**, *34*, 12318–12323.

(108) Luo, J.; Chen, K.; Yin, P.; Li, T.; Wan, G.; Zhang, J.; Ye, S.; Bi, X.; Pang, Y.; Wei, Y.; et al. Effect of Cation–π Interaction on Macroionic Self-Assembly. *Angew. Chem. Int. Ed.* **2018**, *57*, 4067–4072.

(109) Chen, L.; Shi, G.; Shen, J.; Peng, B.; Zhang, B.; Wang, Y.; Bian, F.; Wang, J.; Li, D.; Qian, Z.; et al. Ion Sieving in Graphene Oxide Membranes via Cationic Control of Interlayer Spacing. *Nature* **2017**, *550*, 380–383.

(110) Jho, Y.; Yoo, H. Y.; Lin, Y.; Han, S.; Hwang, D. S. Molecular and Structural Basis of Low Interfacial Energy of Complex Coacervates in Water. *Adv. Colloid Interface Sci.* **2017**, *239*, 61–73.

(111) Huang, K. Y.; Yoo, H. Y.; Jho, Y.; Han, S.; Hwang, D. S. Bicontinuous Fluid Structure with Low Cohesive Energy: Molecular Basis for Exceptionally Low Interfacial Tension of Complex Coacervate Fluids. *ACS Nano* **2016**, *10*, 5051–5062.

(112) Kim, S.; Huang, J.; Lee, Y.; Dutta, S.; Yoo, H. Y.; Jung, Y. M.; Jho, Y.; Zeng, H.; Hwang, D. S. Complexation and Coacervation of Like-Charged Polyelectrolytes Inspired by Mussels. *Proc. Natl. Acad. Sci. U. S. A.* **2016**, *113*, E847–E853.

(113) Degtyar, E.; Harrington, M. J.; Politi, Y.; Fratzl, P. The Mechanical Role of Metal Ions in Biogenic Protein-Based Materials. *Angew. Chem. Int. Ed.* **2014**, *53*, 12026–12044.

(114) Kim, B. S.; Lee, H. I.; Min, Y.; Poon, Z.; Hammond, P. T. Hydrogen-Bonded Multilayer of pH-Responsive Polymeric Micelles with Tannic Acid for Surface Drug Delivery. *Chem. Commun.* **2009**, 4194–4196.

(115) Zeng, H.; Hwang, D. S.; Israelachvilib, J. N.; Waite, J. H. Strong Reversible $Fe^{3+}$-Mediated Bridging between Dopa-Containing Protein Films in Water. *Proc. Natl. Acad. Sci. U. S. A.* **2010**, *107*, 12850–12853.

(116) Ozawa, H.; Haga, M. A. Soft Nano-Wrapping on Graphene Oxide by Using Metal–Organic Network Films Composed of Tannic Acid and Fe Ions. *Phys. Chem. Chem. Phys.* **2015**, *17*, 8609–8613.

(117) Zhou, J.; Lin, Z.; Penna, M.; Pan, S.; Ju, Y.; Li, S.; Han, Y.; Chen, J.; Lin, G.; Richardson, J. J.; et al. Particle Engineering Enabled by Polyphenol-Mediated Supramolecular Networks. *Nat. Commun.* **2020**, *11*, 4804.

(118) Saowalak, K.; Titipun, T.; Somchai, T.; Chalermchai, P. Iron(III)–Tannic Molecular Nanoparticles Enhance Autophagy Effect and $T_1$ MRI Contrast in Liver Cell Lines. *Sci. Rep.* **2018**, *8*, 6647.

(119) Wang, Q.; Gao, Z.; Zhong, Q. Z.; Wang, N.; Mei, H.; Dai, Q.; Cui, J.; Hao, J. Encapsulation of Enzymes in Metal–Phenolic Network Capsules for the Trigger of Intracellular Cascade Reactions. *Langmuir* **2021**, *37*, 11292–11300.

(120) Lin, G.; Rahim, M. A.; Leeming, M. G.; Cortez-Jugo, C.; Besford, Q. A.; Ju, Y.; Zhong, Q. Z.; Johnston, S. T.; Zhou, J.; Caruso, F. Selective Metal–Phenolic Assembly from Complex Multicomponent Mixtures. *ACS Appl. Mater. Interfaces* **2019**, *11*, 17714–17721.

(121) Chen, J.; Pan, S.; Zhou, J.; Zhong, Q.-Z.; Qu, Y.; Richardson, J. J.; Caruso, F. Programmable Permeability of Metal–Phenolic Network Microcapsules. *Chem. Mater.* **2020**, *32*, 6975–6982.

(122) Filippidi, E.; Cristiani, T. R.; Eisenbach, C. D.; Waite, J. H.; Israelachvili, J. N.; Ahn, B. K.; Valentine, M. T. Toughening Elastomers Using Mussel Inspired Iron-Catechol Complexes. *Science* **2017**, *358*, 502–505.

(123) Li, J.; Ejima, H.; Yoshie, N. Seawater-Assisted Self-Healing of Catechol Polymers via Hydrogen Bonding and Coordination Interactions. *ACS Appl. Mater. Interfaces* **2016**, *8*, 19047–19053.

(124) Liu, T.; Zhang, M.; Liu, W.; Zeng, X.; Song, X.; Yang, X.; Zhang, X.; Feng, J. Metal Ion/Tannic Acid Assembly as a Versatile Photothermal Platform in Engineering Multimodal Nanotheranostics for Advanced Applications. *ACS Nano* **2018**, *12*, 3917–3927.

(125) Bertleff-Zieschang, N.; Rahim, M. A.; Ju, Y.; Braunger, J. A.; Suma, T.; Dai, Y.; Pan, S.; Cavalieri, F.; Caruso, F. Biofunctional Metal–Phenolic Films from Dietary Flavonoids. *Chem. Commun.* **2017**, *53*, 1068–1071.

(126) Wei, J.; Liang, Y.; Hu, Y.; Kong, B.; Simon, G. P.; Zhang, J.; Jiang, S. P.; Wang, H. A Versatile Iron–Tannin-Framework Ink Coating Strategy to Fabricate Biomass-Derived Iron Carbide/Fe-N-Carbon Catalysts for Efficient Oxygen Reduction. *Angew. Chem. Int. Ed.* **2016**, *55*, 1355–1359.

(127) Su, X.; Luo, Y.; Tian, Z.; Yuan, Z.; Han, Y.; Dong, R.; Xu, L.; Feng, Y.; Liu, X.; Huang, J. Ctenophore-Inspired Hydrogels for Efficient and Repeatable Underwater Specific Adhesion to Biotic Surfaces. *Mater. Horiz.* **2020**, *7*, 2651–2661.

(128) Cui, C.; Liu, W. Recent Advances in Wet Adhesives: Adhesion Mechanism, Design Principle and Applications. *Prog. Polym. Sci.* **2021**, *116*, 101388.

(129) Xie, C.; Wang, X.; He, H.; Ding, Y.; Lu, X. Mussel-Inspired Hydrogels for Self-Adhesive Bioelectronics. *Adv. Funct. Mater.* **2020**, *30*, 1909954.

(130) Yang, P.; Zhu, F.; Zhang, Z.; Cheng, Y.; Wang, Z.; Li, Y. Stimuli-Responsive Polydopamine-Based Smart Materials. *Chem. Soc. Rev.* **2021**, *50*, 8319–8343.

(131) Liu, J.; Guo, Z.; Liang, K. Biocatalytic Metal–Organic Framework-Based Artificial Cells. *Adv. Funct. Mater.* **2019**, *29*, 1905321.

(132) Yang, Z.; Zhou, Z. W.; Guo, H.; Yao, Z.; Ma, X. H.; Song, X.; Feng, S. P.; Tang, C. Y. Tannic Acid/$Fe^{3+}$ Nanoscaffold for Interfacial Polymerization: Toward Enhanced Nanofiltration Performance. *Environ. Sci. Technol.* **2018**, *52*, 9341–9349.

(133) Luo, W.; Xiao, G.; Tian, F.; Richardson, J. J.; Wang, Y.; Zhou, J.; Guo, J.; Liao, X.; Shi, B. Engineering Robust Metal–Phenolic Network Membranes for Uranium Extraction from Seawater. *Energy Environ. Sci.* **2019**, *12*, 607–614.

(134) Li, K.; Xiao, G.; Richardson, J. J.; Tardy, B. L.; Ejima, H.; Huang, W.; Guo, J.; Liao, X.; Shi, B. Targeted Therapy against Metastatic Melanoma Based on Self-Assembled Metal-Phenolic Nanocomplexes Comprised of Green Tea Catechin. *Adv. Sci.* **2019**, *6*, 1801688.

(135) Zhang, C.; Wu, B.; Zhou, Y.; Zhou, F.; Liu, W.; Wang, Z. Mussel-Inspired Hydrogels: From Design Principles to Promising Applications. *Chem. Soc. Rev.* **2020**, *49*, 3605–3637.

(136) Park, J. H.; Kim, K.; Lee, J.; Choi, J. Y.; Hong, D.; Yang, S. H.; Caruso, F.; Lee, Y.; Choi, I. S. A Cytoprotective and Degradable Metal–Polyphenol Nanoshell for Single-Cell Encapsulation. *Angew. Chem. Int. Ed.* **2014**, *53*, 12420–12425.

(137) Ping, Y.; Guo, J.; Ejima, H.; Chen, X.; Richardson, J. J.; Sun, H.; Caruso, F. pH-Responsive Capsules Engineered from Metal–Phenolic Networks for Anticancer Drug Delivery. *Small* **2015**, *11*, 2032–2036.

(138) Yang, S. J.; Antonietti, M.; Fechler, N. Self-Assembly of Metal Phenolic Mesocrystals and Morphosynthetic Transformation toward Hierarchically Porous Carbons. *J. Am. Chem. Soc.* **2015**, *137*, 8269–8273.

(139) Rahim, M. A.; Björnmalm, M.; Suma, T.; Faria, M.; Ju, Y.; Kempe, K.; Müllner, M.; Ejima, H.; Stickland, A. D.; Caruso, F. Metal–Phenolic Supramolecular Gelation. *Angew. Chem. Int. Ed.* **2016**, *55*, 13803–13807.

(140) Guo, J.; Tardy, B. L.; Christofferson, A. J.; Dai, Y.; Richardson, J. J.; Zhu, W.; Hu, M.; Ju, Y.; Cui, J.; Dagastine, R. R.; et al. Modular Assembly of Superstructures from Polyphenol-Functionalized Building Blocks. *Nat. Nanotechnol.* **2016**, *11*, 1105–1111.

(141) Rahim, M. A.; Björnmalm, M.; Bertleff-Zieschang, N.; Besford, Q.; Mettu, S.; Suma, T.; Faria, M.; Caruso, F. Rust-Mediated Continuous Assembly of Metal–Phenolic Networks. *Adv. Mater.* **2017**, *29*, 1606717.

(142) Kim, B. J.; Han, S.; Lee, K.-B.; Choi, I. S. Biphasic Supramolecular Self-Assembly of Ferric Ions and Tannic Acid across Interfaces for Nanofilm Formation. *Adv. Mater.* **2017**, *29*, 1700784.

(143) Dai, Y.; Yang, Z.; Cheng, S.; Wang, Z.; Zhang, R.; Zhu, G.; Wang, Z.; Yung, B. C.; Tian, R.; Jacobson, O.; et al. Toxic Reactive Oxygen Species Enhanced Synergistic Combination Therapy by Self-Assembled Metal–Phenolic Network Nanoparticles. *Adv. Mater.* **2018**, *30*, 1704877.

(144) Zhong, Q.-Z.; Li, S.; Chen, J.; Xie, K.; Pan, S.; Richardson, J. J.; Caruso, F. Oxidation-Mediated Kinetic Strategies for Engineering Metal–Phenolic Networks. *Angew. Chem. Int. Ed.* **2019**, *58*, 12563–12568.

(145) Chen, J.; Li, J.; Zhou, J.; Lin, Z.; Cavalieri, F.; Czuba-Wojnilowicz, E.; Hu, Y.; Glab, A.; Ju, Y.; Richardson, J. J.; et al. Metal–Phenolic Coatings as a Platform to Trigger Endosomal Escape of Nanoparticles. *ACS Nano* **2019**, *13*, 11653–11664.

(146) Zhong, Q. Z.; Richardson, J. J.; Li, S.; Zhang, W.; Ju, Y.; Li, J.; Pan, S.; Chen, J.; Caruso, F. Expanding the Toolbox of Metal–Phenolic Networks via Enzyme Mediated Assembly. *Angew. Chem. Int. Ed.* **2020**, *59*, 1711–1717.

(147) Lin, Z.; Zhou, J.; Cortez-Jugo, C.; Han, Y.; Ma, Y.; Pan, S.; Hanssen, E.; Richardson, J. J.; Caruso, F. Ordered Mesoporous Metal–Phenolic Network Particles. *J. Am. Chem. Soc.* **2020**, *142*, 335–341.

(148) Mei, H.; Gao, Z.; Zhao, K.; Li, M.; Ashokkumar, M.; Song, A.; Cui, J.; Caruso, F.; Hao, J. Sono-Fenton Chemistry Converts Phenol and Phenyl Derivatives into Polyphenols for Engineering Surface Coatings. *Angew. Chem. Int. Ed.* **2021**, *60*, 21529–21535.

(149) Lin, Z.; Zhou, J.; Qu, Y.; Pan, S.; Han, Y.; Lafleur, R. P. M.; Chen, J.; Cortez-Jugo, C.; Richardson, J. J.; Caruso, F. Luminescent Metal–Phenolic Networks for Multicolor Particle Labeling. *Angew. Chem. Int. Ed.* **2021**, *60*, 24968–24975.

(150) Lee, H.; Lee, B. P.; Messersmith, P. B. A Reversible Wet/Dry Adhesive Inspired by Mussels and Geckos. *Nature* **2007**, *448*, 338–341.

(151) Lee, H.; Dellatore, S. M.; Miller, W. M.; Messersmith, P. B. Mussel-Inspired Surface Chemistry for Multifunctional Coatings. *Science* **2007**, *318*, 426–430.

(152) Duan, J.; Chen, Z.; Liang, X.; Chen, Y.; Li, H.; Tian, X.; Zhang, M.; Wang, X.; Sun, H.; Kong, D.; et al. Construction and Application of Therapeutic Metal-Polyphenol Capsule for Peripheral Artery Disease. *Biomaterials* **2020**, *255*, 120199.

(153) Chen, X.; Yi, Z.; Chen, G.; Ma, X.; Su, W.; Cui, X.; Li, X. DOX-Assisted Functionalization of Green Tea Polyphenol Nanoparticles for Effective Chemo-Photothermal Cancer Therapy. *J. Mater. Chem. B* **2019**, *7*, 4066–4078.

(154) Ju, Y.; Cui, J.; Müllner, M.; Suma, T.; Hu, M.; Caruso, F. Engineering Low-Fouling and pH-Degradable Capsules through the Assembly of Metal–Phenolic Networks. *Biomacromolecules* **2015**, *16*, 807–814.

(155) Ju, Y.; Cui, J.; Sun, H.; Müllner, M.; Dai, Y.; Guo, J.; Bertleff-Zieschang, N.; Suma, T.; Richardson, J. J.; Caruso, F. Engineered Metal–Phenolic Capsules Show Tunable Targeted Delivery to Cancer Cells. *Biomacromolecules* **2016**, *17*, 2268–2276.

(156) Xu, K.; Zhou, M.; Li, M.; Chen, W.; Zhu, Y.; Cai, K. Metal-Phenolic Networks as a Promising Platform for pH-Controlled Release of Bioactive Divalent Metal Ions. *Appl. Surf. Sci.* **2020**, *511*, 145569.

(157) Liu, P.; Liu, X.; Cheng, Y.; Zhong, S.; Shi, X.; Wang, S.; Liu, M.; Ding, J.; Zhou, W. Core–Shell Nanosystems for Self-Activated Drug-Gene Combinations against Triple-Negative Breast Cancer. *ACS Appl. Mater. Interfaces* **2020**, *12*, 53654–53664.

(158) Yun, G.; Richardson, J. J.; Biviano, M.; Caruso, F. Tuning the Mechanical Behavior of Metal-Phenolic Networks through Building Block Composition. *ACS Appl. Mater. Interfaces* **2019**, *11*, 6404–6410.

(159) Zhang, W.; Besford, Q. A.; Christofferson, A. J.; Charchar, P.; Richardson, J. J.; Elbourne, A.; Kempe, K.; Hagemeyer, C. E.; Field, M. R.; McConville, C. F.; et al. Cobalt-Directed Assembly of Antibodies onto Metal–Phenolic Networks for Enhanced Particle Targeting. *Nano Lett.* **2020**, *20*, 2660–2666.

(160) Lin, C.-E.; Zhou, M.-Y.; Hung, W.-S.; Zhu, B.-K.; Lee, K.-R.; Zhu, L.-P.; Fang, L.-F. Ultrathin Nanofilm with Tailored Pore Size Fabricated by Metal-Phenolic Network for Precise and Rapid Molecular Separation. *Sep. Purif. Technol.* **2018**, *207*, 435–442.

(161) Maerten, C.; Lopez, L.; Lupattelli, P.; Rydzek, G.; Pronkin, S.; Schaaf, P.; Jierry, L.; Boulmedais, F. Electrotriggered Confined Self-assembly of Metal–Polyphenol Nanocoatings Using a Morphogenic Approach. *Chem. Mater.* **2017**, *29*, 9668–9679.

(162) Ohtsu, H.; Kawano, M. Kinetic Assembly of Coordination Networks. *Chem. Commun.* **2017**, *53*, 8818–8829.

(163) Zhang, Z.; Maji, S.; da Fonseca Antunes, A. B.; De Rycke, R.; Hoogenboom, R.; De Geest, B. G. Salt-Driven Deposition of Thermoresponsive Polymer-Coated Metal Nanoparticles on Solid Substrates. *Angew. Chem. Int. Ed.* **2016**, *55*, 7086–7090.

(164) Kim, S.; Peterson, A. M.; Holten-Andersen, N. Enhanced Water Retention Maintains Energy Dissipation in Dehydrated Metal-Coordinate Polymer Networks: Another Role for Fe-Catechol Cross-Links? *Chem. Mater.* **2018**, *30*, 3648–3655.

(165) Rahim, M. A.; Ejima, H.; Cho, K. L.; Kempe, K.; Müllner, M.; Best, J. P.; Caruso, F. Coordination-Driven Multistep Assembly of Metal–Polyphenol Films and Capsules. *Chem. Mater.* **2014**, *26*, 1645–1653.

(166) Park, J.; Choi, S.; Moon, H.; Seo, H.; Kim, J.; Hong, S. P.; Lee, B.; Kang, E.; Lee, J.; Ryu, D.; et al. Antimicrobial Spray Nanocoating of Supramolecular Fe(III)-Tannic Acid Metal-Organic Coordination Complex: Applications to Shoe Insoles and Fruits. *Sci. Rep.* **2017**, *7*, 6980.

(167) Kang, J.; Bai, G.; Ma, S.; Liu, X.; Ma, Z.; Guo, X.; Wang, X.; Dai, B.; Zhou, F.; Jia, X. On-Site Surface Coordination Complexation via Mechanochemistry for Versatile Metal–Phenolic Networks Films. *Adv. Mater. Interfaces* **2019**, *6*, 1801789.

(168) Huang, X.; Sheng, P.; Tu, Z.; Zhang, F.; Wang, J.; Geng, H.; Zou, Y.; Di, C. A.; Yi, Y.; Sun, Y.; et al. A Two-Dimensional *π–d* Conjugated Coordination Polymer with Extremely High Electrical Conductivity and Ambipolar Transport Behaviour. *Nat. Commun.* **2015**, *6*, 7408.

(169) Sheberla, D.; Sun, L.; Blood-Forsythe, M. A.; Er, S.; Wade, C. R.; Brozek, C. K.; Aspuru-Guzik, A.; Dinca, M. High Electrical Conductivity in $Ni_3$(2,3,6,7,10,11-hexaiminotriphenylene)$_2$, a Semiconducting Metal–Organic Graphene Analogue. *J. Am. Chem. Soc.* **2014**, *136*, 8859–8862.

(170) Liu, K.; Qi, H.; Dong, R.; Shivhare, R.; Addicoat, M.; Zhang, T.; Sahabudeen, H.; Heine, T.; Mannsfeld, S.; Kaiser, U.; et al. On-Water Surface Synthesis of Crystalline, Few-Layer Two-Dimensional Polymers Assisted by Surfactant Monolayers. *Nat. Chem.* **2019**, *11*, 994–1000.

(171) Dong, R.; Zhang, T.; Feng, X. Interface-Assisted Synthesis of 2D Materials: Trend and Challenges. *Chem. Rev.* **2018**, *118*, 6189–6235.

(172) Wang, Z.; Wang, G.; Qi, H.; Wang, M.; Wang, M.; Park, S.; Wang, H.; Yu, M.; Kaiser, U.; Fery, A.; et al. Ultrathin Two-Dimensional Conjugated Metal–Organic Framework Single-Crystalline Nanosheets Enabled by Surfactant-Assisted Synthesis. *Chem. Sci.* **2020**, *11*, 7665–7671.

(173) Park, J.; Hinckley, A. C.; Huang, Z.; Feng, D.; Yakovenko, A. A.; Lee, M.; Chen, S.; Zou, X.; Bao, Z. Synthetic Routes for a 2D Semiconductive Copper Hexahydroxybenzene Metal–Organic Framework. *J. Am. Chem. Soc.* **2018**, *140*, 14533–14537.

(174) Cherepanov, P. V.; Rahim, M. A.; Bertleff-Zieschang, N.; Sayeed, M. A.; O'Mullane, A. P.; Moulton, S. E.; Caruso, F. Electrochemical Behavior and Redox-Dependent Disassembly of Gallic Acid/Fe(III) Metal–Phenolic Networks. *ACS Appl. Mater. Interfaces* **2018**, *10*, 5828–5834.

(175) Zhu, W.; Liang, S.; Wang, J.; Yang, Z.; Zhang, L.; Yuan, T.; Xu, Z.; Xu, H.; Li, P. Europium−Phenolic Network Coated $BaGdF_5$ Nanocomposites for Tri-Modal Computed Tomography/Magnetic Resonance/Luminescence Imaging. *J. Mater. Sci.: Mater. Med.* **2017**, *28*, 74.

(176) Wu, D.; Zhou, J.; Creyer, M. N.; Yim, W.; Chen, Z.; Messersmith, P. B.; Jokerst, J. V. Phenolic-Enabled Nanotechnology: Versatile Particle Engineering for Biomedicine. *Chem. Soc. Rev.* **2021**, *50*, 4432–4483.

(177) Dai, Y.; Guo, J.; Wang, T. Y.; Ju, Y.; Mitchell, A. J.; Bonnard, T.; Cui, J.; Richardson, J. J.; Hagemeyer, C. E.; Alt, K.; et al. Self-Assembled Nanoparticles from Phenolic Derivatives for Cancer Therapy. *Adv. Healthcare Mater.* **2017**, *6*, 1700467.

(178) Zhang, Z.; Sang, W.; Xie, L.; Li, W.; Li, B.; Li, J.; Tian, H.; Yuan, Z.; Zhao, Q.; Dai, Y. Polyphenol-Based Nanomedicine Evokes Immune Activation for Combination Cancer Treatment. *Angew. Chem. Int. Ed.* **2021**, *60*, 1967–1975.

(179) Dai, Y.; Cheng, S.; Wang, Z.; Zhang, R.; Yang, Z.; Wang, J.; Yung, B. C.; Wang, Z.; Jacobson, O.; Xu, C.; et al. Hypochlorous Acid Promoted Platinum Drug Chemotherapy by Myeloperoxidase-Encapsulated Therapeutic Metal Phenolic Nanoparticles. *ACS Nano* **2018**, *12*, 455–463.

(180) Xu, C.; Wang, Y.; Yu, H.; Tian, H.; Chen, X. Multifunctional Theranostic Nanoparticles Derived from Fruit-Extracted Anthocyanins with Dynamic Disassembly and Elimination Abilities. *ACS Nano* **2018**, *12*, 8255–8265.

(181) Wei, J.; Wang, G.; Chen, F.; Bai, M.; Liang, Y.; Wang, H.; Zhao, D.; Zhao, Y. Sol–Gel Synthesis of Metal–Phenolic Coordination Spheres and Their Derived Carbon Composites. *Angew. Chem. Int. Ed.* **2018**, *57*, 9838–9843.

(182) Ou, R.; Wei, J.; Zhao, C.; Gu, Q.; Zhu, H.; Li, X.; Nguyen, N. S.; Wan, L.; Forsyth, M.; Wang, H. Monovalent Cation–Phenolic Crystals with pH-Driven Reversible Crystal Transformation. *Chem. Eur. J.* **2019**, *25*, 12281–12287.

(183) Grape, E. S.; Flores, J. G.; Hidalgo, T.; Martínez-Ahumada, E.; Gutiérrez-Alejandre, A.; Hautier, A.; Williams, D. R.; O'Keeffe, M.; Öhrström, L.; Willhammar, T.; et al. A Robust and Biocompatible Bismuth Ellagate MOF Synthesized Under Green Ambient Conditions. *J. Am. Chem. Soc.* **2020**, *142*, 16795–16804.

(184) Nguyen, N. T.; Furukawa, H.; Gandara, F.; Trickett, C. A.; Jeong, H. M.; Cordova, K. E.; Yaghi, O. M. Three-Dimensional Metal-Catecholate Frameworks and Their Ultrahigh Proton Conductivity. *J. Am. Chem. Soc.* **2015**, *137*, 15394–15397.

(185) Yang, H.; Bradley, S. J.; Chan, A.; Waterhouse, G. I.; Nann, T.; Kruger, P. E.; Telfer, S. G. Catalytically Active Bimetallic Nanoparticles Supported on Porous Carbon Capsules Derived From Metal–Organic Framework Composites. *J. Am. Chem. Soc.* **2016**, *138*, 11872–11881.

(186) Chen, T.; Huang, R.; Liang, J.; Zhou, B.; Guo, X. L.; Shen, X. C.; Jiang, B. P. Natural Polyphenol–Vanadium Oxide Nanozymes for Synergistic Chemodynamic/Photothermal Therapy. *Chem. Eur. J.* **2020**, *26*, 15159–15169.

(187) Wei, J.; Liang, Y.; Hu, Y.; Kong, B.; Zhang, J.; Gu, Q.; Tong, Y.; Wang, X.; Jiang, S. P.; Wang, H. Hydrothermal Synthesis of Metal–Polyphenol Coordination Crystals and Their Derived Metal/N-Doped Carbon Composites for Oxygen Electrocatalysis. *Angew. Chem. Int. Ed.* **2016**, *55*, 12470–12474.

(188) Chen, E. X.; Qiu, M.; Zhang, Y. F.; Zhu, Y. S.; Liu, L. Y.; Sun, Y. Y.; Bu, X.; Zhang, J.; Lin, Q. Acid and Base Resistant Zirconium Polyphenolate-Metalloporphyrin Scaffolds for Efficient $CO_2$ Photoreduction. *Adv. Mater.* **2018**, *30*, 1704388.

(189) Qiu, X.; Wang, X.; He, Y.; Liang, J.; Liang, K.; Tardy, B. L.; Richardson, J. J.; Hu, M.; Wu, H.; Zhang, Y.; et al. Superstructured Mesocrystals through Multiple Inherent Molecular Interactions for Highly Reversible Sodium Ion Batteries. *Sci. Adv.* **2021**, *7*, 3482.

(190) Zhang, Y.; Xi, K.; Fu, X.; Sun, H.; Wang, H.; Yu, D.; Li, Z.; Ma, Y.; Liu, X.; Huang, B.; et al. Versatile Metal–Phenolic Network Nanoparticles for Multitargeted Combination Therapy and Magnetic Resonance Tracing in Glioblastoma. *Biomaterials* **2021**, *278*, 121163.

(191) Yuan, C.; Chen, J.; Yu, S.; Chang, Y.; Mao, J.; Xu, Y.; Luo, W.; Zeng, B.; Dai, L. Protein-Responsive Assemblies from Catechol–Metal Ion Supramolecular Coordination. *Soft Matter* **2015**, *11*, 2243–2250.

(192) Wang, C.; Sang, H.; Wang, Y.; Zhu, F.; Hu, X.; Wang, X.; Wang, X.; Li, Y.; Cheng, Y. Foe to Friend: Supramolecular Nanomedicines Consisting of Natural Polyphenols and Bortezomib. *Nano Lett.* **2018**, *18*, 7045–7051.

(193) Wang, Y.; Wang, Z.; Xu, C.; Tian, H.; Chen, X. A Disassembling Strategy Overcomes the EPR Effect and Renal Clearance Dilemma of the Multifunctional Theranostic Nanoparticles for Cancer Therapy. *Biomaterials* **2019**, *197*, 284–293.

(194) Qiao, B.; Luo, Y.; Cheng, H. B.; Ren, J.; Cao, J.; Yang, C.; Liang, B.; Yang, A.; Yuan, X.; Li, J.; et al. Artificial Nanotargeted Cells with Stable Photothermal Performance for Multimodal Imaging-Guided Tumor-Specific Therapy. *ACS Nano* **2020**, *14*, 12652–12667.

(195) Liu, F.; Sheng, S.; Shao, D.; Xiao, Y.; Zhong, Y.; Zhou, J.; Quek, C. H.; Wang, Y.; Dawulieti, J.; Yang, C.; et al. Targeting Multiple Mediators of Sepsis Using Multifunctional Tannic Acid-$Zn^{2+}$-Gentamicin Nanoparticles. *Matter* **2021**, *4*, 1–19.

(196) Zhao, G.; Wu, H.; Feng, R.; Wang, D.; Xu, P.; Jiang, P.; Yang, K.; Wang, H.; Guo, Z.; Chen, Q. Novel Metal Polyphenol Framework for MR Imaging-Guided Photothermal Therapy. *ACS Appl. Mater. Interfaces* **2018**, *10*, 3295–3304.

(197) Wu, X.; Qiu, Y.; Chen, Z.; Guan, B.; Hao, X.; Rykov, A. I.; Sun, Y.; Liu, L.; Zou, Y.; Sun, J.; et al. Paramagnetic Conducting Metal–Organic Frameworks with Three-Dimensional Structure. *Angew. Chem. Int. Ed.* **2020**, *59*, 20873–20878.

(198) Rahim, M. A.; Kempe, K.; Müllner, M.; Ejima, H.; Ju, Y.; van Koeverden, M. P.; Suma, T.; Braunger, J. A.; Leeming, M. G.; Abrahams, B. F.; et al. Surface-Confined Amorphous Films from Metal-Coordinated Simple Phenolic Ligands. *Chem. Mater.* **2015**, *27*, 5825–5832.

(199) Hu, M.; Ju, Y.; Liang, K.; Suma, T.; Cui, J.; Caruso, F. Void Engineering in Metal–Organic Frameworks via Synergistic Etching and Surface Functionalization. *Adv. Funct. Mater.* **2016**, *26*, 5827–5834.

(200) Zhu, H.; Cao, G.; Qiang, C.; Fu, Y.; Wu, Y.; Li, X.; Han, G. Hollow Ferric-Tannic Acid Nanocapsules with Sustained $O_2$ and ROS Induction for Synergistic Tumor Therapy. *Biomater. Sci.* **2020**, *8*, 3844–3855.

(201) Wang, H.; Zhu, W.; Ping, Y.; Wang, C.; Gao, N.; Yin, X.; Gu, C.; Ding, D.; Brinker, C. J.; Li, G. Controlled Fabrication of Functional Capsules Based on the Synergistic Interaction between Polyphenols and MOFs under Weak Basic Condition. *ACS Appl. Mater. Interfaces* **2017**, *9*, 14258–14264.

(202) Rahim, M. A.; Hata, Y.; Björnmalm, M.; Ju, Y.; Caruso, F. Supramolecular Metal–Phenolic Gels for the Crystallization of Active Pharmaceutical Ingredients. *Small* **2018**, *14*, 1801202.

(203) Zhang, L.; Bailey, J. B.; Subramanian, R. H.; Groisman, A.; Tezcan, F. A. Hyperexpandable, Self-Healing Macromolecular Crystals with Integrated Polymer Networks. *Nature* **2018**, *557*, 86–91.

(204) Cui, J.; Richardson, J. J.; Bjornmalm, M.; Faria, M.; Caruso, F. Nanoengineered Templated Polymer Particles: Navigating the Biological Realm. *Acc. Chem. Res.* **2016**, *49*, 1139–1148.

(205) Zhao, S.; Caruso, F.; Dähne, L.; Decher, G.; De Geest, B. G.; Fan, J.; Feliu, N.; Gogotsi, Y.; Hammond, P. T.; Hersam, M. C.; et al. The Future of Layer-by-Layer Assembly: A Tribute to *ACS Nano* Associate Editor Helmuth Möhwald. *ACS Nano* **2019**, *13*, 6151–6169.

(206) Björnmalm, M.; Cui, J.; Bertleff-Zieschang, N.; Song, D.; Faria, M.; Rahim, M. A.; Caruso, F. Nanoengineering Particles through Template Assembly. *Chem. Mater.* **2016**, *29*, 289–306.

(207) Ejima, H.; Richardson, J. J.; Caruso, F. Phenolic Film Engineering for Template-Mediated Microcapsule Preparation. *Polym. J.* **2014**, *46*, 452–459.

(208) Shen, G.; Xing, R.; Zhang, N.; Chen, C.; Ma, G.; Yan, X. Interfacial Cohesion and Assembly of Bioadhesive Molecules for Design of Long-Term Stable Hydrophobic Nanodrugs toward Effective Anticancer Therapy. *ACS Nano* **2016**, *10*, 5720–5729.

(209) Lee, J.; Cho, H.; Choi, J.; Kim, D.; Hong, D.; Park, J. H.; Yang, S. H.; Choi, I. S. Chemical Sporulation and Germination: Cytoprotective Nanocoating of Individual Mammalian Cells with a Degradable Tannic Acid–$Fe^{III}$ Complex. *Nanoscale* **2015**, *7*, 18918–18922.

(210) Li, W.; Bing, W.; Huang, S.; Ren, J.; Qu, X. Mussel Byssus-Like Reversible Metal-Chelated Supramolecular Complex Used for Dynamic Cellular Surface Engineering and Imaging. *Adv. Funct. Mater.* **2015**, *25*, 3775–3784.

(211) Delalande, L.; Tsvetkova, I. B.; Zeng, C.; Bond, K.; Jarrold, M. F.; Dragnea, B. Catching a Virus in a Molecular Net. *Nanoscale* **2016**, *8*, 16221–16228.

(212) Han, P.; Shi, J.; Nie, T.; Zhang, S.; Wang, X.; Yang, P.; Wu, H.; Jiang, Z. Conferring Natural-Derived Porous Microspheres with Surface Multifunctionality through Facile Coordination-Enabled Self-Assembly Process. *ACS Appl. Mater. Interfaces* **2016**, *8*, 8076–8085.

(213) Liang, H.; Zhou, B.; Li, J.; Liu, X.; Deng, Z.; Li, B. Engineering Multifunctional Coatings on Nanoparticles Based on Oxidative Coupling Assembly of Polyphenols for Stimuli-Responsive Drug Delivery. *J. Agric. Food Chem.* **2018**, *66*, 6897–6905.

(214) Zheng, D. W.; Lei, Q.; Zhu, J. Y.; Fan, J. X.; Li, C. X.; Li, C.; Xu, Z.; Cheng, S. X.; Zhang, X. Z. Switching Apoptosis to Ferroptosis: Metal−Organic Network for High-Efficiency Anticancer Therapy. *Nano Lett.* **2017**, *17*, 284–291.

(215) Shen, Y.; Du, C.; Zhou, J.; Ma, F. Application of Nano $Fe^{III}$–Tannic Acid Complexes in Modifying Aqueous Acrylic Latex for Controlled-Release Coated Urea. *J. Agric. Food Chem.* **2017**, *65*, 1030–1036.

(216) Long, Y.; Xiao, L.; Cao, Q.; Shi, X.; Wang, Y. Efficient Incorporation of Diverse Components into Metal Organic Frameworks via Metal Phenolic Networks. *Chem. Commun.* **2017**, *53*, 10831–10834.

(217) Wang, X.; Yan, J.; Pan, D.; Yang, R.; Wang, L.; Xu, Y.; Sheng, J.; Yue, Y.; Huang, Q.; Wang, Y.; et al. Polyphenol–Poloxamer Self-Assembled Supramolecular Nanoparticles for Tumor NIRF/PET Imaging. *Adv. Healthcare Mater.* **2018**, *7*, 1701505.

(218) Besford, Q. A.; Ju, Y.; Wang, T. Y.; Yun, G.; Cherepanov, P.; Hagemeyer, C. E.; Cavalieri, F.; Caruso, F. Self-Assembled Metal–Phenolic Networks on Emulsions as Low-Fouling and pH-Responsive Particles. *Small* **2018**, *14*, 1802342.

(219) Cui, J.; Ren, S.; Lin, T.; Feng, Y.; Jia, S. Shielding Effects of $Fe^{3+}$-Tannic Acid Nanocoatings for Immobilized Enzyme on Magnetic $Fe_3O_4$@Silica Core Shell Nanosphere. *Chem. Eng. J.* **2018**, *343*, 629–637.

(220) Liu, T.; Liu, W.; Zhang, M.; Yu, W.; Gao, F.; Li, C.; Wang, S. B.; Feng, J.; Zhang, X. Z. Ferrous-Supply-Regeneration Nanoengineering for Cancer-Cell-Specific Ferroptosis in Combination with Imaging-Guided Photodynamic Therapy. *ACS Nano* **2018**, *12*, 12181–12192.

(221) Guo, Y.; Zhang, X.; Sun, W.; Jia, H.-R.; Zhu, Y.-X.; Zhang, X.; Zhou, N.; Wu, F.-G. Metal–Phenolic Network-Based Nanocomplexes that Evoke Ferroptosis by Apoptosis: Promoted Nuclear Drug Influx and Reversed Drug Resistance of Cancer. *Chem. Mater.* **2019**, *31*, 10071–10084.

(222) Qin, Y.; Wang, J.; Qiu, C.; Hu, Y.; Xu, X.; Jin, Z. Self-Assembly of Metal–Phenolic Networks as Functional Coatings for Preparation of Antioxidant, Antimicrobial, and pH-Sensitive-Modified Starch Nanoparticles. *ACS Sustainable Chem. Eng.* **2019**, *7*, 17379–17389.

(223) Hu, F.; Liu, B.; Chu, H.; Liu, C.; Li, Z.; Chen, D.; Li, L. Real-Time Monitoring of pH-Responsive Drug Release Using a Metal-Phenolic Network-Functionalized Upconversion Nanoconstruct. *Nanoscale* **2019**, *11*, 9201–9206.

(224) Chen, W.; Hu, Y. Multiple Modifications of $BiVO_4$ through the Assembly of Metal-Phenolic Networks for Enhanced Photocatalytic Activity. *Catal. Commun.* **2019**, *123*, 124–128.

(225) Chen, Q.; Shan, X.; Shi, S.; Jiang, C.; Li, T.; Wei, S.; Zhang, X.; Sun, G.; Liu, J. Tumor Microenvironment-Responsive Polydopamine-Based Core/Shell Nanoplatform for Synergetic Theranostics. *J. Mater. Chem. B* **2020**, *8*, 4056–4066.

(226) Li, J.; Li, X.; Gong, S.; Zhang, C.; Qian, C.; Qiao, H.; Sun, M. Dual-Mode Avocado-Like All-Iron Nanoplatform for Enhanced $T_1/T_2$ MRI-Guided Cancer Theranostic Therapy. *Nano Lett.* **2020**, *20*, 4842–4849.

(227) Sun, H.; Hua, W.; Li, Y.; Wang, J. G. Promoting Photoelectrochemical Activity and Stability of $WO_3/BiVO_4$ Heterojunctions by Coating a Tannin Nickel Iron Complex. *ACS Sustainable Chem. Eng.* **2020**, *8*, 12637–12645.

(228) Rahim, M. A.; Centurion, F.; Han, J.; Abbasi, R.; Mayyas, M.; Sun, J.; Christoe, M. J.; Esrafilzadeh, D.; Allioux, F. M.; Ghasemian, M. B.; et al. Polyphenol-Induced Adhesive Liquid Metal Inks for Substrate-Independent Direct Pen Writing. *Adv. Funct. Mater.* **2020**, *31*, 2007336.

(229) Yang, C.; Wu, H.; Yang, X.; Shi, J.; Wang, X.; Zhang, S.; Jiang, Z. Coordination-Enabled One-Step Assembly of Ultrathin, Hybrid Microcapsules with Weak pH-Response. *ACS Appl. Mater. Interfaces* **2015**, *7*, 9178–9184.

(230) Wang, Y.; Zhang, Y.; Hou, C.; He, F.; Liu, M. Facile One-Pot Assembly of Adhesive Phenol/$Fe^{III}$/PEI Complexes for Preparing Magnetic Hybrid Microcapsules. *New J. Chem.* **2016**, *40*, 781–788.

(231) Bartzoka, E. D.; Lange, H.; Thiel, K.; Crestini, C. Coordination Complexes and One-Step Assembly of Lignin for Versatile Nanocapsule Engineering. *ACS Sustainable Chem. Eng.* **2016**, *4*, 5194–5203.

(232) Ju, Y.; Dai, Q.; Cui, J.; Dai, Y.; Suma, T.; Richardson, J. J.; Caruso, F. Improving Targeting of Metal−Phenolic Capsules by the Presence of Protein Coronas. *ACS Appl. Mater. Interfaces* **2016**, *8*, 22914–22922.

(233) Tardy, B. L.; Richardson, J. J.; Guo, J.; Lehtonen, J.; Ago, M.; Rojas, O. J. Lignin Nano- and Microparticles as Template for Nanostructured Materials: Formation of Hollow Metal-Phenolic Capsules. *Green Chem.* **2018**, *20*, 1335–1344.

(234) Pan, S.; Guo, R.; Bertleff-Zieschang, N.; Li, S.; Besford, Q. A.; Zhong, Q. Z.; Yun, G.; Zhang, Y.; Cavalieri, F.; Ju, Y.; et al. Modular Assembly of Host–Guest Metal–Phenolic Networks Using Macrocyclic Building Blocks. *Angew. Chem. Int. Ed.* **2020**, *59*, 275–280.

(235) Zhang, X.; Zang, J.; Ma, S.; Yu, W.; Long, F.; Qi, R.; Guo, G.; Zhou, L.; Han, B. Hollow Microcapsules with Ulcerative Colitis Therapeutic Effects Made of Multifunctional Turkish Galls Extraction. *ACS Appl. Mater. Interfaces* **2019**, *11*, 25054–25065.

(236) Zhang, P.; Hu, W.; Wu, M.; Gong, L.; Tang, A.; Xiang, L.; Zhu, B.; Zhu, L.; Zeng, H. Cost-Effective Strategy for Surface Modification via Complexation of Disassembled Polydopamine with Fe(III) Ions. *Langmuir* **2019**, *35*, 4101–4109.

(237) Wang, X.; Liang, J.; Zhang, C.; Ma, G.; Wang, C.; Kong, D. Coordination Microparticle Vaccines Engineered from Tumor Cell Templates. *Chem. Commun.* **2019**, *55*, 1568–1571.

(238) Ju, Y.; Cortez-Jugo, C.; Chen, J.; Wang, T. Y.; Mitchell, A. J.; Tsantikos, E.; Bertleff-Zieschang, N.; Lin, Y. W.; Song, J.; Cheng, Y.; et al. Engineering of Nebulized Metal–Phenolic Capsules for Controlled Pulmonary Deposition. *Adv. Sci.* **2020**, *7*, 1902650.

(239) Mohammad, M.; Lisiecki, M.; Liang, K.; Razmjou, A.; Chen, V. Metal-Phenolic Network and Metal-Organic Framework Composite Membrane for Lithium Ion Extraction. *Appl. Mater. Today* **2020**, *21*, 100884.

(240) Huang, J.; Meng, J.; Chen, S.; Zhang, S.; Liu, T.; Li, C.; Wang, F. A Soft Metal–Polyphenol Capsule-Based Ultrasensitive Immunoassay for Electrochemical Detection of Epstein-Barr (EB) Virus Infection. *Biosens. Bioelectron.* **2020**, *164*, 112310.

(241) Sun, L.; Wang, C.; Wang, L. A Kind of Coordination Complex Cement for the Self-Assembly of Superstructure. *ACS Nano* **2018**, *12*, 4002–4009.

(242) Zhao, H.; Liu, M.; Zhang, Y.; Yin, J.; Pei, R. Nanocomposite Hydrogels for Tissue Engineering Applications. *Nanoscale* **2020**, *12*, 14976–14995.

(243) Dimatteo, R.; Darling, N. J.; Segura, T. In Situ Forming Injectable Hydrogels for Drug Delivery and Wound Repair. *Adv. Drug. Delivery Rev.* **2018**, *127*, 167–184.

(244) Chen, J.; Peng, Q.; Peng, X.; Han, L.; Wang, X.; Wang, J.; Zeng, H. Recent Advances in Mechano-Responsive Hydrogels for Biomedical Applications. *ACS Appl. Polym. Mater.* **2020**, *2*, 1092–1107.

(245) Wang, Z.; Yang, H.-C.; He, F.; Peng, S.; Li, Y.; Shao, L.; Darling, S. B. Mussel-Inspired Surface Engineering for Water-Remediation Materials. *Matter* **2019**, *1*, 115–155.

(246) Zhang, W.; Wang, R.; Sun, Z.; Zhu, X.; Zhao, Q.; Zhang, T.; Cholewinski, A.; Yang, F. K.; Zhao, B.; Pinnaratip, R.; et al. Catechol-Functionalized Hydrogels: Biomimetic Design, Adhesion Mechanism, and Biomedical Applications. *Chem. Soc. Rev.* **2020**, *49*, 433–464.

(247) Zhao, X.; Liang, Y.; Huang, Y.; He, J.; Han, Y.; Guo, B. Physical Double-Network Hydrogel Adhesives with Rapid Shape Adaptability, Fast Self-Healing, Antioxidant and NIR/pH Stimulus-Responsiveness for Multidrug-Resistant Bacterial Infection and Removable Wound Dressing. *Adv. Funct. Mater.* **2020**, *30*, 1910748.

(248) Kim, S.; Regitsky, A. U.; Song, J.; Ilavsky, J.; McKinley, G. H.; Holten-Andersen, N. In Situ Mechanical Reinforcement of Polymer Hydrogels via Metal-Coordinated Crosslink Mineralization. *Nat. Commun.* **2021**, *12*, 667.

(249) Azevedo, S.; Costa, A. M. S.; Andersen, A.; Choi, I. S.; Birkedal, H.; Mano, J. F. Bioinspired Ultratough Hydrogel with Fast Recovery, Self-Healing, Injectability and Cytocompatibility. *Adv. Mater.* **2017**, *29*, 1700759.

(250) Zhu, W.; Iqbal, J.; Wang, D. A. A DOPA-Functionalized Chondroitin Sulfate-Based Adhesive Hydrogel as a Promising Multi-Functional Bioadhesive. *J. Mater. Chem. B* **2019**, *7*, 1741–1752.

(251) Pham, T. N.; Su, C. F.; Huang, C. C.; Jan, J. S. Biomimetic Hydrogels Based on L-Dopa Conjugated Gelatin as pH-Responsive Drug Carriers and Antimicrobial Agents. *Colloids Surf., B* **2020**, *196*, 111316.

(252) Fan, C.; Fu, J.; Zhu, W.; Wang, D. A. A Mussel-Inspired Double-Crosslinked Tissue Adhesive Intended for Internal Medical Use. *Acta. Biomater.* **2016**, *33*, 51–63.

(253) Mou, C.; Ali, F.; Malaviya, A.; Bettinger, C. J. Electrochemical-Mediated Gelation of Catechol-Bearing Hydrogels Based on Multimodal Crosslinking. *J. Mater. Chem. B* **2019**, *7*, 1690–1696.

(254) Li, Q.; Barrett, D. G.; Messersmith, P. B.; Holten-Andersen, N. Controlling Hydrogel Mechanics via Bio-Inspired Polymer-Nanoparticle Bond Dynamics. *ACS Nano* **2016**, *10*, 1317–1324.

(255) Chen, S.; Zeng, S.; Liu, S.; Liu, H.; Zheng, R.; White, K. L.; Smith, A. T.; Liu, L.; Sun, L. A Biomimetic Interface with High Adhesion, Tailorable Modulus for On-Skin Sensors, and Low-Power Actuators. *Chem. Mater.* **2019**, *31*, 8708–8716.

(256) Zheng, L.-Y.; Shi, J.-M.; Chi, Y.-H. Tannic Acid Physically Cross-Linked Responsive Hydrogel. *Macromol. Chem. Phys.* **2018**, *219*, 1800234.

(257) Fan, H.; Wang, L.; Feng, X.; Bu, Y.; Wu, D.; Jin, Z. Supramolecular Hydrogel Formation Based on Tannic Acid. *Macromolecules* **2017**, *50*, 666–676.

(258) Bjornmalm, M.; Wong, L. M.; Wojciechowski, J. P.; Penders, J.; Horgan, C. C.; Booth, M. A.; Martin, N. G.; Sattler, S.; Stevens, M. M. In Vivo Biocompatibility and Immunogenicity of Metal–Phenolic Gelation. *Chem. Sci.* **2019**, *10*, 10179–10194.

(259) Yu, Y.; Li, P.; Zhu, C.; Ning, N.; Zhang, S.; Vancso, G. J. Multifunctional and Recyclable Photothermally Responsive Cryogels as Efficient Platforms for Wound Healing. *Adv. Funct. Mater.* **2019**, *29*, 1904402.

(260) Zhu, W.; Peck, Y.; Iqbal, J.; Wang, D. A. A Novel DOPA-Albumin Based Tissue Adhesive for Internal Medical Applications. *Biomaterials* **2017**, *147*, 99–115.

(261) Shao, C.; Wang, M.; Meng, L.; Chang, H.; Wang, B.; Xu, F.; Yang, J.; Wan, P. Mussel-Inspired Cellulose Nanocomposite Tough Hydrogels with Synergistic Self-Healing, Adhesive, and Strain-Sensitive Properties. *Chem. Mater.* **2018**, *30*, 3110–3121.

(262) Jia, Z.; Zeng, Y.; Tang, P.; Gan, D.; Xing, W.; Hou, Y.; Wang, K.; Xie, C.; Lu, X. Conductive, Tough, Transparent, and Self-Healing Hydrogels Based on Catechol–Metal Ion Dual Self-Catalysis. *Chem. Mater.* **2019**, *31*, 5625–5632.

(263) Zhou, L.; Fan, L.; Yi, X.; Zhou, Z.; Liu, C.; Fu, R.; Dai, C.; Wang, Z.; Chen, X.; Yu, P.; et al. Soft Conducting Polymer Hydrogels Cross-Linked and Doped by Tannic Acid for Spinal Cord Injury Repair. *ACS Nano* **2018**, *12*, 10957–10967.

(264) Wang, R.; Li, J.; Chen, W.; Xu, T.; Yun, S.; Xu, Z.; Xu, Z.; Sato, T.; Chi, B.; Xu, H. A Biomimetic Mussel-Inspired ε-Poly-L-lysine Hydrogel with Robust Tissue-Anchor and Anti-Infection Capacity. *Adv. Funct. Mater.* **2017**, *27*, 1604894.

(265) Rahim, M. A.; Lin, G.; Tomanin, P. P.; Ju, Y.; Barlow, A.; Björnmalm, M.; Caruso, F. Self-Assembly of a Metal−Phenolic Sorbent for Broad-Spectrum Metal Sequestration. *ACS Appl. Mater. Interfaces* **2020**, *12*, 3746–3754.

(266) Zhang, M.; He, X.; Chen, L.; Zhang, Y. Preparation of IDA-Cu Functionalized Core–Satellite $Fe_3O_4$/Polydopamine/Au Magnetic Nanocomposites and Their Application for Depletion of Abundant Protein in Bovine Blood. *J. Mater. Chem.* **2010**, *20*, 10696–10704.

(267) Fullenkamp, D. E.; Rivera, J. G.; Gong, Y. K.; Lau, K. H.; He, L.; Varshney, R.; Messersmith, P. B. Mussel-Inspired Silver-Releasing Antibacterial Hydrogels. *Biomaterials* **2012**, *33*, 3783–3791.

(268) Zhou, J.; Wang, P.; Wang, C.; Goh, Y. T.; Fang, Z.; Messersmith, P. B.; Duan, H. Versatile Core–Shell Nanoparticle@Metal–Organic Framework Nanohybrids: Exploiting Mussel-Inspired Polydopamine for Tailored Structural Integration. *ACS Nano* **2015**, *9*, 6951–6960.

(269) Zhou, J.; Xiong, Q.; Ma, J.; Ren, J.; Messersmith, P. B.; Chen, P.; Duan, H. Polydopamine-Enabled Approach toward Tailored Plasmonic Nanogapped Nanoparticles: From Nanogap Engineering to Multifunctionality. *ACS Nano* **2016**, *10*, 11066–11075.

(270) Liu, Y.; Li, J.; Zhang, W. Liquid Metal Exfoliation of Two Dimensional Polydopamine Nanosheets for Templated Assembly of Noble Metal Nanoparticles. *Chem. Commun.* **2020**, *56*, 6229–6232.

(271) Milczarek, G.; Rebis, T.; Fabianska, J. One-Step Synthesis of Lignosulfonate-Stabilized Silver Nanoparticles. *Colloids Surf., B* **2013**, *105*, 335–341.

(272) Jia, Z.; Lv, X.; Hou, Y.; Wang, K.; Ren, F.; Xu, D.; Wang, Q.; Fan, K.; Xie, C.; Lu, X. Mussel-Inspired Nanozyme Catalyzed Conductive and Self-Setting Hydrogel for Adhesive and Antibacterial Bioelectronics. *Bioact. Mater.* **2021**, *6*, 2676–2687.

(273) Fei, J.; Zhao, J.; Du, C.; Wang, A.; Zhang, H.; Dai, L.; Li, J. One-Pot Ultrafast Self-Assembly of Autofluorescent Polyphenol-Based Core@Shell Nanostructures. *ACS Nano* **2014**, *8*, 8529–8536.

(274) Yun, G.; Pan, S.; Wang, T. Y.; Guo, J.; Richardson, J. J.; Caruso, F. Synthesis of Metal Nanoparticles in Metal-Phenolic Networks: Catalytic and Antimicrobial Applications of Coated Textiles. *Adv. Healthcare Mater.* **2018**, *7*, 1700934.

(275) Zhou, J.; Jiang, Y.; Hou, S.; Upputuri, P. K.; Wu, D.; Li, J.; Wang, P.; Zhen, X.; Pramanik, M.; Pu, K.; et al. Compact Plasmonic Blackbody for Cancer Theranosis in the Near-Infrared II Window. *ACS Nano* **2018**, *12*, 2643–2651.

(276) Yi, Z.; Li, X.; Xu, X.; Luo, B.; Luo, J.; Wu, W.; Yi, Y.; Tang, Y. Green, Effective Chemical Route for the Synthesis of Silver Nanoplates in Tannic Acid Aqueous Solution. *Colloids Surf., A* **2011**, *392*, 131–136.

(277) Mondal, M.; Begum, T.; Gogoi, P. K.; Bora, U. Gallic Acid Derived Palladium(0) Nanoparticles: An In Situ Formed “Green and Recyclable” Catalyst for Suzuki-Miyaura Coupling in Water. *ChemistrySelect* **2016**, *1*, 4645–4651.

(278) Zhang, X.-L.; Zheng, C.; Zhang, Y.; Yang, H.-H.; Liu, X.; Liu, J. One-Pot Synthesis of Gold Nanostars Using Plant Polyphenols for Cancer Photoacoustic Imaging and Photothermal Therapy. *J. Nanopart. Res.* **2016**, *18*, 174.

(279) Feng, K.; Peng, L.; Yu, L.; Zheng, Y.; Chen, R.; Zhang, W.; Chen, G. Universal Antifogging and Antimicrobial Thin Coating Based on Dopamine-Containing Glycopolymers. *ACS Appl. Mater. Interfaces* **2020**, *12*, 27632–27639.

(280) Hong, S.; Schaber, C. F.; Dening, K.; Appel, E.; Gorb, S. N.; Lee, H. Air/Water Interfacial Formation of Freestanding, Stimuli-Responsive, Self-Healing Catecholamine Janus-Faced Microfilms. *Adv. Mater.* **2014**, *26*, 7581–7587.

(281) Huang, S.; Zhang, Y.; Shi, J.; Huang, W. Superhydrophobic Particles Derived from Nature-Inspired Polyphenol Chemistry for Liquid Marble Formation and Oil Spills Treatment. *ACS Sustainable Chem. Eng.* **2016**, *4*, 676–681.

(282) Li, J.; Liu, L.; Ai, Y.; Liu, Y.; Sun, H.; Liang, Q. Self-Polymerized Dopamine-Decorated Au NPs and Coordinated with Fe-MOF as a Dual Binding Sites and Dual Signal-Amplifying Electrochemical Aptasensor for the Detection of CEA. *ACS Appl. Mater. Interfaces* **2020**, *12*, 5500–5510.

(283) Li, S.; Chen, A.; Chen, Y.; Yang, Y.; Zhang, Q.; Luo, S.; Ye, M.; Zhou, Y.; An, Y.; Huang, W.; et al. Lotus Leaf Inspired Antiadhesive and Antibacterial Gauze for Enhanced Infected Dermal Wound Regeneration. *Chem. Eng. J.* **2020**, *402*, 126202.

(284) Wang, Y.; Chen, S.; Zhao, S.; Chen, Q.; Zhang, J. Interfacial Coordination Assembly of Tannic Acid with Metal Ions on Three-Dimensional Nickel Hydroxide Nanowalls for Efficient Water Splitting. *J. Mater. Chem. A* **2020**, *8*, 15845–15852.

(285) Qin, L.; Huang, D.; Xu, P.; Zeng, G.; Lai, C.; Fu, Y.; Yi, H.; Li, B.; Zhang, C.; Cheng, M.; et al. In-Situ Deposition of Gold Nanoparticles onto Polydopamine-Decorated g-$C_3N_4$ for Highly Efficient Reduction of Nitroaromatics in Environmental Water Purification. *J. Colloid Interface Sci.* **2019**, *534*, 357–369.

(286) Jiang, Y.; Krishnan, N.; Heo, J.; Fang, R. H.; Zhang, L. Nanoparticle–Hydrogel Superstructures for Biomedical Applications. *J. Controlled Release* **2020**, *324*, 505–521.

(287) Thoniyot, P.; Tan, M. J.; Karim, A. A.; Young, D. J.; Loh, X. J. Nanoparticle–Hydrogel Composites: Concept, Design, and Applications of These Promising, Multi-Functional Materials. *Adv. Sci.* **2015**, *2*, 1400010.

(288) Merino, S.; Martı´n, C.; Kostarelos, K.; Prato, M.; Va´zquez, E. Nanocomposite Hydrogels: 3D Polymer–Nanoparticle Synergies for On-Demand Drug Delivery. *ACS Nano* **2015**, *9*, 4686–4697.

(289) Marcelo, G.; López-González, M.; Mendicuti, F.; Tarazona, M. P.; Valiente, M. Poly(*N*-isopropylacrylamide)/Gold Hybrid Hydrogels Prepared by Catechol Redox Chemistry. Characterization and Smart Tunable Catalytic Activity. *Macromolecules* **2014**, *47*, 6028–6036.

(290) Gan, D.; Shuai, T.; Wang, X.; Huang, Z.; Ren, F.; Fang, L.; Wang, K.; Xie, C.; Lu, X. Mussel-Inspired Redox-Active and Hydrophilic Conductive Polymer Nanoparticles for Adhesive Hydrogel Bioelectronics. *Nano-Micro Lett.* **2020**, *12*, 169.

(291) Rak, M. J.; Friščić, T.; Moores, A. Mechanochemical Synthesis of Au, Pd, Ru and Re Nanoparticles with Lignin as a Bio-Based Reducing Agent and Stabilizing Matrix. *Faraday Discuss.* **2014**, *170*, 155–167.

(292) Spitler, E. L.; Dichtel, W. R. Lewis Acid-Catalysed Formation of Two-Dimensional Phthalocyanine Covalent Organic Frameworks. *Nat. Chem.* **2010**, *2*, 672–677.

(293) Xiao, W.; Suby, N.; Xiao, K.; Lin, T. Y.; Al Awwad, N.; Lam, K. S.; Li, Y. Extremely Long Tumor Retention, Multi-Responsive Boronate Crosslinked Micelles with Superior Therapeutic Efficacy for Ovarian Cancer. *J. Controlled Release* **2017**, *264*, 169–179.

(294) Tang, S.; Ma, H.; Tu, H. C.; Wang, H. R.; Lin, P. C.; Anseth, K. S. Adaptable Fast Relaxing Boronate-Based Hydrogels for Probing Cell–Matrix Interactions. *Adv. Sci.* **2018**, *5*, 1800638.

(295) He, L.; Fullenkamp, D. E.; Rivera, J. G.; Messersmith, P. B. pH Responsive Self-Healing Hydrogels Formed by Boronate–Catechol Complexation. *Chem. Commun.* **2011**, *47*, 7497–7499.

(296) Narkar, A. R.; Barker, B.; Clisch, M.; Jiang, J.; Lee, B. P. pH Responsive and Oxidation Resistant Wet Adhesive Based on Reversible Catechol–Boronate Complexation. *Chem. Mater.* **2016**, *28*, 5432–5439.

(297) Wang, M.; Cai, X.; Yang, J.; Wang, C.; Tong, L.; Xiao, J.; Li, L. A Targeted and pH-Responsive Bortezomib Nanomedicine in the Treatment of Metastatic Bone Tumors. *ACS Appl. Mater. Interfaces* **2018**, *10*, 41003–41011.

(298) Demetriades, M.; Leung, I. K.; Chowdhury, R.; Chan, M. C.; McDonough, M. A.; Yeoh, K. K.; Tian, Y. M.; Claridge, T. D.; Ratcliffe, P. J.; Woon, E. C.; et al. Dynamic Combinatorial Chemistry Employing Boronic Acids/Boronate Esters Leads to Potent Oxygenase Inhibitors. *Angew. Chem. Int. Ed.* **2012**, *51*, 6672–6675.

(299) Chen, X.; Wu, F.; Tang, J.; Yang, K.; Ma, Y.; Pan, J. Anisotropic Emulsion Constructed Boronate Affinity Imprinted Janus Nanosheets for Stir Bar Sorptive Extraction of *cis*-Diol-Containing Catechol. *Chem. Eng. J.* **2020**, *395*, 124995.

(300) Naoe, M.; Iwashita, H.; Saito, S.; Koike, M.; Wada, H.; Shimojima, A.; Kuroda, K. Preparation of Porous Pentacoordinate Organosilicon Frameworks Using Organoalkoxysilanes and Tris-Catechol Linkers. *Chem. Lett.* **2020**, *49*, 1075–1077.

(301) Liu, Y.; Meng, H.; Qian, Z.; Fan, N.; Choi, W.; Zhao, F.; Lee, B. P. A Moldable Nanocomposite Hydrogel Composed of a Mussel-Inspired Polymer and a Nanosilicate as a Fit-to-Shape Tissue Sealant. *Angew. Chem. Int. Ed.* **2017**, *56*, 4224–4228.

(302) Skelton, S.; Bostwick, M.; O'Connor, K.; Konst, S.; Casey, S.; Lee, B. P. Biomimetic Adhesive Containing Nanocomposite Hydrogel with Enhanced Materials Properties. *Soft Matter* **2013**, *9*, 3825–3833.

(303) Ding, X.; Vegesna, G. K.; Meng, H.; Lee, B. P.; Winter, A. Nitro-Group Functionalization of Dopamine and Its Contribution to the Viscoelastic Properties of Catechol-Containing Nanocomposite Hydrogels. *Macromol. Chem. Phys.* **2015**, *216*, 1109–1119.

(304) Liu, Y.; Meng, H.; Konst, S.; Sarmiento, R.; Rajachar, R.; Lee, B. P. Injectable Dopamine-Modified Poly(Ethylene Glycol) Nanocomposite Hydrogel with Enhanced Adhesive Property and Bioactivity. *ACS Appl. Mater. Interfaces* **2014**, *6*, 16982–19992.

(305) Weber, F.; Barrantes, A.; Tiainen, H. Silicic Acid-Mediated Formation of Tannic Acid Nanocoatings. *Langmuir* **2019**, *35*, 3327–3336.

(306) Pi, J.; Zeng, J.; Luo, J. J.; Yang, P. H.; Cai, J. Y. Synthesis and Biological Evaluation of Germanium(IV)–Polyphenol Complexes as Potential Anti-Cancer Agents. *Bioorg. Med. Chem. Lett.* **2013**, *23*, 2902–2908.

(307) Bhuiyan, M. S. A.; Liu, B.; Manuel, J.; Zhao, B.; Lee, B. P. Effect of Conductivity on In Situ Deactivation of Catechol–Boronate Complexation-Based Reversible Smart Adhesive. *Biomacromolecules* **2021**, *22*, 4004–4015.

(308) Wu, S.; Qi, R.; Kuang, H.; Wei, Y.; Jing, X.; Meng, F.; Huang, Y. pH-Responsive Drug Delivery by Amphiphilic Copolymer through Boronate–Catechol Complexation. *ChemPlusChem* **2013**, *78*, 175–184.

(309) Wang, Y.; Zhang, X.; Mu, J.; Li, C. Synthesis and pH/Sugar/Salt-Sensitivity Study of Boronate Crosslinked Glycopolymer Nanoparticles. *New J. Chem.* **2013**, *37*, 796–803.

(310) Chen, W.; Cheng, Y.; Wang, B. Dual-Responsive Boronate Crosslinked Micelles for Targeted Drug Delivery. *Angew. Chem. Int. Ed.* **2012**, *51*, 5293–5295.

(311) Guo, R.; Su, Q.; Zhang, J.; Dong, A.; Lin, C.; Zhang, J. Facile Access to Multisensitive and Self-Healing Hydrogels with Reversible and Dynamic Boronic Ester and Disulfide Linkages. *Biomacromolecules* **2017**, *18*, 1356–1364.

(312) Vatankhah-Varnoosfaderani, M.; GhavamiNejad, A.; Hashmi, S.; Stadler, F. J. Mussel-Inspired pH-Triggered Reversible Foamed Multi-Responsive Gel–The Surprising Effect of Water. *Chem. Commun.* **2013**, *49*, 4685–4687.

(313) Wang, Z.; Zou, Y.; Li, Y.; Cheng, Y. Metal-Containing Polydopamine Nanomaterials: Catalysis, Energy, and Theranostics. *Small* **2020**, *16*, 1907042.

(314) Xu, Y.; Rothe, R.; Voigt, D.; Hauser, S.; Cui, M.; Miyagawa, T.; Patino Gaillez, M.; Kurth, T.; Bornhäuser, M.; Pietzsch, J.; et al. Convergent Synthesis of Diversified Reversible Network Leads to Liquid Metal-Containing Conductive Hydrogel Adhesives. *Nat. Commun.* **2021**, *12*, 2407.

(315) Meurer, R. A.; Kemper, S.; Knopp, S.; Eichert, T.; Jakob, F.; Goldbach, H. E.; Schwaneberg, U.; Pich, A. Biofunctional Microgel-Based Fertilizers for Controlled Foliar Delivery of Nutrients to Plants. *Angew. Chem. Int. Ed.* **2017**, *56*, 7380–7386.

(316) Dai, Q.; Yu, Q.; Tian, Y.; Xie, X.; Song, A.; Caruso, F.; Hao, J.; Cui, J. Advancing Metal-Phenolic Networks for Visual Information Storage. *ACS Appl. Mater. Interfaces* **2019**, *11*, 29305–29311.

(317) Yun, G.; Richardson, J. J.; Capelli, M.; Hu, Y.; Besford, Q. A.; Weiss, A. C. G.; Lee, H.; Choi, I. S.; Gibson, B. C.; Reineck, P.; et al. The Biomolecular Corona in 2D and Reverse: Patterning Metal–Phenolic Networks on Proteins, Lipids, Nucleic Acids, Polysaccharides, and Fingerprints. *Adv. Funct. Mater.* **2020**, *30*, 1905805.

(318) Dai, Q.; Geng, H.; Yu, Q.; Hao, J.; Cui, J. Polyphenol-Based Particles for Theranostics. *Theranostics* **2019**, *9*, 3170–3190.

(319) Reitzer, F.; Allais, M.; Ball, V.; Meyer, F. Polyphenols at Interfaces. *Adv. Colloid Interface Sci.* **2018**, *257*, 31–41.

(320) Zhang, H.; Zhao, T.; Newland, B.; Liu, W.; Wang, W.; Wang, W. Catechol Functionalized Hyperbranched Polymers as Biomedical Materials. *Prog. Polym. Sci.* **2018**, *78*, 47–55.

(321) Mrówczyński, R. Polydopamine-Based Multifunctional (Nano)materials for Cancer Therapy. *ACS Appl. Mater. Interfaces* **2018**, *10*, 7541–7561.

(322) Li, H.; Jia, Y.; Peng, H.; Li, J. Recent Developments in Dopamine-Based Materials for Cancer Diagnosis and Therapy. *Adv. Colloid Interface Sci.* **2018**, *252*, 1–20.

(323) Xu, L. Q.; Neoh, K.-G.; Kang, E.-T. Natural Polyphenols as Versatile Platforms for Material Engineering and Surface Functionalization. *Prog. Polym. Sci.* **2018**, *87*, 165–196.

(324) Cheng, W.; Zeng, X.; Chen, H.; Li, Z.; Zeng, W.; Mei, L.; Zhao, Y. Versatile Polydopamine Platforms: Synthesis and Promising Applications for Surface Modification and Advanced Nanomedicine. *ACS Nano* **2019**, *13*, 8537–8565.

(325) Qi, C.; Fu, L.-H.; Xu, H.; Wang, T.-F.; Lin, J.; Huang, P. Melanin/Polydopamine-Based Nanomaterials for Biomedical Applications. *Sci. China Chem.* **2019**, *62*, 162–188.

(326) Wang, H.; Wang, C.; Zou, Y.; Hu, J.; Li, Y.; Cheng, Y. Natural Polyphenols in Drug Delivery Systems: Current Status and Future Challenges. *Giant* **2020**, *3*, 100022.

(327) Zhang, X.; Li, Z.; Yang, P.; Duan, G.; Liu, X.; Gu, Z.; Li, Y. Polyphenol Scaffolds in Tissue Engineering. *Mater. Horiz.* **2021**, *8*, 145–167.

(328) Guo, Y.; Sun, Q.; Wu, F.-G.; Dai, Y.; Chen, X. Polyphenol-Containing Nanoparticles: Synthesis, Properties, and Therapeutic Delivery. *Adv. Mater.* **2021**, *33*, 2007356.

(329) Xie, W.; Guo, Z.; Zhao, L.; Wei, Y. Metal-Phenolic Networks: Facile Assembled Complexes for Cancer Theranostics. *Theranostics* **2021**, *11*, 6407–6426.

(330) Zhang, Z.; Xie, L.; Ju, Y.; Dai, Y. Recent Advances in Metal–Phenolic Networks for Cancer Theranostics. *Small* **2021**, *17*, 2100314.

(331) Zhang, Y.; Shen, L.; Zhong, Q.-Z.; Li, J. Metal-Phenolic Network Coatings for Engineering Bioactive Interfaces. *Colloids Surf., B* **2021**, *205*, 111851.

(332) Thompson, K. H.; Orvig, C. Boon and Bane of Metal Ions in Medicine. *Science* **2003**, *300*, 936–939.

(333) Xie, L.; Wang, G.; Sang, W.; Li, J.; Zhang, Z.; Li, W.; Yan, J.; Zhao, Q.; Dai, Y. Phenolic Immunogenic Cell Death Nanoinducer for Sensitizing Tumor to PD-1 Checkpoint Blockade Immunotherapy. *Biomaterials* **2021**, *269*, 120638.

(334) Yang, Z.; Dai, Y.; Shan, L.; Shen, Z.; Wang, Z.; Yung, B. C.; Jacobson, O.; Liu, Y.; Tang, W.; Wang, S.; et al. Tumour Microenvironment-Responsive Semiconducting Polymer-Based Self-Assembly Nanotheranostics. *Nanoscale Horiz.* **2019**, *4*, 426–433.

(335) Sang, W.; Xie, L.; Wang, G.; Li, J.; Zhang, Z.; Li, B.; Guo, S.; Deng, C.-X.; Dai, Y. Oxygen-Enriched Metal-Phenolic X-Ray Nanoprocessor for Cancer Radio-Radiodynamic Therapy in Combination with Checkpoint Blockade Immunotherapy. *Adv. Sci.* **2021**, *8*, 2003338.

(336) Wang, Y.; Liu, F.; Yan, N.; Sheng, S.; Xu, C.; Tian, H.; Chen, X. Exploration of $Fe^{III}$-Phenol Complexes for Photothermal Therapy and Photoacoustic Imaging. *ACS Biomater. Sci. Eng.* **2019**, *5*, 4700–4707.

(337) Mao, J.; Li, Y.; Cai, Q.; Tang, Z.; Yang, Y.; Yuan, C.; Xu, Y.; Zeng, B.; Luo, W.; Kuo, S.; et al. Tumor Microenvironment-Activated Self-Charge-Generable Metallosupramolecular Polymer Nanocapsules for Photoacoustic Imaging-Guided Targeted Synergistic Photothermal-Chemotherapy. *Chem. Eng. J.* **2021**, *405*, 126690.

(338) Chen, Y.; Ai, K.; Liu, J.; Ren, X.; Jiang, C.; Lu, L. Polydopamine-Based Coordination Nanocomplex for $T_1/T_2$ Dual Mode Magnetic Resonance Imaging-Guided Chemo-Photothermal Synergistic Therapy. *Biomaterials* **2016**, *77*, 198–206.

(339) Lemire, J. A.; Harrison, J. J.; Turner, R. J. Antimicrobial Activity of Metals: Mechanisms, Molecular Targets and Applications. *Nat. Rev. Microbiol.* **2013**, *11*, 371–384.

(340) Tu, Q.; Shen, X.; Liu, Y.; Zhang, Q.; Zhao, X.; Maitz, M. F.; Liu, T.; Qiu, H.; Wang, J.; Huang, N.; et al. A Facile Metal–Phenolic–Amine Strategy for Dual-Functionalization of Blood-

Contacting Devices with Antibacterial and Anticoagulant Properties. *Mater. Chem. Front.* **2019**, *3*, 265–275.

(341) Li, X.; Gao, P.; Tan, J.; Xiong, K.; Maitz, M. F.; Pan, C.; Wu, H.; Chen, Y.; Yang, Z.; Huang, N. Assembly of Metal−Phenolic/Catecholamine Networks for Synergistically Anti-Inflammatory, Antimicrobial, and Anticoagulant Coatings. *ACS Appl. Mater. Interfaces* **2018**, *10*, 40844–40853.

(342) Chen, C.; Zhang, S.; Zhang, R.; Sun, P.; Shi, C.; Abdalla, M.; Li, A.; Xu, J.; Du, W.; Zhang, J.; et al. In Situ Tuning Proangiogenic Factor-Mediated Immunotolerance Synergizes the Tumoricidal Immunity via a Hypoxia-Triggerable Liposomal Bio-Nanoreactor. *Theranostics* **2020**, *10*, 11998–12010.

(343) Yang, L.; Li, L.; Wu, H.; Zhang, B.; Luo, R.; Wang, Y. Catechol-Mediated and Copper-Incorporated Multilayer Coating: An Endothelium-Mimetic Approach for Blood-Contacting Devices. *J. Controlled Release* **2020**, *321*, 59–70.

(344) Liu, L.; Xiao, X.; Li, K.; Li, X.; Yu, K.; Liao, X.; Shi, B. Prevention of Bacterial Colonization Based on Self-Assembled Metal−Phenolic Nanocoating from Rare-Earth Ions and Catechin. *ACS Appl. Mater. Interfaces* **2020**, *12*, 22237–22245.

(345) Liu, P.; Zhang, W.; Li, X.; Liu, Y. Structural Basis for the Biological Effects of Pr(III) Ions: Alteration of Cell Membrane Permeability. *Biol. Trace Elem. Res.* **2007**, *120*, 141–147.

(346) Liu, G.; Li, K.; Wang, H.; Ma, L.; Yu, L.; Nie, Y. Stable Fabrication of Zwitterionic Coating Based on Copper-Phenolic Networks on Contact Lens with Improved Surface Wettability and Broad-Spectrum Antimicrobial Activity. *ACS Appl. Mater. Interfaces* **2020**, *12*, 16125–16136.

(347) Zheng, H.-T.; Bui, H. L.; Chakroborty, S.; Wang, Y.; Huang, C.-J. Pegylated Metal-Phenolic Networks for Antimicrobial and Antifouling Properties. *Langmuir* **2019**, *35*, 8829–8839.

(348) Lee, H. A.; Park, E.; Lee, H. Polydopamine and Its Derivative Surface Chemistry in Material Science: A Focused Review for Studies at KAIST. *Adv. Mater.* **2020**, *32*, 1907505.

(349) Kim, B. J.; Cho, H.; Park, J. H.; Mano, J. F.; Choi, I. S. Strategic Advances in Formation of Cell-in-Shell Structures: From Syntheses to Applications. *Adv. Mater.* **2018**, *30*, 1706063.

(350) Yang, S. H.; Kang, S. M.; Lee, K.-B.; Chung, T. D.; Lee, H.; Choi, I. S. Mussel-Inspired Encapsulation and Functionalization of Individual Yeast Cells. *J. Am. Chem. Soc.* **2011**, *133*, 2795–2797.

(351) Park, T.; Kim, J. Y.; Cho, H.; Moon, H. C.; Kim, B. J.; Park, J. H.; Hong, D.; Park, J.; Choi, I. S. Artificial Spores: Immunoprotective Nanocoating of Red Blood Cells with Supramolecular Ferric Ion-Tannic Acid Complex. *Polymers* **2017**, *9*, 140.

(352) Lee, H.; Park, J.; Han, S. Y.; Han, S.; Youn, W.; Choi, H.; Yun, G.; Choi, I. S. Ascorbic Acid-Mediated Reductive Disassembly of $Fe^{3+}$-Tannic Acid Shells in Degradable Single-Cell Nanoencapsulation. *Chem. Commun.* **2020**, *56*, 13748–13751.

(353) Zhou, T.; Yan, L.; Xie, C.; Li, P.; Jiang, L.; Fang, J.; Zhao, C.; Ren, F.; Wang, K.; Wang, Y.; et al. A Mussel-Inspired Persistent ROS-Scavenging, Electroactive, and Osteoinductive Scaffold Based on Electrochemical-Driven In Situ Nanoassembly. *Small* **2019**, *15*, 1805440.

(354) Pan, X.; Wang, Q.; Guo, R.; Ni, Y.; Liu, K.; Ouyang, X.; Chen, L.; Huang, L.; Cao, S.; Xie, M. An Integrated Transparent, UV-Filtering Organohydrogel Sensor via Molecular-Level Ion Conductive Channels. *J. Mater. Chem. A* **2019**, *7*, 4525–4535.

(355) Shin, M.; Park, E.; Lee, H. Plant-Inspired Pyrogallol-Containing Functional Materials. *Adv. Funct. Mater.* **2019**, *29*, 1903022.

(356) Stewart, R. J.; Wang, C. S.; Shao, H. Complex Coacervates as a Foundation for Synthetic Underwater Adhesives. *Adv. Colloid Interface Sci.* **2011**, *167*, 85–93.

(357) Ahn, B. K. Perspectives on Mussel-Inspired Wet Adhesion. *J. Am. Chem. Soc.* **2017**, *139*, 10166–10171.

(358) Saiz-Poseu, J.; Mancebo-Aracil, J.; Nador, F.; Busque, F.; Ruiz-Molina, D. The Chemistry behind Catechol-Based Adhesion. *Angew. Chem. Int. Ed.* **2019**, *58*, 696–714.

(359) Wei, W.; Petrone, L.; Tan, Y.; Cai, H.; Israelachvili, J. N.; Miserez, A.; Waite, J. H. An Underwater Surface-Drying Peptide Inspired by a Mussel Adhesive Protein. *Adv. Funct. Mater.* **2016**, *26*, 3496–3507.

(360) Stewart, R. J.; Weaver, J. C.; Morse, D. E.; Waite, J. H. The Tube Cement of *Phragmatopoma Californica*: A Solid Foam. *J. Exp. Biol.* **2004**, *207*, 4727–4734.

(361) Shao, H.; Bachus, K. N.; Stewart, R. J. A Water-Borne Adhesive Modeled after the Sandcastle Glue of *P. californica*. *Macromol. Biosci.* **2009**, *9*, 464–471.

(362) Shao, H.; Stewart, R. J. Biomimetic Underwater Adhesives with Environmentally Triggered Setting Mechanisms. *Adv. Mater.* **2010**, *22*, 729–733.

(363) Winslow, B. D.; Shao, H.; Stewart, R. J.; Tresco, P. A. Biocompatibility of Adhesive Complex Coacervates Modeled after the Sandcastle Glue of *Phragmatopoma Californica* for Craniofacial Reconstruction. *Biomaterials* **2010**, *31*, 9373–9381.

(364) Mann, L. K.; Papanna, R.; Moise, K. J., Jr.; Byrd, R. H.; Popek, E. J.; Kaur, S.; Tseng, S. C.; Stewart, R. J. Fetal Membrane Patch and Biomimetic Adhesive Coacervates as a Sealant for Fetoscopic Defects. *Acta Biomater.* **2012**, *8*, 2160–2165.

(365) Pandey, N.; Soto-Garcia, L. F.; Liao, J.; Zimmern, P.; Nguyen, K. T.; Hong, Y. Mussel-Inspired Bioadhesives in Healthcare: Design Parameters, Current Trends, and Future Perspectives. *Biomater. Sci.* **2020**, *8*, 1240–1255.

(366) Liu, M.; Zeng, G.; Wang, K.; Wan, Q.; Tao, L.; Zhang, X.; Wei, Y. Recent Developments in Polydopamine: An Emerging Soft Matter for Surface Modification and Biomedical Applications. *Nanoscale* **2016**, *8*, 16819–16840.

(367) Guo, Q.; Chen, J.; Wang, J.; Zeng, H.; Yu, J. Recent Progress in Synthesis and Application of Mussel-Inspired Adhesives. *Nanoscale* **2020**, *12*, 1307–1324.

(368) Jia, Z.; Wen, M.; Cheng, Y.; Zheng, Y. Strategic Advances in Spatiotemporal Control of Bioinspired Phenolic Chemistries in Materials Science. *Adv. Funct. Mater.* **2021**, *31*, 2008821.

(369) Yang, L.; Guo, X.; Jin, Z.; Guo, W.; Duan, G.; Liu, X.; Li, Y. Emergence of Melanin-Inspired Supercapacitors. *Nano Today* **2021**, *37*, 101075.

(370) Li, A.; Mu, Y.; Jiang, W.; Wan, X. A mussel-Inspired Adhesive with Stronger Bonding Strength under Underwater Conditions than Under Dry Conditions. *Chem. Commun.* **2015**, *51*, 9117–9120.

(371) Sha, X.; Zhang, C.; Qi, M.; Zheng, L.; Cai, B.; Chen, F.; Wang, Y.; Zhou, Y. Mussel-Inspired Alternating Copolymer as a High-Performance Adhesive Material Both at Dry and Under-Seawater Conditions. *Macromol. Rapid Commun.* **2020**, *41*, 2000055.

(372) Mu, Y.; Wu, X.; Pei, D.; Wu, Z.; Zhang, C.; Zhou, D.; Wan, X. Contribution of the Polarity of Mussel-Inspired Adhesives in the Realization of Strong Underwater Bonding. *ACS Biomater. Sci. Eng.* **2017**, *3*, 3133–3140.

(373) Kim, D.-S.; Park, W.-J.; Jun, C.-H. Metal–Organic Cooperative Catalysis in C–H and C–C Bond Activation. *Chem. Rev.* **2017**, *117*, 8977–9015.

(374) Gao, C.; Lyu, F.; Yin, Y. Encapsulated Metal Nanoparticles for Catalysis. *Chem. Rev.* **2021**, *121*, 834–881.

(375) Ai, K.; Liu, Y.; Ruan, C.; Lu, L.; Lu, G. $Sp^2$ C-Dominant N-Doped Carbon Sub-Micrometer Spheres with a Tunable Size: A Versatile Platform for Highly Efficient Oxygen-Reduction Catalysts. *Adv. Mater.* **2013**, *25*, 998–1003.

(376) Zhou, J.; Duan, B.; Fang, Z.; Song, J.; Wang, C.; Messersmith, P. B.; Duan, H. Interfacial Assembly of Mussel-Inspired Au@Ag@Polydopamine Core–Shell Nanoparticles for Recyclable Nanocatalysts. *Adv. Mater.* **2014**, *26*, 701–705.

(377) Zhou, J.; Wang, C.; Wang, P.; Messersmith, P. B.; Duan, H. Multifunctional Magnetic Nanochains: Exploiting Self-Polymerization and Versatile Reactivity of Mussel-Inspired Polydopamine. *Chem. Mater.* **2015**, *27*, 3071–3076.

(378) Álvarez-Paino, M.; Marcelo, G.; Muñoz-Bonilla, A.; Fernández-García, M. Catecholic Chemistry To Obtain Recyclable and Reusable Hybrid Polymeric Particles as Catalytic Systems. *Macromolecules* **2013**, *46*, 2951–2962.

(379) Dubey, A. V.; Kumar, A. V. A Biomimetic Magnetically Recoverable Palladium Nanocatalyst for the Suzuki Cross-Coupling Reaction. *RSC Adv.* **2016**, *6*, 46864–46870.

(380) Zhang, Z.; He, X.; Zhou, C.; Reaume, M.; Wu, M.; Liu, B.; Lee, B. P. Iron Magnetic Nanoparticle-Induced ROS Generation from Catechol-Containing Microgel for Environmental and Biomedical Applications. *ACS Appl. Mater. Interfaces* **2020**, *12*, 21210–21220.

(381) Guo, H.; Yao, Z.; Yang, Z.; Ma, X.; Wang, J.; Tang, C. Y. A One-Step Rapid Assembly of Thin Film Coating Using Green Coordination Complexes for Enhanced Removal of Trace Organic Contaminants by Membranes. *Environ. Sci. Technol.* **2017**, *51*, 12638–12643.

(382) Kim, H. J.; Kim, D.-G.; Yoon, H.; Choi, Y.-S.; Yoon, J.; Lee, J.-C. Polyphenol/$Fe^{III}$ Complex Coated Membranes Having Multifunctional Properties Prepared by a One-Step Fast Assembly. *Adv. Mater. Interfaces* **2015**, *2*, 1500298.

(383) Bliznyuk, V. N.; Kołacińska, K.; Pud, A. A.; Ogurtsov, N. A.; Noskov, Y. V.; Powell, B. A.; DeVol, T. A. High Effectiveness of Pure Polydopamine in Extraction of Uranium and Plutonium from Groundwater and Seawater. *RSC Adv.* **2019**, *9*, 30052–30063.

(384) Derami, H. G.; Jiang, Q.; Ghim, D.; Cao, S.; Chandar, Y. J.; Morrissey, J. J.; Jun, Y.-S.; Singamaneni, S. A Robust and Scalable Polydopamine/Bacterial Nanocellulose Hybrid Membrane for Efficient Wastewater Treatment. *ACS Appl. Nano Mater.* **2019**, *2*, 1092–1101.

(385) Li, B.; Wu, L.; Li, L.; Seeger, S.; Zhang, J.; Wang, A. Superwetting Double-Layer Polyester Materials for Effective Removal of Both Insoluble Oils and Soluble Dyes in Water. *ACS Appl. Mater. Interfaces* **2014**, *6*, 11581–11588.

(386) Oulad, F.; Zinadini, S.; Zinatizadeh, A. A.; Derakhshan, A. A. Fabrication and Characterization of a Novel Tannic Acid Coated Boehmite/PES High Performance Antifouling NF Membrane and Application for Licorice Dye Removal. *Chem. Eng. J.* **2020**, *397*, 125105.

(387) Wang, R.; Zhao, X.; Lan, Y.; Liu, L.; Gao, C. In Situ Metal-Polyphenol Interfacial Assembly Tailored Superwetting PES/SPES/MPN Membranes for Oil-in-Water Emulsion Separation. *J. Membr. Sci.* **2020**, *615*, 118566.

(388) Zhang, N.; Yang, N.; Zhang, L.; Jiang, B.; Sun, Y.; Ma, J.; Cheng, K.; Peng, F. Facile Hydrophilic Modification of PVDF Membrane with Ag/EGCG Decorated Micro/Nanostructural Surface for Efficient Oil-in-Water Emulsion Separation. *Chem. Eng. J.* **2020**, *402*, 126200.

(389) You, F.; Xu, Y.; Yang, X.; Zhang, Y.; Shao, L. Bio-Inspired $Ni^{2+}$-Polyphenol Hydrophilic Network to Achieve Unconventional High-Flux Nanofiltration Membranes for Environmental Remediation. *Chem. Commun.* **2017**, *53*, 6128–6131.

(390) Zhu, Q.; Pan, Q. Mussel-Inspired Direct Immobilization of Nanoparticles and Application for Oil–Water Separation. *ACS Nano* **2014**, *8*, 1402–1409.

(391) Li, W.; Shi, J.; Zhao, Y.; Huo, Q.; Sun, Y.; Wu, Y.; Tian, Y.; Jiang, Z. Superhydrophobic Metal–Organic Framework Nanocoating Induced by Metal-Phenolic Networks for Oily Water Treatment. *ACS Sustainable Chem. Eng.* **2020**, *8*, 1831–1839.

(392) Wang, R.; Zhao, X.; Jia, N.; Cheng, L.; Liu, L.; Gao, C. Superwetting Oil/Water Separation Membrane Constructed from In Situ Assembled Metal–Phenolic Networks and Metal–Organic Frameworks. *ACS Appl. Mater. Interfaces* **2020**, *12*, 10000–10008.

(393) Geng, H.; Zhuang, L.; Li, M.; Liu, H.; Caruso, F.; Hao, J.; Cui, J. Interfacial Assembly of Metal–Phenolic Networks for Hair Dyeing. *ACS Appl. Mater. Interfaces* **2020**, *12*, 29826–29834.

(394) Im, K. M.; Kim, T.-W.; Jeon, J.-R. Metal-Chelation-Assisted Deposition of Polydopamine on Human Hair: A Ready-to-Use Eumelanin-Based Hair Dyeing Methodology. *ACS Biomater. Sci. Eng.* **2017**, *3*, 628–636.

(395) Han, S. Y.; Hong, S.-P.; Kang, E. K.; Kim, B. J.; Lee, H.; Kim, W. I.; Choi, I. S. Iron Gall Ink Revisited: Natural Formulation for Black Hair-Dyeing. *Cosmetics* **2019**, *6*, 23.

(396) Han, S. Y.; Kang, E. K.; Choi, I. S. Iron Gall Ink Revisited: A Surfactant-Free Emulsion Technology for Black Hair-Dyeing Formulation. *Cosmetics* **2021**, *8*, 9.

(397) Zhang, L.; Liu, R.; Gung, B. W.; Tindall, S.; Gonzalez, J. M.; Halvorson, J. J.; Hagerman, A. E. Polyphenol–Aluminum Complex Formation: Implications for Aluminum Tolerance in Plants. *J. Agric. Food Chem.* **2016**, *64*, 3025–3033.

(398) Kim, B. J.; Lee, J. K.; Choi, I. S. Iron Gall Ink Revisited: Hierarchical Formation of Fe(III)–Tannic Acid Coacervate Particles in Microdroplets for Protein Condensation. *Chem. Commun.* **2019**, *55*, 2142–2145.

Table of Content graphic